A Computational Approach for Understanding Adaptation in Vertebrate Hair Cells

by

Paul D. Niksch

B.S. Electrical Engineering
Purdue University, 2001

SUBMITTED TO THE DEPARTMENT OF HEALTH SCIENCES AND TECHNOLOGY IN PARTIAL FULFILLMENT OF THE REQUIREMENTS FOR THE DEGREE OF DOCTOR OF PHILOSOPHY IN HEALTH SCIENCES AND TECHNOLOGY
AT
HARVARD/MASSACHUSETTS INSTITUTE OF TECHNOLOGY

FEBRUARY 2012

Signature of Author: _____
Department of Health Sciences and Technology
October 11, 2011

Certified by:

_____
David P. Corey
Professor of Neurobiology, Harvard Medical School
Investigator, Howard Hughes Medical Institute
Thesis Supervisor

Accepted by: _____
Ram Sasisekharan
PhD/Director, Harvard-MIT Division of Health Sciences and Technology
Edward Hood Taplin Professor of Health Sciences & Technology and Biological Engineering

A Computational Approach for Understanding Adaptation in Vertebrate Hair Cells

by

Paul D. Niksch

Submitted to the Department of Health Sciences and Technology on October 11, 2011 in Partial Fulfillment of the Requirements for the Degree of Doctor of Philosophy in Health Sciences and Technology

ABSTRACT

Vertebrate hair cells respond to mechanical stimuli with an inward current that is carried by extracellular cations through mechanically-gated transmembrane ion channels called transduction channels, located in the hair cell's specialized apical surface called the stereocilia. The current is characterized as having a rapid onset and adapting exponentially with a fast and slow time constant. The fast component is usually attributed to calcium binding directly to the transduction channels to promote channel reclosure. Myosin-1C, an unconventional myosin motor protein that is also modulated by calcium, adjusts the tension applied to the transduction channel to cause slow adaptation. Neither adaptation typically acts completely to restore the transduction current back to the baseline level.

Recent evidence has suggested that the transduction channel is further away from myosin-1C than previously believed, creating a spatial separation that changes the nature of the calcium feedback. I developed a computational model to explore the motion of vertebrate hair cells simultaneously with calcium diffusion within the cell. The model is also capable of simulating many other experimental techniques that are commonly applied to hair cells.

The results of the model suggest a fundamentally different viewpoint for understanding adaptation in vertebrate hair cells. Calcium can create unique responses from different transduction channels within the same hair cell. The implications of these findings help to explain the incompleteness of adaptation as well as implicate myosin-1C for fast adaptation as well as slow adaptation. In addition, groundwork for better understanding stereocilia-based amplification in the mammalian cochlea was developed. Experimental predictions were created to test these theories.

Thesis Supervisor: David P. Corey

Title: Professor of Neurobiology, Harvard Medical School / Investigator, Howard Hughes Institute

Table of Contents

Acknowledgments

In the (many) years since I first began graduate school, Boston has become a true home for me. I have made, what most would consider, several lifetimes' worth of wonderful friends and enjoyed countless experiences. Throughout the more stressful days of my studies, I could often find a pleasant distraction. Whether this took the form of a nice conversation with someone from the other side of the world or flying through the air with the greatest of ease, it will forever be appreciated. I would be completely ungrateful if I did not especially thank Vanessa, who provided many wonderful memories and support during graduate school.

I also would like to thank for family for all of the support that they have given me. Growing up, my parents made sure that I had more than every opportunity to succeed. They always encouraged me no matter how bizarre my interest was at the time. My two older brothers toughened me up when I was younger which made me quite persistent as an adult, a trait that is sometimes very handy in science. They, and their families, have always provided wonderful respites from graduate life.

I could not have asked for a better environment to work in than the Corey lab. I'm quite sure that I could not have quite as interesting luncheon conversations with any other lab. Every member of the lab would provide assistance without even a second's thought. This, of course, is a reflection of the leader, Dr. David Corey. Any member of the lab knows that David ranks his priorities as such:

1. The well-being and happiness of his family and members of the lab.
2. Pursuing true discovery and knowledge about the world.
3. Sailing.

It has been a true pleasure working and learning with David throughout the years.

Chapter 1

Review of Transduction Adaptation

Introduction

Hair cells have evolved to be remarkably sensitive to mechanical stimulation. They are the primary transducer for vibrations arising from sound in hearing organs, fluid flow in the lateral line of fish, as well as head motion in the vestibular system. Each specialty varies in design to fit its function; however, all hair cells have a specialized apical portion that contains the hair bundle. The hair bundle is made up of rigid structures called stereocilia, with the primary component of each stereocilium being actin fibers bundled tightly together (DeRosier, Tilney, & Egelman, 1980). The stereocilia are arranged in a staircase formation, with each stereocilium being progressively larger than its neighbor along a column. A deflection towards the tallest stereocilia produces an excitatory, inward current, but the hair cell is unresponsive to orthogonal deflections (Shotwell, Jacobs, & Hudspeth, 1981). Vestibular hair bundles and immature cochlear hair bundles contain a kinocilium adjacent to the tallest stereocilia, which is not responsible for the excitatory current (Hudspeth & Corey, 1977). Early work in hair cell transduction indicated that current enters the hair bundle near the tips of the stereocilia (Hudspeth, 1982) and that the latency of the current response to a mechanical deflection was around 10 μsec at mammalian temperatures, indicating that a second messenger system is not involved in generating the excitatory current (Corey & Hudspeth, 1979b). The discovery of tip links provided a mechanism for how the applied force could be sensed by the hair bundle (Pickles, Comis, & Osborne, 1984). During a deflection, the stereocilia maintain physical contact with each other, due to horizontal top connectors, and shear relative to one another (Karavitaki & Corey, 2010; Goodyear & Richardson, 1999). A deflection toward the tallest stereocilium thus increases the distance between the tips of neighboring stereocilia. Shearing increases the length of the tip link, or at least elements in series with the tip link. The increase in length along the tip link axis provides the necessary final stimulus in converting a physical stimulus into energy that is sufficient to activate a force-gated transmembrane ion channel, termed the transduction channel.

The hair cell transduction channel is similar to voltage-gated channels in that a force will bias the channel towards an open configuration (Hudspeth et al., 2000). In the case of voltage-gated channels, the bias force comes in the form of an intrinsic voltage sensor responding to a transmembrane voltage (Hille, 1992). In general, mechanically gated channels directly respond to the force applied to them. The hair cell transduction channel is thought to be connected in series with an elastic element termed the gating spring (Corey & Hudspeth, 1983b). The tension in the gating spring will cause a conformational change in the channel, resulting in a movement of the gating elements by a distance, d, known as the gate swing. The gate swing does not simply refer to the change in diameter of the pore of the channel, but refers to the net movement of elements in series with the channel during a conformational change (Howard & Hudspeth, 1988). This direct coupling of the force to the channel implies that the gate swing itself causes a change in the stretch of transduction elements. The further implication is that the change in stretch will directly affect the force acting on elements in the tip link axis, as well as affect the overall motion of the hair bundle.

A linear deflection of the hair bundle by a displacement, X, should stretch the gating springs by a fraction (termed the shear factor, γ) of that displacement so that the total gating-spring stretch along the tip link axis is γ*X (Howard, Roberts, & Hudspeth,1988). This stretch will result in a proportional increase in force to the transduction channel. The net force is the product of the tip link stretch and the stiffness of the gating spring, k_G, with the resulting force being $F= k_G*\gamma*X$. A gating sensitivity, z, can be defined as the product of the gating spring stiffness and the channel during gating, d, so that $z=k_G*\gamma*d$; it has units of force. The channel gating is governed by a sigmoidal gating equation:

$$P(X) = \frac{1}{1+e^{-\frac{z(X-Xo)}{kT}}}$$

in which P is the open probability of the transduction channels, X_o is the displacement for which the open probability is 0.5, and k is Boltzmann's constant and T is temperature. In this viewpoint, a displacement step applied to the hair bundle should yield a steady change in transduction current. However, an absolute position sensor would not be ideal for the function of hair cells. A strong deflection produced by gravity detection might saturate the detector. It is therefore not surprising that the transduction current often adapts: it quickly reaches a peak value and then declines towards its baseline level (Corey & Hudspeth, 1983a; Eatock *et. al*, 1987). This occurs as well for negative deflections, in which the instantaneous current is reduced from the baseline level. This mechanism provides high pass filtering that allows hair cells to reject static offset and thus to be more sensitive to new stimuli. Much of the work done on hair cells from the past two decades has sought to explore this process, termed transduction adaptation.

Adaptation of hair bundle transduction currents is certainly a difficult field to comprehend. Subtle variations amongst species and an incomplete knowledge of the molecular components involved make it hard to integrate the findings of the field. This review seeks to explain what has been discovered about adaptation by viewing the knowledge in the field from three separate approaches. First, the current and position response of the hair bundle to deflections will be analyzed. Following this, the various attempts to explain the molecular mechanisms of adaptation will be explored. Finally, I will discuss how recent findings might support some models and describe which experiments would be most useful in creating a better understanding of hair cell adaptation.

Mechanical and Electrical Aspects of Adaptation

Components of Adaptation:

Adaptation can be divided into fast and slow adaptation. The principal basis for this distinction is that the transduction current returns to a steady state value in a roughly exponential manner. The current decline is better fit with the sum of two exponentials rather than one (Crawford, Evans & Fettiplace, 1989; Wu, Ricci & Fettiplace, 1999). The time constants for these fits depend on the species examined and overall experimental conditions. Time constants measured with a stiff probe in bullfrog saccular hair cells for fast and slow adaptation have been measured as 2.3 msec and 18.1 msec,

respectively. This is compared to 5.2 msec and 45.6 msec in mouse utricle obtained by the same researchers (Vollrath & Eatock, 2003). Turtle adaptation time constants are around 0.75 msec, with slow adaptation seemingly absent (Ricci, Wu & Fettiplace, 1998). Rat outer hair cell bundles have shown extremely fast time constants in the range of 60 μsec for small stimuli (Ricci *et.al.*,2005). For larger stimuli, outer hair cells have displayed time constants of 3 msec and 13 msec and inner hair cells have time constants on the order of 4 msec and 15 msec (Stauffer & Holt, 2007).

The transduction current directly following stimulation with a fast probe can be used to determine the instantaneous transduction curve, I-X. This curve generally fits a sigmoidal profile as predicted by gating theory. The steepness of the curve is determined by the gating spring stiffness and gate swing. In theory, adaptation could work by either adjusting the steepness of the I-X curve or by shifting the curve along the deflection axis. Both fast and slow adaptation appear to be best explained by shifting the I-X curve as adaptation progresses (Corey & Hudspeth, 1983a; Cheung & Corey, 2006). Both processes shift the I-X curve so that the transduction current approaches its baseline level. The relative ratio of fast adaptation to slow adaptation varies depending on the size of the deflection. Smaller deflections tend to elicit fast adaptation, whereas larger deflections produce more slow adaptation (Stauffer *et. al.*, 2005). It appears that fast adaptation can only have an effect for small deflections. As it shifts the I-X curve in the same direction as slow adaptation, fast adaptation inherently reduces the drive for slow adaptation. This ratio depends on the hair cell type as well as the magnitude of the stimulus (Vollrath & Eatock, 2003).

Stimulating the hair bundle with a probe that is relatively compliant when compared to the hair bundle allows one to observe the forces produced by the hair bundle. For a positive deflection, the hair bundle tends to decrease in stiffness, initially. This effect is thought to be due to the opening of transduction channels, termed gating compliance (Howard & Hudspeth, 1988). In addition, fast adaptation and slow adaptation produce bundle motions following the stimulus. Directly following a deflection, the bundle will sometimes move in the direction opposite of the stimulus, on a time course similar to fast adaptation. This reverse motion of the bundle has been termed the twitch. In bullfrog saccular hair cells, it is only on the order of a few nanometers (Cheung & Corey, 2004). Turtle hair cells have displayed a much larger twitch (Ricci, Crawford, & Fettiplace, 2002) that occasionally rebounds further negative than the initial position of the hair bundle at rest (Ricci, Crawford, & Fettiplace, 2000). Strangely, the twitch has never been observed in mammalian hair bundles (Kennedy, Crawford, & Fettiplace, 2005; Beurg *et. al.*,2008).

On a time course with slow adaptation, the bundle relaxes in the same direction of the stimulus (Howard & Hudspeth, 1987). This motion is rather robust and takes much longer than one would expect from the passive drag of the hair bundle. This slower motion correlates well with the rate of slow adaptation of the transduction current. This active positive motion has even been shown to move the hair bundle further than the stimulus probe in rat outer hair cells, requiring that the hair bundle provide energy (Kennedy, Crawford, & Fettiplace, 2005). The difference in direction of bundle motion associated with fast and slow adaptation, at least in non-mammals, is another reason that researchers distinguish these two processes.

For a step deflection of the bundle, the current rarely returns back to the baseline level for both negative and positive deflections; that is, adaptation is rarely complete. Shepherd *et. al.* (1994) measured the extent of adaptation to be roughly 85% for positive deflections and constant for negative deflections. This means that most of the current does not return to the baseline level if a sufficiently large enough negative deflection is delivered. However, the I-X curve is still shifting while the bundle is held in a negative position. This is evident in the fact that when the bundle is returned to the baseline position, a positive rebound current is often seen (Shepherd *et. al.*, 1994; Cheung & Corey, 2006). This rebound current is larger for larger negative deflections, implying that the I-X had shifted further for such deflections.

Calcium's Effect on Adaptation:

Calcium plays a very important role in modulating the strength and speed of both fast and slow adaptation. Early work in early epithelia microphonic preparations showed that external calcium concentrations had a direct effect on transduction (Corey & Hudspeth, 1983b; Eatock, Corey, & Hudspeth, 1987). Recordings made directly from hair cells showed that external calcium acted to partially block the transduction channel as well as decrease the time constants for both fast and slow adaptation (Crawford, Evans, & Fettiplace, 1989, 1991). Removing all the external calcium is a very effective way of breaking the tip links and abolishing functional transduction (Assad *et. al.*,1991). Researchers can decrease the intracellular calcium by lowering the external calcium to as low as a few tens of micro-molar without breaking the tip links, or by depolarizing the cell so as to reduce the driving force for calcium influx. Reducing the external calcium concentration also acts to slow the mechanical correlates of adaptation (Cheung & Corey, 2006). As the external calcium is lowered, or the holding potential of the cell is depolarized, the resting current increases, an effect thought to be caused by the weakening of the adaptation mechanisms (Crawford, Evans, & Fettiplace, 1991; Assad, Hacohen, & Corey, 1989). In outer hair cells, the resting current is around 6% for 1.5 mM external calcium concentration and 46% for 20 μM external calcium concentration (Johnson *et. al.*, 2011). In addition, the extent of adaptation is lowered in the presence of less calcium. For transduction recordings done in bullfrog saccular hair cells, the resting current shifted from 15% to 70% of the total current when the holding potential was changed from -80 mV to +80 mV. At +80 mV, adaptation becomes almost non-existent (Assad, Hacohen, & Corey, 1989). In general, the presence of calcium makes adaptation more complete.

There is a general broadening of the instantaneous I-X curve when the cell is held at +80 mV in bullfrog saccular hair cells (Assad, Hacohen, & Corey, 1989) and turtle cochlear hair cells (Crawford, Evans, & Fettiplace, 1991). Essentially, it appears as if the gating sensitivity, z, is reduced under this condition. It is not clear if this effect stems from reduced adaptation or from some other process. It does seem slightly counter-intuitive to believe that reducing adaptation would broaden the transduction curve, as one would expect robust adaptation to reduce current even during the rise time of the bundle's deflection. Therefore, one might expect weakened adaptation to create a steeper transduction curve. I-X curves in rat outer hair cells occasionally show increased maximum current as well as a steeper slope when calcium is reduced (Beurg *et. al.*, 2008). This would fit well with this interpretation that robust adaptation can reduce the measured instantaneous current. However, in other reports

reducing the calcium concentration broadens the I-X curve (Johnson *et. al.*, 2011). Two different responses to calcium obtained in the same model system highlights the difficulty in interpreting this result.

Active Hair Bundle Motion:

The amount of transduction current is a measure of the open probability of the transduction channels, which is proportional to the force being exerted on the channels by the gating springs. Tension in the gating springs acts to move the bundle in the negative direction. Therefore, adaptation, which reduces transduction current, would be expected to move the bundle in the positive direction. However, the opening of transduction channels creates gating compliance, which also acts to move the bundle in the positive direction. In light of this, it is not surprising that hyperpolarizing the cell, which reduces the strength of adaptation, produces conflicting results in different hair cell types. Assad *et. al.* (1989) found that bullfrog saccular hair bundles moved in the negative direction by 97 nm when the cell was hyperpolarized to +80 mV. For the same voltage change, Ricci *et. al.* (2002) found that turtle cochlear hair bundles initially move 30 nm in the positive direction followed by a negative motion past the baseline position. Turtle hair bundles also exhibit a larger twitch corresponding with fast adaptation. It could be that a larger gate swing, which produces a larger gating compliance, explains both of these differences in turtle hair bundles.

In a free standing bundle, any motion of the hair bundle will change the tension in the gating springs, regardless of whether the motion comes from an external stimulus or from components of the gating complex. Slow adaptation, which corresponds to decreasing current and positive bundle movement, will create additional shear and tension in the gating springs from the positive motion. Opening of the transduction channels also creates a positive bundle motion, whereas closure of transduction channels causes the bundle to move in the negative direction. Every motion of the bundle causes a series of changes at the level of the transduction complex, which in turn create additional hair bundle motions. The freestanding system is in a constant struggle to reach equilibrium. This complex balance of forces is thought to be responsible for the observation of free standing bundles occasionally displaying spontaneous oscillations (Martin, Hudspeth, & Jülicher, 2001; Martin *et. al.*, 2003; Le Goff, Bozovic, & Hudspeth, 2005; Nam & Fettiplace, 2008). Martin *et. al.* (2003) reported bullfrog saccular hair bundles oscillate at peak to peak displacements up to 80 nm at frequencies of 5-50 Hz. Tinevez *et. al.* (2007) reported the oscillation behavior is dependent on the amount of free calcium in the external solution. 250 μM Ca^{+2} in the external solution was more likely to produce oscillations, whereas higher calcium created negative twitches in response to positive bundle deflections. Currently, oscillations in mammalian hair bundles have not been observed (Kennedy, Crawford, & Fettiplace, 2005; Beurg *et. al.*,2008). It remains to be seen if this missing behavior stems from experimental conditions or a fundamental difference intrinsic to mammalian hair cells.

The mechanism thought to be responsible for self-oscillating bundles is dependent on a region of negative slope, or negative stiffness in the force versus displacement curve, F-X (Martin, Mehta, &

Hudspeth, 2000). Over the region of negative stiffness, any positive deflection of the bundle will actually act to reduce the intrinsic force opposing such motion. This is an inherently unstable situation in which the bundle will continue to move until it has moved passed the region of negative stiffness. The negative stiffness region always corresponds with the most sensitive region of the I-X curve. The obvious inference is that the negative stiffness region stems from the gating compliance associated with the opening of transduction channels. This negative stiffness region does not always appear in hair cell recordings. It is dependent on the external calcium levels (Tinevez *et. al.* ,2007), as well as the overall health of the hair bundle post dissection (Cheung & Corey, 2008). Freestanding oscillations have two components of motion: a slow component in which the bundle creeps in one direction on the order of milliseconds as well as a rapid component in the opposite direction that is on a sub-millisecond time scale. The slow component most likely arises from slow adaptation resetting the setpoint of the I-X curve. The fast component of oscillation arises when the bundle rapidly moves through the unstable region of negative stiffness (Martin *et. al.*, 2003; Le Goff, Bozovic, & Hudspeth, 2005).

Variations across Hair Bundle Type:

There are apparent differences in the manner in which hair bundles behave from various preparations. This is not altogether surprising based on the functions of the organs and species that the hair bundles are taken from. One would expect that hair cells from various organs would individually evolve to serve their specific function. Even within the same cochlea, single channel conductance of the transduction channel varies across the tonotopic gradient and between cell types (Beurg *et. al.*, 2006). In outer hair cells, single channel conductance varies from 145 to 210 pS from low to high center frequencies, whereas it is roughly constant at 260 pS in inner hair cells. One would expect that similar specialization might be present for all of the elements of the transduction complex. However, there should also be great conservation across species and hair cell type. The seemingly disparate behavior across species should have a similar molecular basis, with subtle changes within the proteins to account for the differences.

Molecular Components of Adaptation

Determining the molecular components of hair bundles is notoriously difficult. With very little protein available, researchers have to resort to painstaking techniques in an attempt to analyze the contents of the hair bundle (Gillespie & Hudspeth, 1989; Peng *et. al.*, 2009). Even with this limitation, the electrical and mechanical data have allowed researchers to make theories as to what components need to be present for transduction adaptation. By modeling these data, constraints can be placed on certain parameters involved with these components. The following is a discussion of the progress that has been made on determining the molecular components of adaptation.

Slow Adaptation Mechanism:

Strictly from the positive motion of the bundle during slow adaptation, Martin and Hudspeth (1987) speculated that a myosin motor might be involved with slow adaptation. Gillespie, Wagner &

Hudspeth (1993) discovered that myo 1β, also known as myosin-1C, was expressed in hair bundles. Adaptation was found to be inhibited in the presence of phosphate analogs which inhibit the ATPase activity of myosin motors (Yamoah & Gillespie, 1996; Wu, Ricci, & Fettiplace, 1999). Immunogold electron microscopy showed that antibodies to myosin-1C displayed their highest concentration at both ends of tip links (Garcia *et. al.*, 1998). Evidence was mounting that myosin-1C is involved in adaptation, however a straight knockout of myosin-1C was lethal. A more subtle approach, which involves structural knowledge of myosin-1C, was needed to determine if myosin-1C was indeed responsible for adaptation.

X-ray crystallography was used to solve the structure of the head domain for a myosin fragment (Rayment *et. al.*, 1993). The structure of myosin-1C can be determined in various configurations using cryo-EM and image analysis (Batters *et. al.*,2004). Myosin-1C consists of a single head and tail region. Contained within the head region is the ATP binding pocket. Myosin-1C binds tightly to actin in the absence of ATP as well as when ADP is bound to the binding pocket. When ATP binds, the head region releases from the actin core and the tail region prepares for the power stroke. After ATP is hydrolyzed into ADP and P_i, the head domain binds tightly to the actin core and the tail undergoes a power stroke when P_i is ejected from the ATP binding pocket. The head domain remains tightly bound to the actin core until the ADP is released from the binding pocket and ATP binds, starting the cycle over again.

Knowledge of myosin-1C's structure was used with great effect to test its function in hair cells (Holt *et. al.*, 2002). A single amino acid mutation of myosin-1C in the ADP binding domain was made in which tyrosine-61 was changed to glycine (Y61G). The introduced mutation in myosin-1C increases the affinity of the ATP binding pocket only to a special form of ADP, N^6(2-methylbutyl) ADP (NMB-ADP). Originally, the Y61G version of myosin-1C was expressed in hair cells using a transgenic approach. NMB-ADP introduced through a patch pipette takes minutes to diffuse up the stereocilia from the patch pipette. This creates a very elegant experiment in which the control and experimental condition can be accessed in the same cell. The introduction of NMB-ADP to Y61G transgenic mice produced a severe reduction in slow adaptation. This provided strong evidence that myosin-1C was involved, and perhaps solely responsible for slow adaptation.

Myosin-1C moves towards the barbed end of actin, located at the tips of stereocilia. The basic model incorporating myosin-1C into the transduction apparatus puts it in series with the gating spring, tip link and transduction channels (Assad & Corey, 1992). Each tip link is thought to have dozens to hundreds of myosin-1C molecules attached to it (Gillespie, Wagner, & Hudspeth, 1993). It is unclear how this collection of motors is connected to each other or attached to the tip link, but this implies that they work collectively to maintain tension on a single tip link. At any given instant, some of the myosins are tightly bound to actin while others are unbound preparing for their next power stroke. This complex is constantly climbing up the actin core which acts to apply tension in the tip link. The tip link tension correspondingly moves the hair bundle in the negative direction. When the tension in the tip links is too high, then the myosin motors can no longer climb and a dynamic equilibrium is reached. During a positive deflection, the gating spring is stretched and the increased tension causes the myosin motors to slip down the actin. The slipping of the myosin motors reduces overall tension in the bundle which allows for the slow positive motion associated with slow adaptation. For negative deflections, tension is

reduced in the gating spring and the myosin motor can climb back up the actin to restore tension to resting levels. Under this model a large enough negative deflection should provide slack in the tip link and create a period of zero force in the gating spring directly following the deflection. This explains why adaptation doesn't occur quickly in response to a large enough negative displacement (Shepherd & Corey, 1994). There simply is not enough tension in the tip link to open transduction channels, even as the myosin motors climb.

The binding of myosin-1C to actin has been studied *in vitro* using an optical trap (Batters *et. al.*, 2004). The researchers found that the power stroke occurred in two phases with a displacement of 3.1 nm and 1.1 nm (4.2 nm total motion) in low calcium. The data are consistent with the idea that the tail of myosin-1C must undergo an additional motion following the power stroke in order to release ADP and allow the ATP binding pocket to bind ATP. Strain, produced by the tip link *in vivo*, can reverse the power stroke and cause the motors to have less affinity for actin, essentially causing myosin-1C to slip down actin. This study found that increased calcium had the following effects: it increased the net power stroke size to 7.2 nm, increased the rate at which myosin-1C detached from actin, and increased the rate for back detachment. Taken as a whole, this means that the adaptation motors would slip faster as tension is applied to them as well as climb faster in the absence of tension, explaining how calcium can increase the rate of adaptation to both positive and negative deflections.

Fast Adaptation Mechanism:

Myosin-1C may be well suited to explain slow adaptation but fast adaptation appears to be a separate process from slow adaptation. Also, it seems difficult to see how myosin-1C could respond in the sub-millisecond time scale, which is required for fast adaptation. The phosphate analogue, vandate, inhibits myosin function (Wu, Ricci, & Fettiplace, 1999). Vandate was shown to double the slow adaptation time constant while maintaining the fast adaptation time constant. In addition, the presence of NMB-ADP delivered to hair cells of Y61G transgenic mice inhibited slow adaptation without a major effect on the rate of fast adaptation (Holt *et. al.*, 2002). These results indicated that myosin-1C is not likely to be responsible for fast adaptation.

Any mechanism responsible for fast adaptation would have to be sensitive to calcium, as well as work in a sub-millisecond time scale. Many groups came to the conclusion that the fast adaptation mechanism needs to be in very close proximity to the transduction channel, but different groups have speculated different mechanisms as to the action that calcium takes to cause fast adaptation. The general theory is that calcium will enter through the transduction channel and bind to a calcium binding site associated with the channel. The presence of calcium acts to close the channel in some manner. Three separate mechanisms were hypothesized to describe the manner in which calcium closes the transduction channel. It could act to weaken the gating spring, thus requiring more force to open the channel (Bozovic & Hudspeth, 2003). Alternatively, it could activate a release mechanism, essentially decreasing the stretch on the gating spring, which would then decrease the force applied to the channel causing it to close (Gillespie & Corey, 1997). Finally, calcium could bias the transduction channel towards the closed configuration, requiring more force to cause it to open (Howard & Hudspeth, 1988; Wu, Ricci, & Fettiplace, 1999). All three of these ideas were tested with a model and data obtained by

deflecting bullfrog saccular bundles utilizing a laser tweezers setup (Cheung & Corey, 2006). Of the three alternatives tested, the data and model support the third idea, and that a calcium-bound channel requires an additional 3 pN of force to open.

The original paper involving the Y61G mutant of myosin-1C involved a transgenic expression of the mutated form of the protein (Holt *et. al.*, 2002). This means that the hair bundle had both native and mutated copies of myosin-1C present. Therefore, the adaptation response was a composite response stemming from both forms of myosin-1C. It was thought that the mutant forms would tightly bind to actin and thus tightly bind the entire motor complex of a whole tip link. To ensure that this truly was the case, a knock-in version of the Y61G mouse line was made (Stauffer *et. al.*, 2005). This mouse only contained myosin-1C with a mutated ATP binding pocket. Introduction of NMB-ADP through the patch pipette in these hair cells disrupted both fast and slow adaptation rates. This result shed doubt on the idea that fast adaptation stems from a mechanism other than myosin-1C. The disruption of native myosin-1C behavior could also have had a secondary disruption on the function of an additional mechanism responsible for fast adaptation. Alternatively, fast adaptation could be associated with a movement of the myosin motor not typically associated with climbing and slipping along actin.

Tinevez, Jülicher, & Martin (2007) theorized that the climbing and slipping motion of myosin-1C could adequately explain both fast and slow adaptation. In simple terms, the seemingly different nature between the two processes arises because of the sigmoidal open probability versus displacement curve. The current adapts faster when the slope of this curve is steeper. Small deflections, which tend to be dominated by fast adaptation, would inherently operate along the steepest part of the curve. On the other hand, large deflections push the hair bundle into the less steep part of the I-X curve, therefore adaptation takes longer to drive the current back towards the baseline level. This theory can explain a lot about fast adaptation, but it is also very difficult to design a test that distinguishes it from alternatives. Leading some support to this theory, Stauffer and Holt (2007) display fast adaptation in outer hair cells even to supersaturating deflections, which does not agree with the model that calcium binds to the channel to promote channel reclosure.

Extent of Adaptation Mechanism:

The incompleteness of adaptation has been well characterized and is a very robust phenomenon. Even so, no strong theory has been presented as to the molecular mechanism involved. Typically, the incompleteness of adaptation is modeled by declaring that some portion of the deflection is not connected to the adaptation motor (Shepherd & Corey, 1994). One could imagine any number of ideas as to how this is accomplished at the level of the tip link.

The extent of adaptation is dependent on calcium concentration. Low calcium tends to reduce the completeness of adaptation whereas high calcium makes adaptation more complete (Assad, Hacohen, & Corey, 1989; Crawford, Evans, & Fettiplace, 1990). Outer hair cells from rats show very complete adaptation to small deflections but rather incomplete adaptation to larger deflections (Ricci *et. al.*, 2005; Kennedy *et. al.*, 2006; Stauffer & Holt, 2007; Johnson *et. al.*, 2011). These results indicate that the extent of adaptation is more complicated than the hair bundle simply containing an absolute

position sensor. Any theory that attempts to explain the molecular origin of incomplete adaptation would also have to incorporate calcium dependence into the mechanism.

Integrating Transduction Apparatus Knowledge

Understanding adaptation in all of its forms is a truly difficult task. Not enough is known about the components involved, yet there is a strong foundation as to how the components need to behave. When a hair bundle is deflected, the shearing force affects all of the elements in series with the tip link. The interconnectedness of elements means that any incremental gain in knowledge about one element comes with the added benefit of providing more knowledge about the other elements in series. The remainder of this review will describe how each element in this chain affects adaptation, as well as what future discoveries are needed to further our understanding of adaptation.

Transduction Channel:

The identity of the hair cell transduction channel has been quite elusive (Corey *et. al.*, 2004; Cheung *et. al.*, 2006). The best candidates came from the superfamily of TRP (transient receptor potential) channels (see Christensen & Corey, 2007 for review). The transduction channel is a non-selective cation channel with a large Ca^{2+} permeability (Corey & Hudspeth, 1979a; Ricci & Fettiplace, 1998). The pore of the channel is rather large, with the channel even being permeable to the fluorescent dye FM1-43 (Gale *et. al.*, 2001; Meyers *et. al.*, 2003). The single channel conductance is also rather large, in the 100-300 pS range, and varies along the cochlear length in turtle hair cells (Ricci, Crawford, Fettiplace, 2003) and mammalian outer hair cells (Beurg *et. al.*, 2006). The variation in single channel conductance not only affects the intracellular voltage, but also the amount of calcium influx, which affects adaptation.

If calcium does indeed bind to the transduction channel to promote channel reclosure during fast adaptation, then the channel is likely to include a calcium binding domain, or perhaps several. When the transduction channel is identified, calcium binding domains in the structure would support a model for fast adaptation in which calcium binds directly to the channel to promote closure. Of course, calcium might instead bind to a beta subunit of the channel encoded by a different gene.

Originally, a transduction channel was thought to be at the upper and lower end of the tip link, with myosin motors being only at the upper end (Denk *et. al.*, 1995). This configuration allows calcium to pass through the upper channel and directly interact with the myosin motors, in addition to the channels. More recent data has suggested that two transduction channels are present only at the lower insertion point of a tip link, and that myosin motors are present only at the upper insertion point (Beurg *et. al.*, 2009). This configuration is perplexing, in that myosin motors in one stereocilium will be under the calcium control of transduction channels that are higher up in the stereocilium and attached to a different tip link. This also means that any influx of calcium through transduction channels will have direct access to the transduction channels but will have a delayed effect on the myosin motors due to the necessary diffusion time. In addition, calcium takes time to diffuse and be pumped away from the

site of myosin motors (Beurg *et. al.*, 2008). This, in effect, means that rapid changes to the calcium influx through transduction channels will have an instantaneous effect on any mechanism that involves calcium binding to the transduction channel but will have a delayed effect on the regulation of myosin-1C. This delay of a few milliseconds can be exploited by changing the calcium driving force at the same time that the hair bundle is deflected. Such experiments will be difficult to perform, given the small time window, but they do provide a means of separating calcium's effect on either the transduction channel or myosin motors. This would greatly elucidate the mechanisms responsible for fast and slow adaptation.

Gate Swing:

The size and mechanism for the gate swing is a bit mysterious. The increase in compliance always corresponds with an increase in transduction current, which strongly links the compliance with the opening of transduction channels (Howard & Hudspeth, 1987). The conformational change associated with the channel going from a closed to open state would not be expected to be more than a few Ångstroms (Hille, 1992; Hudspeth *et. al.*, 2000). However, some estimates of the gate swing range as high as 10 nm (Tinevez, Jülicher, Martin, 2007). Even lower estimates of the gate swing place it in excess of 2 nm (Cheung & Corey, 2006), which might still be too large to be caused by a conformational change of the transduction channel. Either the estimates of the gate swing are inaccurate, or the conformational change of the channel gate moves an additional lever arm (Hudspeth *et. al.*, 2000). This lever arm could either be another protein attached to the transduction channel or be a specialized end of the channel.

Tip Link:

The tip link is perhaps one of the best characterized elements of the transduction complex. It is visible in carefully prepared electron micrographs (Pickles, Comis, Osborne, 1984; Kachar *et. al.*, 2000) and transduction ceases when the tip link is cut by lowering the external free calcium below a few micromolar (Assad, Shepherd, & Corey, 1991). Recently, the identity of the tip link was determined (Siemens *et al.*, 2004; Söllner *et. al.*, 2004; Ahmed *et al.*, 2006; Kazmierczak *et al.*, 2007). Protocadherin-15 makes up the lower portion of the tip link which connects to cadherin-23 on the end with the taller stereocilium. cadherin-23 is roughly 130 nm and protocadherin-15 is 50 nm long (Kazmierczak *et al.*, 2007). The partial crystal structure of cadherin-23 has been determined and examined using molecular dynamic simulations (Sotomayor *et. al.*, 2010). From these simulations, the stiffness of cadherin-23 was determined to be roughly 2 orders of magnitude larger than expected for the gating spring. Therefore, cadherin-23 most likely does not stretch considerably during a deflection of the hair bundle. The structure of protocadherin-15 has not yet been determined and so it is difficult to determine its physical properties. It remains to be discovered how cadherin-23 and protocadherin-15 interact with each other. It is still unknown how cadherin-23 binds to myosin motors at the upper insertion point as well as how Protocadherin-15 attaches to the transduction channels (or gating lever arm) at the lower insertion point. Determining the properties of the tip link will determine how much of the shearing force stretches the tip link. The remaining stretch will have to be incorporated by the other transduction elements. In addition, specific mutations in the tip link could be made to determine other transduction

parameters. The stiffness of the tip link could be selectively changed, noting the effect that this has on transduction. In its native form, the tip link breaks without the stabilizing presence of calcium. A tip link that does not require calcium maintenance could be engineered so that adaptation could be studied in the absence of external calcium.

Gating Spring:

Currently, the gating spring is a necessary concept provided by electrophysiological results. The transduction current responds very rapidly to deflections implying that transduction channels must be directly mechanically gated (Corey & Hudspeth, 1979b). The gating spring element provides force as it stretches. The stiffness of individual gating springs have been estimated as 620 μN/m (Martin *et. al.*, 2000), 780 μN/m (Cheung & Corey, 2006) and 1100 μN/m (Tinevez, Jülicher, & Martin, 2007). One would expect that the gating spring would be formed by a molecular element that resembles a spring. *In silico* examination of ankyrin repeats shows that they have properties similar to those expected from the gating spring model (Sotomayor, Corey, & Schulten, 2005). Ankyrin repeats also have the attractive property that the number of repeats can be varied depending on the hair cell type. This would allow various species and types of hair cells to customize their gating spring stiffness to fit the particular function of the cell. The precise stiffness value can be inferred from electrophysiology, but is still difficult to determine exactly because of the complex interaction of the gating elements in series. Determining how the stiffness of the gating spring varies from cell to cell is crucial in understanding how the stretch created by shearing is transmitted to the transduction channels, as well as to the adaptation motor.

The relative position of the gating spring is also important. Each tip link most likely connects to two transduction channels (Beurg *et. al.*, 2009). The most likely theory is that each channel has its own gating spring associated with it. An alternative theory is that each tip link has a gating spring which somehow transmits its force to both transduction channels. These two alternatives have consequences for the cooperativity between the two channels. In the first scenario, the gate swing of a single channel would not affect the force on its neighboring channel, but it would affect the force that the myosin motors feel. In the latter scenario, the gate swing of one channel would essentially give more tension to its neighboring channel. This would create positive cooperativity between the two channels on a tip link. For the configuration in which each transduction channel contains its own gating spring, it is also important to know if the gating spring connects with the lever arm of the gate swing or connects on the intracellular side of the channel. This difference would affect the properties of the gate swing.

Linking Proteins and Additional Proteins:

Researchers can theorize as to which elements must be present in order for transduction and adaptation to occur. Even so, there are certainly additional proteins involved whose function isn't well understood. Other proteins might be needed to link the transduction components together. An example of this is the mechanism used to bundle myosin-1C proteins together. A collection of motors must be held together as well as attached to the cadherin-23 end of the tip link. Electron dense regions show up in electron microscopy of tip links at the lower and upper insertion points termed the lower tip

link density (LTLD) and upper tip link density (UTLD), respectively (Kachar *et. al.*, 2000). It is unclear exactly what role these densities play. Recently, harmonin, a protein that binds to actin, was found to be present at the UTLD (Grillet *et. al.*, 2009; Michalski *et. al.*, 2009). Disrupted function of harmonin, by either a missense mutation in the gene (Grillet *et. al.*, 2009), or deletion of the most prevalent isoform, harmonin-b (Michalski *et. al.*, 2009), created no noticeable morphological defect. However, the UTLDs were no longer present in these hair cells, the rate of adaptation slowed slightly, the extent of adaptation was slightly diminished, and the I-X curve broadened slightly. This implies a very subtle effect on the myosin-1C motors. This only goes to highlight how many proteins are involved in adaptation, and their effects can be difficult to properly explain. More work is needed on how exactly harmonin affects adaptation and what other proteins are involved in supporting roles.

Myosin-1C:

Myosin-1C is the only component of the transduction complex that has been strongly implicated in adaptation. Even so, there are still many aspects as to how it functions *in vivo* that need answering. The basic model as to how myosin-1C works is that it climbs up the actin core while tension in the tip link provides a counter force that makes it slip down actin (Assad & Corey, 1992). But it isn't known how many molecules of myosin-1C are bound to a single tip link. Estimates have varied from 130/tip-link (Gillespie, Wagner, & Hudspeth, 1993), to 200/tip-link (Walker & Hudspeth, 1995) to 400/tip link (Garcia *et. al.*, 1998). All of these estimates come with the caveat that they are likely extreme underestimates of the number of myosin motors per tip link. Even if the average number is determined precisely, each tip link could have a variation on the average, which would affect how adaptation behaves in that bundle. Also, calcium seems to reduce the strength of actin-myosin crossbridges while at the same time increasing the size of its power stroke (Batters *et. al.*, 2004). It is difficult to fully understand how changes in calcium and force would affect a group of myosin-1C molecules working together. The speed at which myosin-1C can respond to changes in force is also an interesting question that needs answering. Previously, it was speculated that myosin-1C could not respond fast enough to be responsible for fast adaptation (Wu, Ricci, & Fettiplace, 1999). This may be true for one molecule of myosin-1C, but a myosin-1C complex may be capable of responding much faster to changes in tension.

Additional knowledge about myosin-1C should prove very useful in understanding all aspects of adaptation in hair cells. Having a proper understanding of how it behaves will allow researchers to determine what components of the transduction current and bundle motion stem from myosin-1C. Other mechanisms can then be incorporated to explain what myosin-1C cannot explain.

Conclusion

Understanding adaptation in hair cells requires integrating knowledge from a variety of sources. Physiological experiments provide insight into the molecular components that must be involved in the transduction apparatus. The molecular identity of these components, as well as specifics about how they function, allow for a better understanding of experimental data. All of this knowledge must be

incorporated into a model that is sufficiently sophisticated to simulate a functional hair cell. Such a model needs to independently calculate the forces along the transduction apparatus, calculate the forces and motion of the stereocilia, stochastically determine the open state of transduction channels, and track the calcium concentration within the hair cell. Combining all of these factors provides for the most realistic simulation of a hair cell, which creates increased knowledge of adaptation.

Chapter 2

Quantitative Model Design

Introduction

Stereocilia of hair cells are extremely complex biological components. All stereocilia share many common features. They have a gradation in height with a deflection towards the tallest stereocilia eliciting an excitatory response in the form of an inward current. This is accomplished by a relative shear amongst the tips of the stereocilia. Adjacent stereocilia are connected by a variety of links; most important amongst these are the tip links which only connect the tips along an excitatory column of stereocilia. Tip links relay this extension to an element that produces force from extension termed the gating spring (Pickles, Comis, & Osborne, 1984). Each gating spring provides force which gates a transmembrane protein called the transduction channel (Corey & Hudspeth, 1983b). The transduction channel is currently not identified but is a relatively non-selective cation channel that provides the means for which the excitatory current enters the cell (Corey & Hudspeth, 1979a; Ricci & Fettiplace, 1998). . All hair cells display some form of adaptation that occurs after the stimulus. This adaptation generally has a fast and slow time constant which are both calcium dependent (Assad & Corey, 1992; Cheung & Corey, 2006). Myosin motors, and in particular Myosin-1C, have been strongly implicated as the responsible mechanism for slow adaptation. Calcium binding directly to the transduction channel is generally thought to cause fast adaptation.

This chain of mechanical elements necessitates a good quantitative model to properly understand its behavior. Early models utilized a lumped element approach to understand how hair cell mechanotransduction works (Assad & Corey, 1992). Under this approach, the hair bundle is composed of rootlet springs and responds to a deflection under the influence of the viscous drag. Shearing from the stereocilia is directly translated into a stretch of elements along the tip link axis. The gating spring is a spring element that responds to the stretch by producing force. As the open probability of the transduction channel increases, this also decreases the amount of stretch on the gating spring element. Finally, a motor element acts to restore the system to its resting position, incompletely.

This type of model does a good job of explaining transduction. However, it doesn't quite explain all of the results that researchers observe, especially as additional animal models become more commonplace. Different species and organ types have hair bundles that have strikingly different morphologies. They also produce different rates and extent of adaptation, as well as differences in the mechanical response of the hair bundle. With increased computing power throughout the years, models have become more complicated. Most models have moved to a finite-element approach, in which each individual stereocilium is modeled individually (Nam & Fettiplace, 2008; Nam, Cotton, Grant, 2007; Kozlov *et. al.*, 2011). These mechanical models allow for the hair bundle to be deflected as a whole but the calcium concentration simply increases to a discrete value once transduction channels open. Other models examine how calcium diffuses within the cell but do not allow calcium to have a direct feedback on the adaptation response (Lumpkin & Hudspeth, 1998; Beurg *et. al.*. 2010).

Recent findings have suggested that transduction channels exist only at the lower end of the tip link while myosin motors are present at the upper end of the tip link (Beurg *et. al.*. 2009). This result alone produces a very complicated scenario for how adaptation can occur. Calcium has a direct effect

on how adaptation occurs which in turn limits the amount of adaptation into the stereocilia. They are intimately linked. For this reason, a model in which the hair bundle can move under a stimulus probe and produce internal calcium diffusion was produced. The goal of this model is to explain even the subtle aspects of transduction and adaptation as well as make experimental predictions to test these theories. This chapter describes how the model is designed to accomplish these goals.

General Model Design

The model attempts to simulate a hair bundle during stimulation. In principle, the model should reproduce experimental results. Primarily, the majority of experiments that study single hair cells consist of deflecting the hair bundle and measuring the transduction current as well as the position of the bundle. In addition, because of calcium's important role in adaptation, experiments look at the calcium concentration inside of the hair cell during stimulation. At its core, this model simply allows the hair bundle to be deflected while the position, current, and calcium concentration are calculated. However, this model also tracks and controls the details of this process. The motion of elements in the transduction apparatus can be carefully examined, or even manipulated to determine the overall effect.

The model uses a Monte Carlo approach to simulate the hair bundle. The change of status for each element is calculated for a very small time step after the appropriate forces have acted on it. The time differential must be very small to ensure that the calculation is accurate. An appropriate value for the time step is determined by running the simulation for a small length of time with an extremely small time step. As the time step is increased, then the output of the model changes as the error in the calculation increases. Acceptable values for the time step are those in which the error only deviates by less than 1% from the asymptote of the best possible value.

The model is designed in three separate main parts. The first section calculates the movement of the stereocilia to a mechanical deflection. It also tracks the movement of the adaptation motors as well as stochastically determines the conformation of the transduction channels, which determines the transduction current. The second part looks at the calcium diffusion in the hair bundle and hair cell body. This part also allows for diffusion of calcium buffers as well as uncaging of calcium via calcium cages. The third component displays the concentration of calcium or selected buffers in the hair cell. The display can show the concentration for their proper position or in confocal mode, which convolves the display to determine how a real confocal image would look after the point spread function of the confocal microscope, is considered. Each part can be run independently and has its own time step. For example, the transduction channels and bundle position can be held in a certain state while calcium is allowed to diffuse. Alternatively, the bundle can be deflected while the internal calcium concentration is held constant.

Mechanical Model Design

Hair Bundle Structure

Each hair bundle is made up of several individual stereocilium that are held in close contact to one another by connecting links. The stereocilia are composed primarily of actin which creates a rigid structure. Each stereocilium has a cylindrical shape that is thickest at the top of the stereocilium and decreases in diameter near the insertion point in the apical surface of the hair cell body. This portion of a stereocilium is known as the rootlet. The stereocilia grow in height along an excitatory column but have roughly the same height perpendicular to this axis, along a shared row.

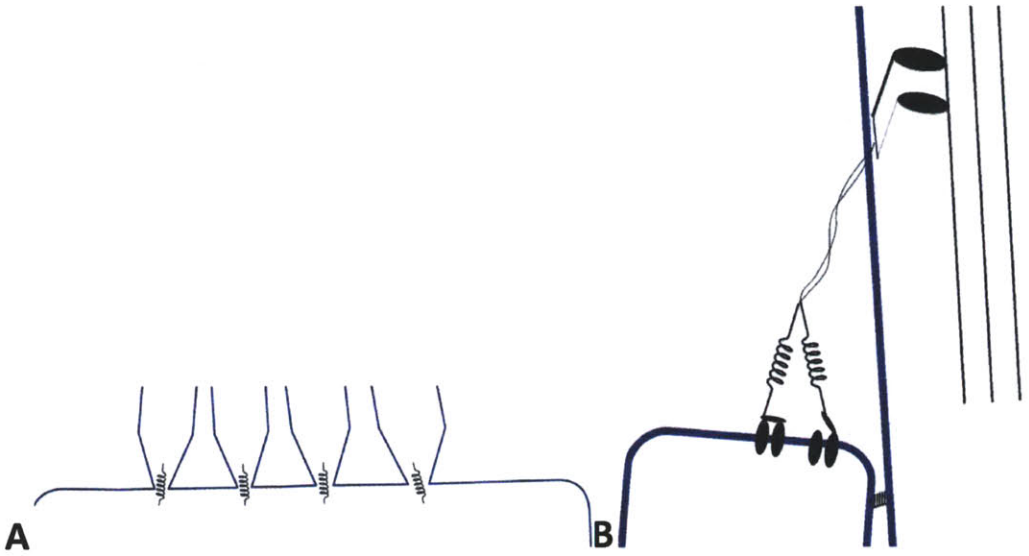

Figure 1: Components of the mechanical model. (**A**) Diagram of the rootlet portion of the stereocilia. The stereocilia spacing, diameter, and taper shape are all user-defined parameters. In addition, rootlet springs act to provide a torsion force. (**B**) Diagram of the transduction apparatus used in the standard configuration. Horizontal top connectors maintain close contact between adjacent stereocilia. Myosin motors produce force at the upper insertion point. The tip link connects adjacent stereocilia and is infinitely stiff. The gating springs are attached directly to the transduction channels and produce force when extended. The transduction channels gate stochastically as a function of the force provided from the attached gating spring.

In the model, each stereocilium is viewed as a rigid line segment of variable length. The sterocilia pivot at their insertion points on a flat apical surface of the hair cell body. The thickness of each stereocilium is factored so that when two stereocilia become too close to one another, a small repulsive force keeps them from overlapping. The number of stereocilia in each row and column, as

well as the height of stereocilia in each row, can be varied to reflect the different kinds of hair bundle geometries. The overall spacing of the stereocilia is also determined by setting the spacing of the insertion points along both dimensions. Generally, the stereocilia along a row are spaced at the maximum diameter of the stereocilia. This simplification ensures that the stereocilium are all touching along a row in a neutral position and therefore only deflect along an excitatory column, which reduces the overall computational time. The overall layout of the stereocilia is shown in figure 1 for reference.

Connecting Links and Forces

Each stereocilium is originally positioned with no angular deflection. The stereocilia have intrinsic forces exerted on them by linking proteins. Rootlet springs acts to keep the stereocilia with no deflection. When a stereocilium is deflected, then the rootlet stiffness increases the force that opposes this deflection. Column top links maintain close proximity of stereocilia along a single column. Typically, this stiffness is kept quite high so that each stereocilium maintains close contact with the taller stereocilium adjacent to it. This has been shown to be the case from physiological results (Karavitaki, & Corey, 2010). Row top links act to minimize the relative position difference between adjacent stereocilia of the same row. Finally, the tip of a stereocilium connects with its tallest neighbor via a tip link. The tip link is connected in the transduction chain and therefore affects channel gating, which will be discussed shortly. However, the tip link also acts to reduce the shear between the connected stereocilia by producing a negative force that acts at the tip of the stereocilia.

In general, there are two potential sources that can act on a hair bundle: intrinsic and external. The intrinsic forces are caused by the links and are mostly linear with displacement, except for the tip link which depends on the state of transduction elements. The main external force is delivered by an external stimulus. Experimenters generally deflect hair bundles in a couple of ways: with a small glass probe of a known stiffness, a pipette that blows a fluid jet across the bundle, or by attaching a refractive sphere to the hair bundle that is controlled by a laser tweezers setup. The external stimulus is modeled either as a force stimulus or as a probe deflection where the stiffness of the probe is an independent variable. For either case, the external force is distributed amongst the stereocilia of the tallest row. For the probe case, the probe is moved to a displacement a certain distance from the tallest stereocilia. The force of the probe is determined by multiplying the net displacement of the probe obtained from the average position of the tallest stereocilia by the stiffness of the stimulus probe. This means that the probe force changes as the hair bundle moves. The force, or position of the probe, can be changed as a step function, triangle wave, or sine wave of various frequency, duration, phase, and magnitude.

From the point of view of a hair bundle, viscous drag and Brownian motion are also considered external stimuli. Brownian motion causes small random disturbances of a hair bundle. To reduce the execution time of the model, Brownian motion is not simulated. The viscous drag is an important component that affects how far a stereocilium moves during a given time step. The force on each stereocilium is calculated for each time step. The force from the links and external stimulus do not inherently provide information on how far the stereocilium moves for a particular time step. The force provided by the drag force is a product of the drag coefficient and the velocity of a stereocilium, in discrete terms this is:

$$Fdrag = \beta * \frac{\Delta x}{\Delta t}$$

(eq. 1)

β is the drag coefficient, Δt is the time step and Δx is the deflection of the stereocilium for that time step. The system is at rest for the condition when all of the forces are balanced, that is when $F_{drag}=\Sigma F_{links}+F_{external}$. Therefore, the drag force for a single time step simply opposes the other forces acting on a stereocilium. The deflection of a stereocilium in a single time step is therefore:

$$\Delta x = Fdrag * \frac{\Delta t}{\beta}$$

(eq. 2)

This assumes that the time step is very small because the relative motion of the stereocilia creates a change in the forces involved. To ensure that the time step is small enough, the time step is reduced until the solution has less than a 1% error.

Transduction Complex Setup

Probably the most complicated section of the hair bundle is the region that is directly responsible for transduction, termed the transduction complex. This region spans from one stereocilium to its neighbor along a column. The attachment to the smaller stereocilium is called the lower insertion point and the connection to the side of the taller stereocilium is called the upper insertion point. Although there is some evidence that the adaptation motor is concentrated at both insertion points (Garcia *et. al.*, 1998), it is most likely not in a functional form at the lower insertion point. In the model, myosin motors are only located at the upper insertion point. The most recent evidence suggests that two transduction channels are present only at the lower insertion point (Beurg *et. al.*, 2009). However, the model also allows three configurations for the transduction channels: two channels at the lower insertion point, two channels at the upper insertion point, or one channel at each insertion point. Each channel has a gating spring and gate swing that is directly associated with the channel, regardless of the configuration. Finally, the tip link is modeled as an infinitely stiff line segment that has a user defined length. This is a good estimation because steered molecular dynamic simulations have shown that the tip link is roughly 100 times stiffer than the stiffness of the gating spring (Sotomayor *et. al.*, 2010).

Adaptation Motors

The actual motion of the myosin-1C adaptation motors is quite complex. Each myosin motor moves through an ATP dependent power stroke (Batters *et. al.*, 2004). The myosin motor can also be bound to the actin core with high or low affinity depending on its state in the power stroke cycle. In addition, multiple myosin motors are thought to be bound together at a single upper insertion point. These considerations make it extremely difficult to accurately model myosin motor behavior at the level

of single proteins. An entire myosin-1C complex is modeled as producing a constant force that climbs up the actin towards the tip of the stereocilium. A myosin drag factor represents the interactions that the myosin has with the actin core, which slows both the rate at which the myosin motor falls and climbs on the actin core.

The myosin motors are constantly reacting to the force produced in the gating complex by the gating springs. The myosin force is constantly directed up and parallel to the attached stereocilium. The force from the gating springs pulls the myosin complex in roughly the opposite direction but at a small angle to the direction of the stereocilium. Because of this, only the component of force along the stereocilium axis pulls the myosin complex in the negative direction. The force from the gating springs is essentially the product of the stretch across the gating springs and the gating spring stiffness. If the channels are closed, the stretch is the distance from the upper insertion point to the lower insertion point minus the length of the tip link, which does not contribute to the overall stiffness. When a transduction channel opens, the stretch across that particular gating spring is reduced by the gate swing of the transduction channel. If the two transduction channels are both at the same end of the tip link, then the forces from the two gating springs add because they are in parallel. If a channel is at both ends of the tip link, then the inverse of the forces add together. The net force acting on a myosin motor complex is calculated for each time step. The motion of a complex during each time step is calculated by balancing the myosin motor drag force, in a similar manner to the technique used to determine the motion of a stereocilium to force.

The force produced by the myosin motor complex also changes throughout time. Calcium has a well characterized effect of increasing the speed of adaptation (Cheung & Corey, 2006). For a positive deflection, this could be interpreted as reducing the drag coefficient of the myosin motors on the actin core. In addition, increased calcium reduces the resting current of a hair bundle, this has the implication that calcium reduces the overall force that the myosin motors are capable of producing. In the model, the calcium concentration near the position of the upper insertion point is used to reduce the myosin motor force and myosin drag coefficient according to the equation:

$$Post\ Calcium\ Value = \frac{Pre\ Calcium\ Value}{1 + [Ca^{+2}]calcium_{slope}} \qquad \text{(eq. 3)}$$

This general formula is used for both the motor force and drag coefficient. The calcium concentration used is the internal calcium concentration immediately adjacent to the myosin motor complex for that particular stereocilium. $Calcium_{slope}$ is set for both the motor drag and force terms separately to allow for unique modification for each of the two terms.

Transduction Channel

Each channel can be controlled in a deterministic manner, so that the fraction of the current entering through the channel is determined by a user defined equation. Alternatively, the state of the channel can be determined stochastically, which is the typical mode of operation. In the stochastic

mode, each transduction channel can exist in either the closed state or an open state. The rate at which the channel transitions from its current state to the opposite state is determined by a rate equation that changes based on the force exerted by the attached gating spring (Nam & Fettiplace, 2008). The rate equations are:

$$R_{C\to O} = \Delta t * K_F \exp\left(\frac{\mu dF}{kT}\right)$$

(eq. 4)

and

$$R_{O\to C} = \Delta t * K_R \exp\left(\frac{-1 * (1-\mu) dF}{kT}\right)$$

(eq. 5)

$R_{C\to O}$ is the rate that the channel transitions from the closed state to the open state and $R_{O\to C}$ is the rate at which the channel transitions from the open state to the closed state. K_F and K_R are the forward and reverse rate constants, respectively. F is the force applied to the channel by the gating spring. D is the gate swing, μ is a constant that biases the equation towards the open or closed configuration, and kT is the product of Boltzmann's constant and temperature in Kelvin. When the rate is multiplied by the time step of the model, then the result is the probability that a transition occurs during that time step. This number is compared with a random number generated between 0 and 1. If the random number is less than the probability of a state transition, then the state of the channel is changed.

The transduction channel is treated as a conductance element when determining the overall current flow through the channel. The channel has a conductance value defined in the model. The single channel current is simply the product of the holding potential and the single channel conductance of the channel. The overall current in the hair bundle is therefore the product of the single channel current and the number of channels in the open configuration. The fraction of the current carried by calcium depends on the external concentration of calcium as well as the holding potential and is determined by the following equation:

$$Fraction_{Calcium} = \frac{Calcium_{gain} * [Ca^{+2}]_{ext} * \exp\left(\frac{-V}{25}\right)}{V}$$

(eq. 6)

$Calcium_{gain}$ is an empirically derived constant in mV/μM that adjusts the slope of the relationship (Beurg *et. al.*, 2010). V is the voltage of the hair cell. $Fraction_{Calcium}$ gives the fraction of current carried by calcium and is always limited between 0 and 1.

The whole cell transduction current varies from cell to cell quite strongly during physiological experiments. It should be expected that hair bundles are slightly damaged during the dissection process. After all, hair bundles are extremely sensitive to mechanical stimuli, and dissection would be viewed as a rather large mechanical stimulus. To represent this, a certain percentage of the tip links can

be randomly destroyed before a simulation begins. For each tip link, a random number between 0 and 1 is called. If the number is higher than the desired fraction of healthy tip links, then the tension on that tip link is permanently set to 0. This technique leaves the transduction channels present without any tension on them, so that they can occasionally create a current, albeit with an extremely low probability.

Fast adaptation has been theorized to be caused by calcium binding to the transduction channel directly. Each transduction channel has 4 calcium binding locations (Nam & Fettiplace, 2008). Each bound calcium ion decreases the force applied to the transduction channel by a user defined amount. This essentially requires more force to open the transduction channel. The calcium binding affinity can also be defined for the calcium binding locations on the channel.

Calcium Diffusion Model Design

Calcium plays a very important role in transduction adaptation. It acts to increase the rate of fast and slow adaptation. The direct mechanisms responsible for the effect on adaptation remain difficult to fully understand. It is thought that calcium acts directly on the myosin adaptation motors as well as the transduction channels. The calcium concentration within the hair cell changes as calcium diffuses, binds to buffers, and is pumped out by calcium pumps. Therefore, it is very difficult to obtain a simple estimate of the calcium concentration near the adaptation motors or transduction channels. The calcium diffusion section of the model seeks to accurately determine the calcium concentration within the hair cell. This section can be used in conjunction with the mechanical model to obtain more realistic hair bundle behavior.

Voxels and Compartments

With the exception of calcium uncaging, the intracellular calcium sources are the transduction channels. If the channels are associated with the upper insertion point, then the transduction channel position is determined by the mechanical model as the myosin motors climb and slip. If the channels are on the lower insertion point, then the position of the channels is determined by a variable that sets the lower insertion point distance from the edge of the stereocilium. Each stereocilium then consists of a diffusible volume and a calcium source in the form of the transduction channels, the angle of the stereocilium is not important to determine how calcium diffuses.

The overall dimensions of the stereocilia are set by the mechanical model section of the model. For each stereocilium, the maximum height and the diameter at any position above the hair cell body is already defined. Near the top of a stereocilium, the volume is broken up into small voxels whose width is defined depending on the desired resolution. A maximum number of voxels is created to fill up the diameter of the stereocilium at a particular height. A separate time step is used for the voxel diffusion than the mechanical model. Based on the single channel current, channel open state, and calcium

fraction of current, the rate of calcium influx is used to add additional calcium to the voxel closest to the position of the transduction channel for every diffusion time step.

Ideally, one would like to have extremely small voxels in order to accurately represent the calcium concentration within the stereocilia. However, decreasing the voxel length by half implies that the number of voxels needs to be increased by a factor of eight. In addition, the diffusion time step must be decreased in order to ensure accurate results. This makes increasing the resolution take increasingly long to execute a simulation. If the calcium comes from the transduction channel, then the calcium diffuses in a hemispherical manner down the stereocilium. After a few hundred nanometers, the calcium diffusion more closely resembles one dimensional diffusion. This effect can be utilized by creating cylindrical compartments further down in the stereocilia. Each stereocilium is therefore represented by a combination of voxels in the top region, where resolution is most important, and cylindrical compartments further down to increase the speed of the calculations. The cylindrical compartments have a separate time step for diffusion. This arrangement is displayed in figure 2.

The hair cell body can be represented as a large diffusible volume with calcium sources at the apical surface. The location of the stereocilia insertion points is determined by variables that set the relative x and y positions of the hair bundle with respect to the hair cell body. The hair cell body is represented in a similar manner as the stereocilia. The diameter of the hair cell body is kept constant throughout its depth. The apical portion is composed of voxels with their own size and time step. Below that, the remainder of the hair cell body is represented by cylindrical compartments that also have their own dimension and time step.

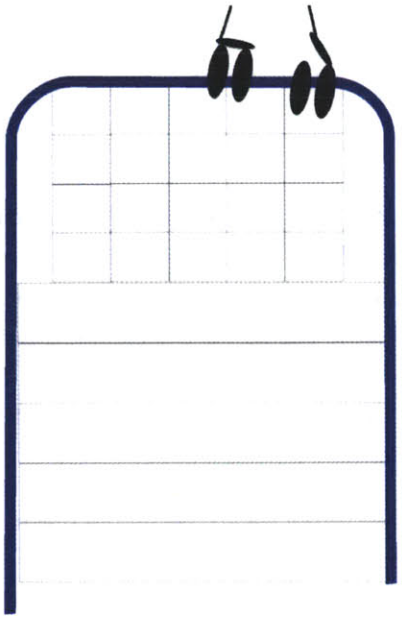

Figure 2: Diagram demonstrating the variable compartment size approach for diffusion. Voxels with a user-defined width are utilized in the apical section of the stereocilia. Below a user-defined transition point, diffusion is calculated using cylindrical compartments that are the diameter of the stereocilia.

Internal Diffusible Contents of the Cell

The hair cell contains a range of intracellular molecules. This model is only concerned with calcium and molecules that interact with calcium. Experiments done using whole cell patch clamp, typically contain at least one diffusible calcium chelator. Calcium chelators bind to calcium with a known affinity. The bound and unbound forms of a chelator diffuse as if they are two separate molecules. Therefore, each voxel or compartment within the hair cell contains the concentration of both forms of any calcium chelator used during a simulation. The model allows for several kinds of calcium chelators. EGTA or BAPTA are typically added to patch pipettes to maintain low internal calcium, the concentration of either one of these compounds can be uniformly added throughout the volume of the hair cell, in the unbound form. A variety of calcium indicator dyes can also be added, which produce florescence in the bound form. Finally, calcium cages can be added to the hair cell. Calcium cages have high affinities for calcium prior to an irreversible chemical change following the interaction with a photon, which reduces their affinity for calcium. Adding calcium cage to the hair cell essentially adds two additional diffusible species: the pre and post photo-exposed versions of the cage. To reduce the execution time of the model, the diffusion code only executes if the diffusible molecule is actually present within the hair cell.

Calcium binds or unbinds to a molecule based on its affinity for the molecule. The affinity for the model is defined in terms of its dissociation constant,k_d, given in μM and its on-rate,k_{on}, given in $\frac{1}{\mu M - \mu sec}$. The off rate, k_{off}, is simply the product of the on rate and dissociation constant (Lumpkin & Hudspeth, 1998). The rate, $R_{calcium\ bound}$, at which calcium binds to a buffer is:

$$R_{calcium\,bound} = k_{on} * [Ca^{+2}] * [buffer]_{free} - k_{off} * [buffer]_{bound} \quad \text{(eq. 7)}$$

Determining the change in bound calcium buffer is just a matter of multiplying by the diffusion time step.

Diffusion

Diffusion is most accurately represented as a second order partial differential equation. For small time steps, this can be approximated as a simple difference equation. A diffusion coefficient is defined for each diffusible molecule in terms of $\frac{nm^2}{\mu sec}$. This coefficient is multiplied by the surface area of diffusion and divided by the volume and distance of diffusion to yield a diffusion constant. This constant is simply multiplied by the concentration difference between adjacent regions to yield the diffusion rate per unit time (Lumpkin & Hudspeth, 1998). The net effect is that two adjacent volumes tend to reach the same concentration as time progresses. This equation is calculated at every time step for every pair of adjacent volumes, whether they are voxels or cylindrical compartments. The diffusion coefficient changes for each diffusible compound, but is the same for the bound and unbound forms of the molecule.

Diffusion at the interface between voxels and cylindrical compartments requires additional computations. Diffusion is calculated over the largest surface area shared between the two regions. For the interface between the voxels and highest cylindrical compartment in a stereocilium, this requires combining several voxels together. The average calcium concentration is used across the voxels to determine the amount of diffusion across the interface. This technique is accurate if there is little concentration variance across the voxels, which is typically the case at the interface, where the diffusion starts to be approximated as a one-dimensional case. Diffusion across the interface only occurs according to the larger of the two time steps for the interface.

Intrinsic Calcium Stores and Calcium Pumps

In addition to calcium being chelated by diffusible molecules, free calcium is reduced by molecules that remain fixed in the hair cell. In the stereocilia, a fixed calcium buffer has been theorized to accurately account for results obtained using calcium indicator dyes. The identity of the fixed buffer is not known. In addition, mitochondria, located within the hair cell body, act as a calcium chelator. Calcium influx into the mitochondria occurs from the calcium uniporter and is extruded from the cell by a sodium calcium exchanger. The system of equations describing the calcium balance is as follows (Beurg *et. al.*, 2010):

$$Mitochondria\ Influx = \frac{k_m}{\gamma_m} * (J_{uni} - J_{NCX})$$

(eq. 8)

where

$$J_{mit,uni} = v_{max,uni} * \frac{[Ca^{+2}]_{free}{}^2}{k_{uni}{}^2 + [Ca^{+2}]_{free}{}^2}$$

(eq. 9)

and

$$J_{NCX} = \frac{v_{max,NCX}}{1 + \frac{K_{NCX}}{[Ca^{+2}]_{mitochondria}}}$$

(eq. 10)

J_{uni} is the uniporter current and J_{NCX} is the sodium calcium exchanger current. K_m is the free to fixed mitochondrial ratio and γ_m is the mitochondrial volume ratio. V_{max} is the maximum transport rate and k is the half activation point for the respective transporters. The mitochondria are maintained within a region defined within the center of the hair cell body. Calcium within this volume is subject to the additional chelation from the mitochondria.

Calcium pumps are present in the cell membrane. They act to keep the internal calcium low. The pumps change the calcium concentration along the cell membrane according to the following rate (Lumpkin & Hudspeth, 1998):

$$R_{calcium\ concentration} = \frac{-1 * pump\ density * SA * v_{max}}{N_A * volume * \left(1 + \frac{K_M}{[Ca^{+2}]_{free}}\right)}$$

(eq. 11)

N_A is Avogadro's number. K_M is Michaeli's constant for a calcium pump. Pump density is the density of calcium pumps in that region. SA is the surface for the pumps in that region. Volume is the volume of the voxel or cylinder. There is some speculation that the density of the pump is higher near the transduction channels. In the model, the density can be set for the upper region of the stereocilia as well as a separate density for lower in the stereocilia. This division is independent of the boundary setup by the voxels and cylindrical compartment interface. For voxels, the pumps are only present on the voxel surface that is touching the outside of the stereocilium. The surface area used for the cylindrical compartments is the surface area that coincides with the diameter of the stereocilium.

Calcium Uncaging

Calcium uncaging is a unique tool that allows calcium to be released quickly in the hair cell. In an experiment, the calcium cage diffuses into the hair cell via a patch electrode. For the model, the calcium cage can be uniformly distributed throughout the hair cell. To fill the cage quickly, the internal calcium concentration can also be increased uniformly at the start of a simulation. A large percentage of the free calcium will bind to the high affinity calcium cage.

The calcium cage changes configuration by being exposed to photons of the appropriate wavelength. The photons can come from any sort of light source but this model assumes that they come from a pulsed UV laser. Each pulse occurs faster than the duration of a single time step, but many pulses occur within a small span of time. The power of the laser, pulse repetition rate, and number of pulses per burst are all variables. In addition, the number of bursts and bursts repetition rate can all be controlled.

The excitation laser is focused so that the beam forms a diffraction limited spot near the hair bundle. This means that the beam waist reaches a diameter that is limited by the wavelength of the laser and the numerical aperture of the objective lens. The intensity of the beam weakens away from the focus of the uncaging laser as such:

$$R_{excitation} = \frac{\lambda}{NA} + NA * abs(z_{off})$$

(eq. 12)

and

$$I_{fraction} = \frac{S}{\pi * R_{excitation}{}^2}$$

(eq. 13)

$R_{excitation}$ is the excitation radius for the laser. NA is the numerical aperture for the objective lens. Z_{off} is the distance in the z dimension that the pixel is from the focus of the laser. S is the surface area and λ is the wavelength of the uncaging laser. The interaction between the laser and the hair cell is extremely complicated. Each stereocilium is at an angle that intersects the laser. In addition, the laser will excite voxel regions and cylindrical compartments. Finally, the calcium cages change configuration with an exponential time constant following interacting with photons (Ellis-Davies, 2008). After some complicated trigonometry, the model calculates the number of photons absorbed for a single pulse in every voxel and compartment. The cages in those regions change configuration with an exponential time course, even if the hair bundle moves during that time. Up to three uncaging pulses can independently affect calcium cage molecules in this manner. The absorbed photons affect both the calcium bound and unbound versions of the cage molecules. The conformational change essentially changes the cage into a different diffusible molecular that behaves in the same manner as the other diffusible calcium chelators.

Display Design

Interpreting the combined results of the calcium diffusion model and the mechanical model can be difficult. It is easier to see how the calcium changes throughout the hair bundle as the hair bundle moves. In addition, it is useful to have a representation of the calcium-induced-fluorescence that is similar to what one would see from a confocal microscope. The model can produce images to display how the hair bundle looks from a side profile as well as from the top, by producing cross-sections through the bundle. The resolution of these cross-sections can either be increased or blurred, to mimic confocal images.

Cross-Section Images

A nice feature of the model is that the concentration of several diffusible molecules is tracked. Typically, one would like to know the calcium concentration in the hair cell during a simulation but occasionally one might also like to get insight from one of the calcium buffers. Any of the diffusible molecules can be used to create an image of the hair cell. This allows the user to further understand why the calcium concentration varies as it does during a stimulus.

To create a cross-section of the hair bundle, the appropriate plane must be chosen. For the side profile, an x position is chosen that defines which voxels are used to create an image in the y-z plane. This includes data created from voxels and cylindrical compartments in both the stereocilia and hair cell body. Similarly, a z position is chosen which defines the position of the x-y plane. This plane can either be located in the stereocilia or hair cell body. If the plane is in the stereocilia, then the image could be

formed by a combination of voxels and cylindrical compartments. To create an image for display, all of the data is converted to pixels of the same size.

For the calcium diffusion portion of the model, it is advantageous to use voxels and cylindrical compartments that are not too small in order to decrease the overall computation time. However, these small compartments also create an image that appears pixilated. To correct this problem, an algorithm was implemented to create an image that uses pixels smaller than those used for the diffusion portion of the model. The basic principle used to get the concentrations for the smaller pixels is to use a weighted average of the surrounding voxels. Voxels that are closest to the center of the pixel of interest are weighted more than those further away. In this manner, pixels of uniform size are created that will accurately represent the hair cell. Often, much larger voxels are used for the hair cell body than in the stereocilia. This creates a small amount of spatial aliasing in the hair cell body. Also, the stereocilia is at an angle that is mapped onto an image made up of pixels that form a grid. Occasionally, a pixel is missed in this representation which creates a dark pixel in the image. These problems don't unduly take away from the information that the image is presenting, and are therefore tolerated.

Like most portions of the model, a separate time step is defined for how often images are created. These images capture the state of the hair bundle or hair cell at various times throughout the simulation. The images can be combined and turned into a movie which shows the motion of the hair bundle along with the concentration of the desired diffusible molecule. This is a very useful tool in understanding how the calcium concentration throughout the hair bundle influences the motion of the hair bundle.

Confocal Imaging Mode

Obtaining cross section images of the hair bundle is a useful tool for displaying the actual concentration of calcium or calcium buffers throughout a simulation. However, a precise display of this sort is not possible during an actual experiment. In reality, one is limited by the optics of the imaging microscope. A typical approach to examining the calcium concentration within the hair cell is to use a calcium indicator dye in conjunction with a laser scanning confocal microscope. A confocal microscope uses a laser that scans the sample to selectively excite regions of the fluorescent dye. A pinhole prior to the microscope photon multiplier tubes blocks light from out of regions that are out of plane with the focus of the confocal laser. This allows a confocal microscope to provide cross-sections in the z-plane of the specimen.

A true confocal microscope scans the specimen with a laser in a line scan pattern. For the model, this process is ignored and multiple image planes are produced at intervals determined by the time step for the confocal imaging mode. This produces x-y cross sections throughout the hair cell similar to the process used for the cross-section imaging mode. The difference for the confocal mode comes from how the images are produced. Even with the technology of a confocal microscope, the resolution of the sample is still limited by the wave nature of light. Each fluorescent molecule produces a three-dimensional blur of light rather than a precise point of light. The density of the light produced from any given fluorescent source is known as the point spread function. The overall point spread

function depends on the numerical aperture of the objective lens as well as the wavelength of light. A true point spread function is determined by the airy function which produces concentric rings of light in the x-y plane and a very complex interference pattern in the z plane. This was simplified in the model to only include the central intensity of the point spread function. In the x-y plane, the intensity of the light falls off from the maximum based on the square of distance from the focus of the laser. To model this, a two-dimensional filter array was created of the following form:

$$Filter\ Value(r) = Filter\ Constant * \exp\left(\frac{-5.2r^2}{\lambda^2 NA^2}\right)$$

(eq. 14)

Here a filter constant sets the maximum of the pixel intensity and is dependent on factors such as the strength of the confocal laser and yield of the photon detector. R is the distance from the focus of the laser, or in the case of the model, the pixel of interest. NA is the numerical aperture of the microscope and λ is the wavelength of the excitatory laser. The filter is only created for the effective radius of the laser central intensity which is defined for the model as $Filter\ Radius = \frac{0.7\lambda}{NA}$. In the z dimension, the effective distance is twice this value. Also in the z dimension, the filter constant is reduced in the following manner:

$$Reduced\ Filter\ Constant(z) = Original\ Filter\ Constant * \exp\left(\frac{-5.2z^2}{4\lambda^2 NA^2}\right)$$

(eq. 15)

Z refers to the height from the pixel of interest and the reduced filter constant is used to create a filter in planes above and below the pixel of interest. By combining these two equations, the effect of the point spread function can be estimated in 3 dimensions away from a fluorescent point source.

For each confocal plane, the appropriate filter is convolved with the bound calcium indicator concentration in the x-y plane. Filters are also convolved in planes above and below the confocal plane of interest. The sum of this filtering creates the actual intensity of the pixels in the confocal plane. In this manner, each pixel is blurred with the surrounding fluorescence which is essentially what occurs during confocal microscopy. This allows the user of the model to predict what the confocal image will look like during a calcium indicator dye experiment, which is the best way to visualize the calcium concentration within the hair cell. The calcium indicator dye can be used to produce the fluorescent image as well as calcium or any one of the calcium buffers. This is not possible during an actual experiment but can be useful in demonstrating how one might see them under a confocal microscope if they could fluoresce. A comparison of calcium images obtained from a model bullfrog saccular hair bundle in normal and confocal mode is displayed in figure 3.

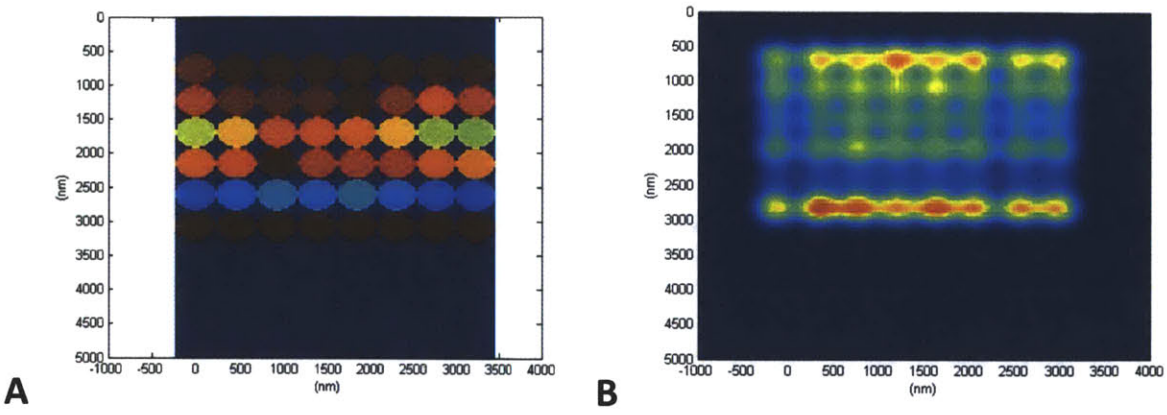

Figure 3: Comparing normal display mode with confocal display mode. Red indicates increased calcium concentration and blue indicates less calcium concentration. (**A**) Cross section image of the calcium concentration obtained in a model bullfrog saccular hair bundle at a height of 700 nm displayed in normal display mode. (**B**) The same cross section as in A, but displayed in confocal display mode.

Overall Model Use

The model is essentially capable of performing any operation that an experimenter can do for a real experiment. The added benefit of a computational model is that each component can be monitored during the simulation. This allows for a better understanding of how the hair cell responds to stimulation. The model can be used to verify physiological results, but the primary purpose of the model is to better understand what is happening within the hair bundle during an experiment and to use this knowledge to design unique and useful experiments. Simulating the complex interactions between the mechanical aspects of the bundle and calcium feedback allows for a better understanding of hair cell mechanotransduction that cannot be obtained with a simple model.

Chapter 3

Calcium Diffusion in Hair Cells

Introduction

Calcium has a ubiquitously important role in regulating processes across biology. Calcium has a well known regulatory function in hair cells. In the hair cell body, calcium influx through voltage activated $Ca_v1.3$ channels acts at the ribbon synapse to initiate vesicle release (Fuchs, Evans, & Murrow, 1990; Brandt, Striessnig, & Moser, 2003). Therefore, the calcium concentration near the basal surface of the hair cell must be tightly regulated. In the hair bundle, calcium acts to mediate the rate of fast and slow adaptation. The calcium concentration in the endolymph, the solution bathing the apical surface of hair cells in the mammalian cochlea, is kept exceptionally low, around 20 micro-molar (Bosher & Warren, 1978). Additional supporting cells could potentially increase the calcium concentration in the vicinity of cochlear hair cells but it still does not reach levels above 1 mM that are often used during physiological experiments. With the importance of calcium for regulating hair cell processes including adaptation, a careful examination of the intracellular calcium concentration is imperative.

With the prevalence of calcium indicator dyes, calcium can be exploited as a visual indicator of transduction current flow. Recent data measuring the fluorescence increase of a calcium indicator dye have demonstrated that transduction channels are present only at the lower insertion point of tip links (Beurg *et. al.*, 2009). This is contradictory to evidence from earlier work which placed transduction channels at both ends of the tip link (Denk *et. al.*, 1995). This result also has the very important implication that myosin motors are regulated by transduction channels attached to a neighboring tip link.

This chapter examines calcium diffusion in detail, to obtain a thorough understanding of how the calcium concentration changes near important elements of the transduction apparatus. In addition, the evidence used to determine the location of the transduction channel will be carefully examined, as well as its implications.

Basic Principles of Diffusion

Diffusion is a thoroughly studied phenomenon. It can best be described by Fick's second law:

$$\frac{\partial \phi}{\partial t} = D\nabla^2\phi$$

ϕ is the concentration of the substance, t is time, and D is the diffusion coefficient for the substance. For the discrete case of the model, diffusion can be represented as a difference equation. In this case, diffusion is a measure of flux across compartment interfaces so that:

$$\Delta\phi = \frac{DA\Delta t}{Vl}$$

A is the surface area between neighboring compartments, V is the volume of each compartment, and l is the path length of diffusion between compartments. This equation can be calculated for each surface of a compartment during a given time step to compute the overall change in calcium concentration for that particular compartment (Lumpkin & Hudspeth, 1998). This solution is valid assuming that the net diffusion for each time step is a small fraction of the overall concentration within a compartment. This can be assured by decreasing the value for Δt until the diffusion percentage is smaller than one percent of the total volume.

Much of the diffusion within stereocilia can be approximated as occurring along one dimension. The increase in area from the diameter of the stereocilia simply acts to slow diffusion down as it travels from the transduction channel towards the hair cell body. This is even more the case when the diameter of stereocilia decreases, such as in outer hair cells. Therefore, a good approximation of diffusion can be estimated by the one-dimensional solution in which the calcium concentration is held constant at the top of the stereocilium and calcium is allowed to diffuse in one direction. For this scenario, the diffusion length can be estimated as $2\sqrt{Dt}$, where the diffusion length is the distance away from the source that the concentration is approximately the source value after a time of t. This can be used to estimate how quickly the calcium concentration has changed away from the transduction channel, which acts as the calcium source in this case. This indicates that the calcium concentration roughly depends on the square of the distance of diffusion. This makes diffusion have a rapid change on calcium concentration near to the calcium source but a weaker role over larger distances.

The hair cell stereocilia are full of actin molecules (DeRosier, Tilney, & Egelman,1980) as well as many other proteins. For this reason, the stereocilia contain obstructions that reduce the ability of calcium to diffuse within the cell. The exact percentage of diffusible volume is rather difficult to obtain. For the case of the stereocilia, diffusible obstructions are represented as reducing the diffusion coefficient by a factor of two (Beurg *et. al.*, 2010).

Diffusion near the Transduction Channel

The calcium concentration near the transduction channel is of great importance for determining how calcium might affect a fast adaptation mechanism attached to the transduction channel. Ideally, one would like to model calcium as it moves through the pore of the channel, interacting with the pore and other cations. This idea is impractical as it would take too long to model and the identity of the transduction channel is not known. For this model, the transduction channel acts as a calcium source that increases the calcium in the nearest voxel. The rate at which calcium enters the voxel is determined by the external calcium concentration, holding potential, and the single channel conductance. The fraction of the current carried by calcium depends on the holding potential and external calcium concentration (Beurg *et. al.*, 2010). Because of the negative holding potential, the inward calcium current should be much larger than any potential outward calcium current, even as the calcium concentration increases inside of the cell.

Defining exactly what "close to the transduction channel" implies is an interesting matter. The purpose of examining the calcium concentration near the transduction channel is to understand how much calcium is present to interact with the transduction channel. 5 nm voxels were used to represent a small enough distance that calcium can quickly interact with the transduction channel. It should be pointed out that a 5 nm wide voxel is very small. If one could somehow squeeze together calcium ions so that they are touching at their minimum diameter, you could only fit about 15,000 calcium ions into this volume. This is only about $3 * 10^{-20}$ moles of calcium ions. A single calcium ion increases the molarity of a voxel by 13 mM which is an extremely high intracellular calcium concentration. The calcium concentration for such a small volume should be viewed as the average calcium concentration as calcium ions move in and out of the voxel.

Figure 1 displays the calcium concentration near the transduction channel in typical experimental conditions. The calcium concentration rises to over 100 μM in 50 ns in the voxel closest to the transduction channel. Even up to 50 nm away, the calcium concentration rises quickly and then follows an exponential increase as time progresses. Panel B of figure 1 displays how the calcium rises as time progresses. There is a visible pattern that the calcium concentration distribution creates that is easiest to see when plotted in this manner. The calcium concentration rises with the peak concentration always occurring close to the channel and dropping off further away from the channel. As time progresses, the volume that contains calcium becomes much larger. Therefore, it begins to take much longer to increase the calcium concentration in the voxel closest to the transduction channel. Diffusion takes longer to fill a larger volume, which makes intuitive sense.

As calcium enters through the transduction channel, it immediately has a large volume to fill through diffusion but there are also molecules waiting to interact with it. Intrinsic fixed buffers and diffusible buffers added through a patch pipette can quickly bind to calcium. There are also calcium extrusion pumps on the cell membrane. However, these are too weak to have a strong effect over very short time scales. How do the buffers change the calcium concentration near the transduction channel? Figure 2 compares the calcium concentration for various buffer conditions. The on/off rates in $(\mu M\text{-}\mu sec)^{-1}$ and μsec^{-1} used for the buffers are 1e-5/1e-4 for the fixed buffer, 1.5e-6/0.3e-6 for EGTA, and 5e-4/3.5e-5 for calcium green (Ricci, Wu, & Fettiplace, 1998; Beurg *et. al.*, 2010). None of the buffers really slow the rapid influx of calcium in the initial microseconds after the channel is opened. The fixed buffer decreases the peak of the calcium concentration. It has a decent on rate but an even higher off rate. EGTA is the weakest of the buffers added. It has a tenfold slower on rate than the fixed buffer. The addition of EGTA has very little impact on the calcium concentration. Calcium green-1 was chosen because it has a very high on rate and a weak off rate. It should therefore quickly and strongly bind to free calcium. This buffer has the greatest effect on decreasing the free calcium concentration. Overall, the calcium distribution across several voxels doesn't change much for the various buffer conditions, it just takes longer for the change to occur in the presence of high affinity buffer. It should be noted that BAPTA, which is often used instead of EGTA inside of a patch pipette, has an on rate similar to calcium green-1. This shows how the choice in calcium buffer can affect the kinetics of calcium increase near the transduction channel, this should influence the choice of buffer used during an experiment.

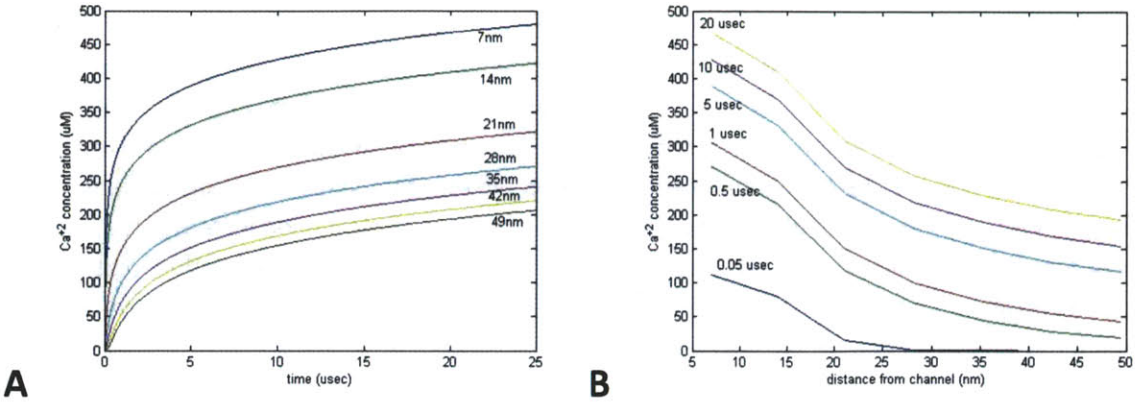

Figure 1: (**A**) Calcium concentration versus time recorded in 5 nm voxels. Two transduction channels are placed at the top of the stereocilium, 7.5 nm from the positive end (towards the tallest stereocilia) of the stereocilium. The displayed voxels are diagonally adjacent, moving 1 voxel towards the base of the hair bundle and 1 voxel towards the negative end of the stereocilium. The distances from the transduction channel are displayed on the figure. V_{hold}=-80 mV, $[Ca^{+2}]_{ext}$=1.5 mM, $[\text{fixed buffer}]_{int}$=1 mM, $[EGTA]_{int}$=1 mM, calcium extrusion pumps turned on. (**B**) Same data plotted as calcium concentration versus distance from the transduction channel, with the time post transduction displayed on the figure.

Changing the external calcium concentration is a technique often used by experimenters to change the adaptation rate. One would assume that decreasing the amount of external calcium would have a linear decrease in the amount of calcium near the transduction channel. However, there could also be a complicated interaction with the calcium buffers that causes an additional decrease in the calcium concentration. Figure 3 reduces the external calcium concentration to 0.1 mM from 1.5 mM in figure 1. This is a 15 fold decrease in the external calcium concentration. The calcium concentration near the transduction channel decreases from 475 μM to 32.5 μM, which is around a 15 fold decline in the calcium concentration near the transduction channels. This demonstrates that the short term internal calcium concentration near the transduction channel changes roughly linearly with the change in external calcium concentration.

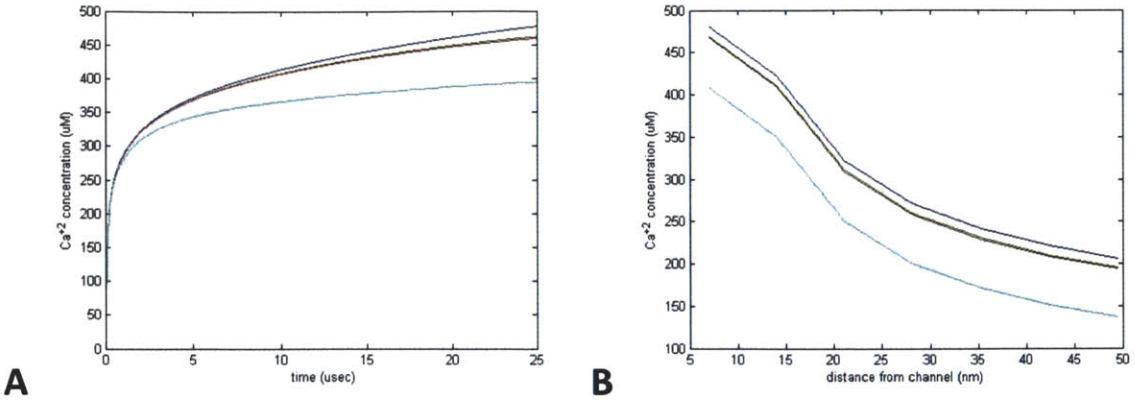

Figure 2: (**A**) Calcium concentration versus time recorded in 5 nm voxels measured at a voxel 7.5 nm below the transduction channel. The plots show the effects of increased buffering conditions. V_{hold}=-80 mV, $[Ca^{+2}]_{ext}$=1.5 mM for all traces. Blue: no fixed buffer or calcium extrusion pumps, green: [fixed buffer]$_{int}$=1 mM, calcium extrusion pumps turned on, red: [EGTA]$_{int}$=1 mM added to previous condition, cyan: [Calcium Green-1]$_{int}$=250 μM added to previous condition. (**B**) Same data plotted as calcium concentration versus distance from the transduction channel for 20 μsec post transduction.

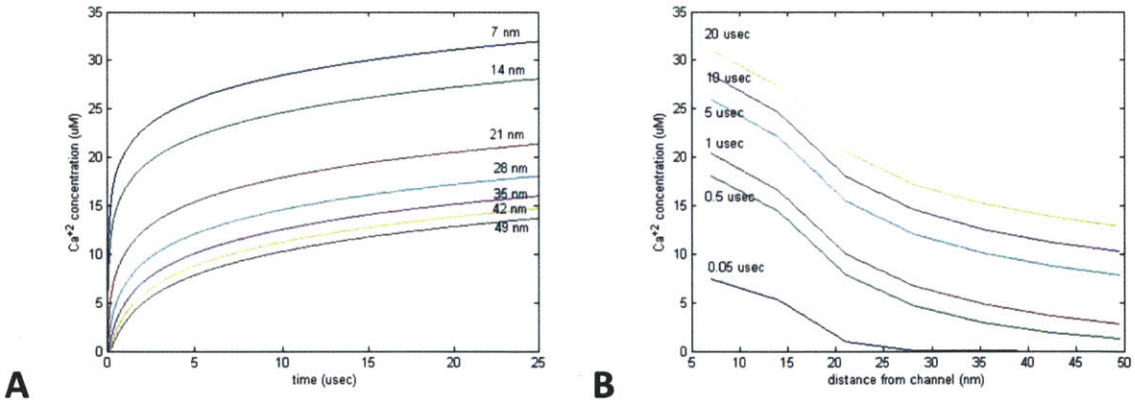

Figure 3: (**A**) Calcium concentration versus time recorded in 5 nm voxels. The distances from the transduction channel are displayed on the figure.V_{hold}=-80 mV, $[Ca^{+2}]_{ext}$=0.1 mM, [fixed buffer]$_{int}$=1 mM, EGTA]$_{int}$=1 mM, calcium extrusion pumps turned on. (**B**) Same data plotted as calcium concentration versus distance from the transduction channel, with the time post transduction displayed on the figure.

Diffusion to the Myosin Motors

Recent evidence suggests that transduction channels only exist at the lower insertion point and myosin motors are only at the upper insertion point (Beurg *et. al.*, 2009). This is a confusing result because lowering the external calcium concentration also reduces the slow adaptation time constant (Crawford, Evans, & Fettiplace, 1989, 1991). It would seem that this effect must be caused by a transduction channel that is almost a micron from the adaptation motors and connected to another tip link. In addition, there is speculation that fast adaptation is caused by the myosin-1C (Tinevez *et. al.*, 2007; Stauffer *et. al.*, 2005). The fast adaptation time constant also decreases with a decrease in external calcium. Therefore, it is important to know how the internal calcium concentration changes within the first few milliseconds of a stimulus down to the approximate location of the myosin motor complex.

Figure 4 uses 25 nm voxels to examine the calcium concentration down to 820 nm, which could be considered a typical distance from the lower insertion point of one tip link to the upper insertion point of the adjacent tip link, which share a common stereocilium. The pattern looks slightly different from figure 1. The calcium concentration initially rises very quickly and then rises slowly after the first few microseconds. Distances further away from the transduction channel take much longer to reach concentrations similar to that near the transduction channel. The voxel located 820 nm from the transduction channel reaches a calcium concentration of around 12 μM after 3 msec of the transduction channels being turned on.

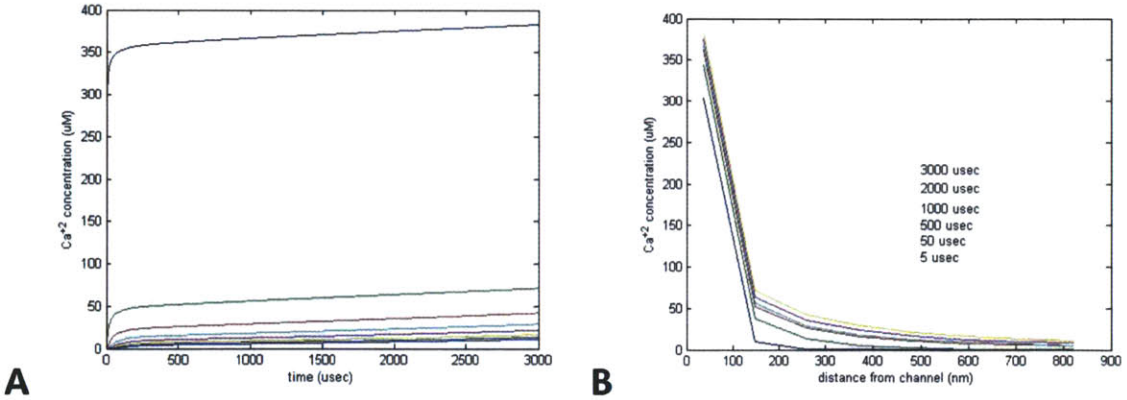

Figure 4: (**A**) Calcium concentration versus time recorded in 25 nm voxels. The displayed voxels move 4 voxels towards the base of the hair bundle and 2 voxels towards the negative end of the stereocilium. The distances from the transduction channel, going from the top plot down are: 37nm, 148nm, 260nm, 372nm, 484nm, 596nm, 708nm, and 820nm.V_{hold}=-80 mV, $[Ca^{+2}]_{ext}$=1.5 mM, $[\text{fixed buffer}]_{int}$=1 mM, $[EGTA]_{int}$=1 mM, calcium extrusion pumps turned on. (**B**) Same data plotted as calcium concentration versus distance from the transduction channel, with the time post transduction displayed on the figure.

A lot of the decline in calcium concentration over the distance to the adaptation motors may be caused by the presence of calcium buffers and calcium extrusion pumps. Figure 5 shows that adding buffers or calcium extrusion pumps reduces the calcium concentration that diffuses down to the adaptation motors. The calcium extrusion pumps even reduce the rate of the initial calcium peak. The calcium pumps remove free calcium from the cell so that it takes longer for the free calcium to reach the myosin motors. The reduction in calcium concentration when EGTA is added is different than the case in the vicinity of the channel. Over a larger distance, EGTA is more capable of binding calcium which reduces the overall amount of free calcium diffusing down the stereocilium, which effectively slows the rate of calcium diffusion. Adding 250 μM of Calcium Green-1 greatly reduces the rate at which calcium makes it down to the site of adaptation motors. Calcium Green-1 has a high affinity for calcium and therefore greatly impedes the free calcium. It is also a diffusible buffer, meaning that the bound form of the buffer will diffuse down the stereocilium while more unbound buffer diffuses up the stereocilium to take its place. The hair cell body acts as a vast reservoir of unbound buffer to diffuse up the stereocilia. Any high affinity buffer will act in this manner to continuously impede the downward flow of free calcium.

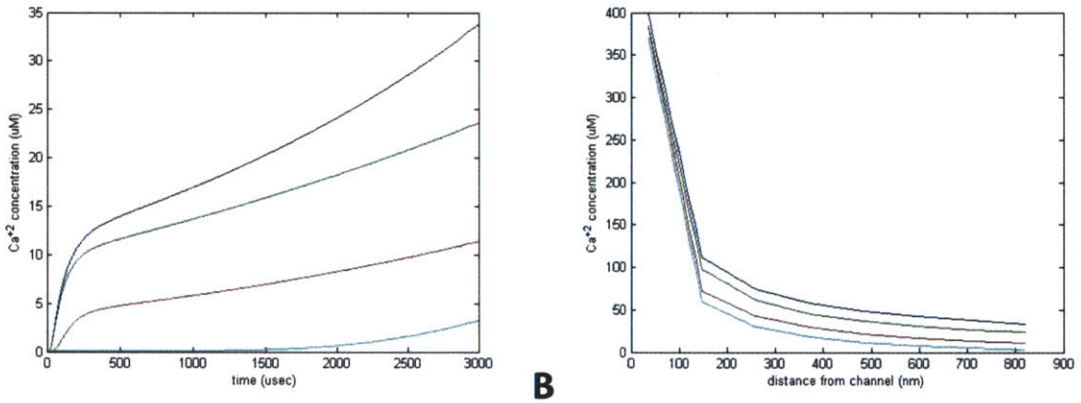

Figure 5: (**A**) Calcium concentration versus time recorded in 25 nm voxels measured at a voxel 800 nm from the transduction channel, to represent the location of the myosin motor. The plots show the effects of increased calcium buffering conditions. V_{hold}=-80 mV, $[Ca^{+2}]_{ext}$ =1.5 mM for all traces. Blue: $[\text{fixed buffer}]_{int}$=1 mM, green: $[EGTA]_{int}$=1 mM added to previous condition, red: calcium pumps turned on in addition to previous condition, cyan: $[\text{Calcium Green-1}]_{int}$=250 μM added to previous condition (**B**) Same data plotted as calcium concentration versus distance from the transduction channel for 3 msec after transduction is turned on.

Reducing the external calcium concentration increases the effect that the calcium buffers have on impeding calcium flow down the stereocilium. As figure 6 shows, reducing the external calcium concentration by 15 fold reduces the calcium concentration near the myosin motors by about 40 fold in the presence of fixed buffer, calcium extrusion pumps and EGTA. This non-unity decrease in calcium at the myosin motors is different than what is seen when examining the effect of decreasing the external calcium concentration near the transduction channels. The increased distance to the myosin motors gives calcium buffers more time to bind to the free calcium. This means that under normal

experimental conditions, changing the external calcium concentration should have a nonlinear effect on the calcium concentration near the myosin motors but a linear effect on the calcium concentration near the transduction channels. This is a very subtle effect, one that involves comparing time constants of adaptation, but still could be used to elucidate the location of fast adaptation.

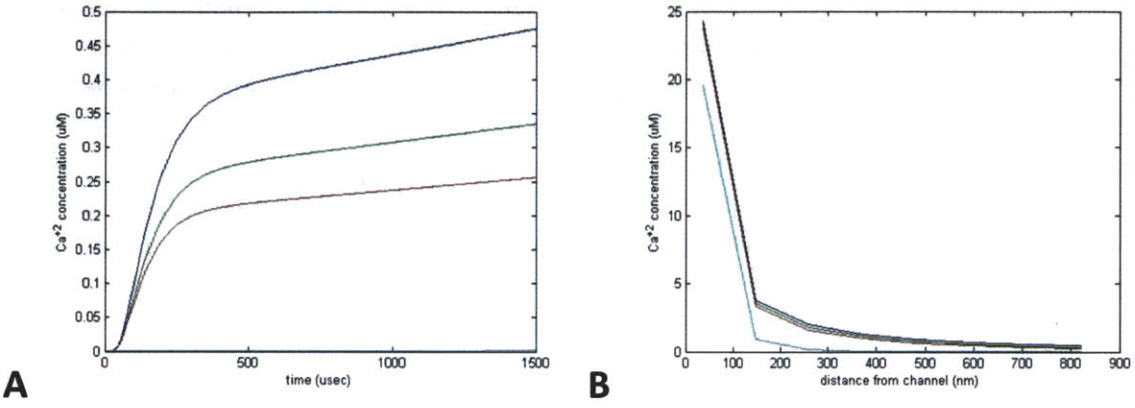

Figure 6: (**A**) Calcium concentration versus time recorded in 25 nm voxels measured at a voxel 800 nm from the transduction channel, to represent the location of the myosin motor. The plots show the effects of increased calcium buffering conditions. V_{hold}=-80 mV, $[Ca^{+2}]_{ext}$=0.1 mM for all traces. Blue: $[\text{fixed buffer}]_{int}$=1 mM, green: calcium pumps turned on in addition to previous condition,red: $[EGTA]_{int}$=1 mM added to previous condition, cyan: $[\text{Calcium Green-1}]_{int}$=250 μM added to previous condition (**B**) Same data plotted as calcium concentration versus distance from the transduction channel for 1.5 msec post transduction.

It is important to make sure that the results using 25 nm voxels are consistent with those produced using 5 nm voxels. Figure 7 compares the average calcium concentration of five voxels at 5 nm on an edge that are within the same space as a 25 nm voxel near the transduction channel. This shows that for both calcium conditions, the results are approximately consistent no matter what voxel size is used. There is some error, but there are actually 125 voxels with a 5 nm edge within a single 25 nm voxel. Therefore, using just 5 voxels produces a sample of the calcium concentration within the 25 nm voxel.

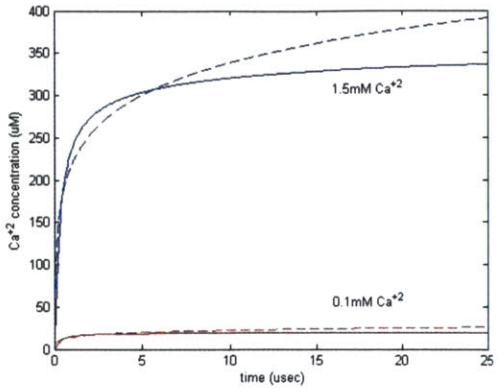

Figure 7: Calcium concentration versus time for $[Ca^{+2}]_{ext}$=1.5 mM (blue lines) and $[Ca^{+2}]_{ext}$=0.1 mM (red lines). Solid lines are values from a 25 nm voxel centered at the transduction channel and dashed lines are the average of five, 5 nm voxels that span the 25 nm voxel region diagonally. V_{hold}=-80 mV, $[\text{fixed buffer}]_{int}$=1 mM, $[\text{EGTA}]_{int}$=1 mM, calcium extrusion pumps turned on.

Diffusion with Deterministic Transduction Channels in Bullfrog Saccular Hair Cells

In a real hair cell, the transduction current will adapt within a matter of milliseconds which reduces the calcium influx through the transduction channel. Even so, the effects of the calcium pulse will still linger even after adaptation has reduced the current. Furthermore, adaptation is never complete and even the residual current after adaptation could cause a buildup in the internal calcium concentration. To model the calcium concentration over longer periods of time, a combination of voxels and cylindrical compartments were used. 125 nm voxels were used for the apical portion of the stereocilia volume. This ensures that calcium enters into a region that is not excessively large, which would tend to overestimate the calcium concentration. Cylindrical compartments with a depth of 200 nm were used below the voxels. Using cylindrical compartments greatly speeds up the computation time, allowing the simulations to take a more reasonable amount of time to execute. Modeling adaptation in a deterministic channel involves changing the fraction of current that enters through the channel as time progresses. This is equivalent to reducing the fraction of time that the channel is open. The transduction current opens with 100% current and then declines to its post adaptation value following a double exponential curve. The fast adaptation time constant for the model is 3 msec and the slow adaptation time constant is 15 msec.

Figure 8 examines the calcium concentration in a situation where the transduction channel remains on for the entire length of the simulation. This situation would not likely happen *in vivo* because of adaptation but it is still useful in understanding the maximum calcium concentration that

could occur in a hair cell. The calcium concentration climbs steadily throughout the stereocilium but then the rate of increase begins to decline. The main obstacle that slows the calcium buildup is the hair cell body. The hair cell body is a rather large volume when compared to the stereocilia. Calcium and bound buffer diffuse into this large volume which acts as a diffusion sink. In addition, the hair cell body acts as a large unbound calcium buffer source, allowing a large amount of unbound buffer to diffuse into the stereocilia. This effect prevents the calcium concentration in the stereocilia from becoming too large even without adaptation.

Figure 9 displays how a diffusible calcium buffer reduces the free calcium concentration further down the stereocilium. The transduction channel at the top of the displayed stereocilium adapted to 10 percent of the maximum current after 20 milliseconds. For the figure, the green trace still has fixed buffer and calcium extrusion pumps turned on and the blue trace has an additional 1 mM of EGTA in the intracellular solution. In the absence of EGTA, the free calcium begins to buildup after 100 msec, well after the transduction current had adapted. In the presence of EGTA, the free calcium concentration never significantly increased near the site of the adaptation motors. This shows how a diffusible buffer can continuously diffuse into the stereocilia and act to buffer the free calcium, especially if the calcium influx is reduced by adaptation. Panel B shows how EGTA slows the overall rate at which calcium fills up the volume of the stereocilium. The free calcium can't diffuse down towards the hair cell soma before EGTA buffers it.

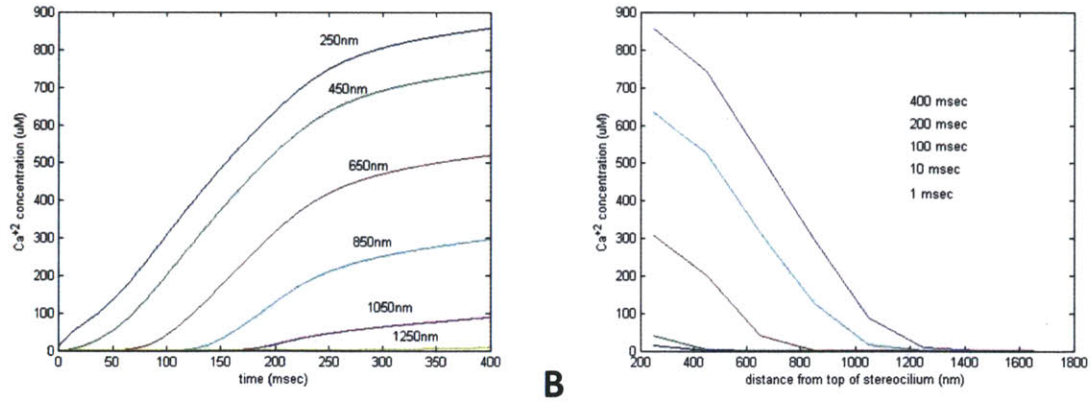

Figure 8: (**A**) Calcium concentration versus time recorded in 200nm deep cylinders. 125nm voxels were included for the top 125 nm to create proper calcium entry through the transduction channel. The transduction channel is open fully at t=0 and remains open throughout the simulation. The calcium concentrations are taken from cylindrical compartments centered at the distances shown on the plot. V_{hold}=-80 mV, $[Ca^{+2}]_{ext}$=1.5 mM, $[\text{fixed buffer}]_{int}$=1 mM, $[EGTA]_{int}$=1 mM, calcium extrusion pumps turned on. (**B**) Same data plotted as calcium concentration versus distance from the top of the stereocilium, with the times post transduction displayed on the figure.

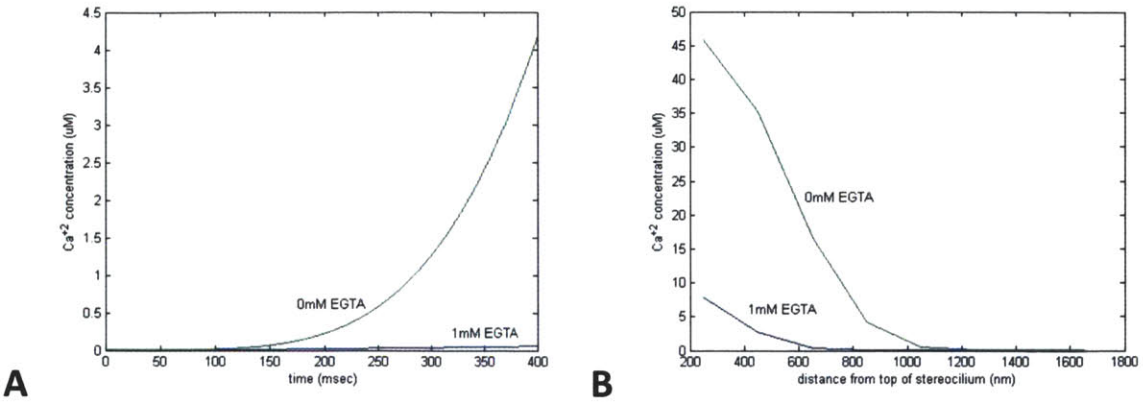

Figure 9: (**A**) Calcium concentration versus time recorded in 200nm deep cylinders measured 850 nm from the top of the stereocilium. The current source starts with the channel being open at 0 msec but decays exponentially to 10% of full current with two time constants of 3 msec and 15 msec. V_{hold}=-80 mV, $[Ca^{+2}]_{ext}$=1.5 mM, $[\text{fixed buffer}]_{int}$=1 mM, calcium extrusion pumps turned on. The blue trace has an addition of $[EGTA]_{int}$=1 mM. (**B**) Same data plotted as calcium concentration versus distance from the top of the stereocilium at 400 msec.

The weak buildup of free calcium becomes exaggerated in the presence of low calcium. Figure 10 examines the free calcium near the top of the stereocilium. In the case of 0.1 mM external calcium and 1 mM internal EGTA, there is very little increase in the free calcium concentration even at the top of the stereocilium. This raises a very interesting point. Calcium is known to affect slow adaptation, which occurs at the site of the myosin motors. However, in the presence of adaptation, the free calcium concentration does not rise significantly in the region near the adaptation motors. These results argue that not all of the channels are always at their resting current when no deflection is present. More likely, 10% of the total transduction current is the average of the entire population of transduction channels in a hair bundle. Some tip links have channels that have a higher open probability while others are lower. This would allow a change in external calcium concentration to have a significant effect on slow adaptation while still maintaining a low resting current. The manner in which transduction channels in a hair bundle obtain different open probabilities will be discussed further when stochastic channels are examined.

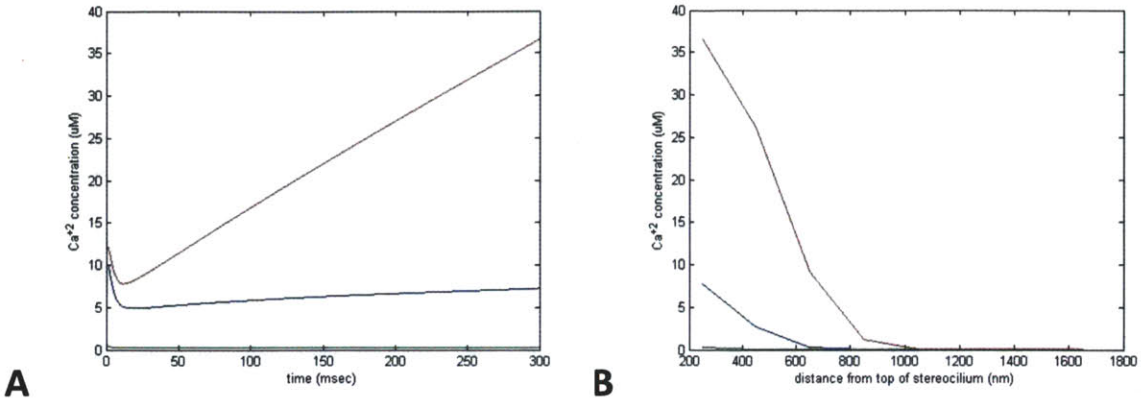

Figure 10: (**A**)Calcium concentration versus time recorded in 200nm deep cylinders measured 225 nm from the top of the stereocilium. The current source starts with the channel being open at 0 msec but decays exponentially to 10% of full current with two time constants of 3 msec and 15 msec. V_{hold}=-80 mV, extrusion pumps turned on, $[\text{fixed buffer}]_{int}$=1 mM for all traces. Red: $[Ca^{+2}]_{ext}$=1.5 mM, blue: $[Ca^{+2}]_{ext}$=1.5 mM, $[EGTA]_{int}$=1 mM, green: $[Ca^{+2}]_{ext}$=0.1 mM, $[EGTA]_{int}$=1 mM. (**B**) same data as in A but plotted as calcium concentration versus distance from the top of the stereocilium at 300 msec.

Diffusion with Deterministic Transduction Channels in Outer Hair Cells

The stereocilia of outer hair cells have a different structure than those of bullfrog saccular hair cells. The diameter of outer hair cell stereocilia is typically smaller than their bullfrog saccular counterparts. The model uses a stereocilium diameter of 250 nm for outer hair cells and 450 nm for saccular hair cells. In addition, outer hair cell bundles tend to be shorter than saccular hair cells. Outer hair cells get taller towards the apex of the cochlea so the model uses dimensions typical for the middle of the cochlea: 1 μm for the smallest stereocilia and 4 μm for the tallest in along an excitatory column. The stereocilia in the saccule span from 3.5 μm to 8.3 μm. Both of these factors have a significant effect on the speed at which calcium diffuses. The smaller diameter means that calcium has less volume to fill as it diffuses down the stereocilia. This fact alone allows the calcium concentration to build up much higher than in saccular hair cells. The smaller stereocilia allow a much larger calcium concentration to enter into the hair cell body which allows calcium to flow up into adjacent stereocilia.

This effect is demonstrated in figure 11. Panel A shows the calcium concentration in stereocilia from the second and third row without adaptation. The calcium concentration at the top of the stereocilium reaches around 15 mM whereas the calcium concentration never got above 1 mM in a bullfrog saccular hair cell for the same conditions. This effect arises strictly because of the decreased diameter of the stereocilium. The calcium concentration begins to plateau as the calcium diffuses into the hair cell body. The second row of stereocilia have transduction channels at the top but the third row

are lacking transduction channels. The dotted lines on the figure show the calcium concentration in a stereocilium from row 3. The calcium concentration rises in this stereocilium almost to 10 mM, even in the absence of a transduction channel. The calcium concentration in this stereocilium becomes relatively uniform throughout the entire stereocilium. This is in contrast to the stereocilium from row 2 that has a calcium concentration gradient from the top of the stereocilium to the bottom. The reason for this difference is the source of the calcium input. For the stereocilium from row 2, the calcium source is a current source located at the top of the stereocilium. The current source does not establish a constant calcium concentration but instead ensures that calcium flows down the stereocilium. The direction of diffusion always flows from higher calcium concentrations to lower concentrations. Therefore, there is approximately a linear calcium gradient from the top of the stereocilium to the bottom because there is approximately a steady current source of calcium. By contrast, the hair cell body provides a near constant calcium concentration source at the bottom of the stereocilium from row 3. The steady state calcium concentration must become near uniform in this stereocilium in order to prevent calcium flow, which cannot exist because of the constrained apical surface, with the minor exception of current flow from the calcium extrusion pumps.

Even with adaptation to 10% of the maximum current, the calcium concentration continues to increase in 1.5 mM calcium. Panel B of figure 11 shows that the calcium concentration does not plateau even after 300 msec of simulation. The intracellular calcium concentration near the transduction channel will be above 1 mM, which is a very large intracellular concentration for any cell. The external calcium concentration and intracellular solutions are those that are typically used during patch clamping experiments. 1.5 mM external calcium concentration would never occur in the endolymph surrounding outer hair cells which is held closer to 20 μM. This simulation shows that the calcium concentration builds up to excessive values at 1.5 mM external calcium concentration if 10% of the transduction current is present even after adaptation.

Figure 12 displays the intracellular calcium concentration for 20 μM external calcium, a value more in line with *in vivo* conditions. As expected, lowering the external calcium concentration reduces the calcium buildup inside of the outer hair cell. Even in the absence of adaptation, the calcium concentration does not significantly increase in the tallest stereocilium. With uniform adaptation for all transduction channels, the calcium concentration near the adaptation motors in the tallest stereocilia would never be expected to exceed 1 μM. This means that under *in vivo* conditions there is very little calcium regulation of the myosin motors in the tallest stereocilia, which make up one half of the myosin motors in outer hair cells. This could explain the reports of outer hair cells having 50% transduction current at rest in 20 μM external calcium concentration but a percentage closer to 3 percent in the presence of 1.5 mM external calcium that is typically used during experiments.

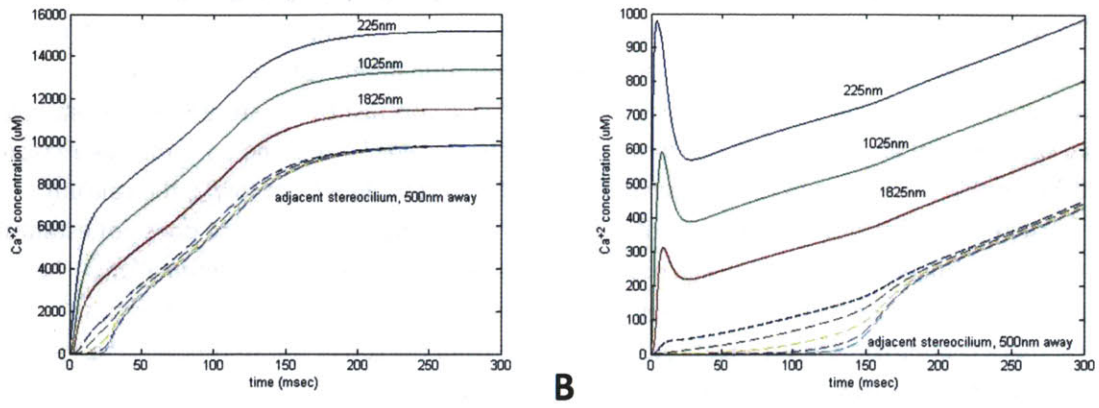

Figure 11: (**A**) Calcium concentration versus time recorded in 200nm deep cylinders in an outer hair cell without adaptation. 125nm voxels were included for the top 125 nm to create proper calcium entry through the transduction channel. The transduction channel is open fully at t=0 and remains open throughout the simulation. The calcium concentrations are taken from cylindrical compartments centered at the distances shown on the plot. V_{hold}=-80 mV, $[Ca^{+2}]_{ext}$=1.5 mM, $[\text{fixed buffer}]_{int}$=1 mM, $[EGTA]_{int}$=1 mM, calcium extrusion pumps turned on. The solid line traces are in a stereocilium from the second row with a transduction channel at the top. The distance on the plot refer to the distance down from the top of the stereocilium. The dotted lines are in a stereocilium from the third row, which does not have a transduction channel. The distances are taken with reference to the base of the stereocilium and at 800 nm increments. (**B**) Same configuration as in the previous panel but with adaptation changing the transduction current from 100% to 10% with two time constants of 3 msec and 15 msec.

There is clearly a calcium difference from the shortest to tallest stereocilia along a single column. There are not even transduction channels in the tallest stereocilia, therefore their only source of calcium is from the hair cell body which is ultimately supplied from the base of adjacent stereocilia. Figure 13 shows a calcium concentration map at the top surface of the hair cell body. The area in red is directly below the stereocilia. The interesting thing to note is that left edge of the image is not as red as the center of the image. Panel B shows this graphically. There are 30 stereocilia per row in this hair bundle, the center plot is taken directly below the 15th column and the edge plot is taken directly below the 1st column. There is always less calcium towards the edge of the stereocilia than at the middle of the hair bundle. The base of each stereocilium acts as a calcium source for diffusion. There are more calcium sources near the middle of the bundle than at the edge, so that the calcium sums to a higher concentration near the middle of the hair bundle. The higher calcium concentration in the center of the bundle increases the calcium concentration in all of the stereocilia in this region. This complicates things considerably in that every single stereocilium within a hair bundle is predicted to have a different calcium concentration and therefore a different level of feedback on adaptation.

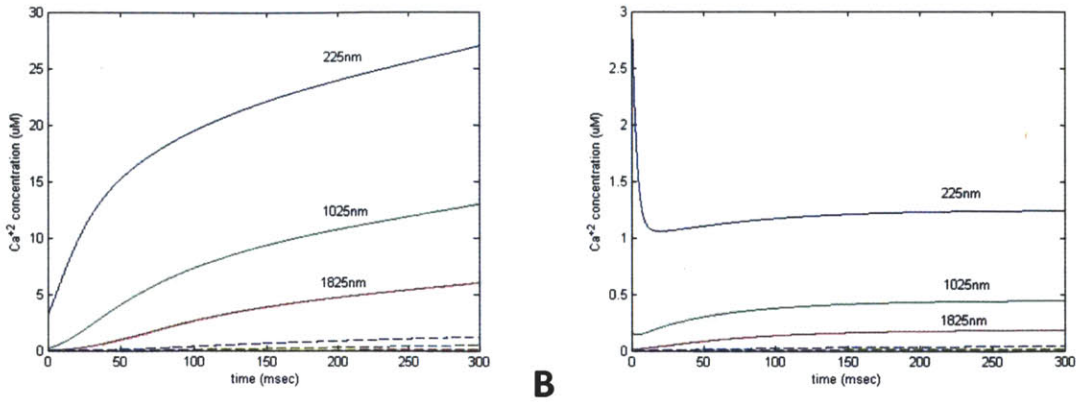

Figure 12: (**A**) Calcium concentration versus time recorded in 200nm deep cylinders in an outer hair cell without adaptation. 125nm voxels were included for the top 125 nm to create proper calcium entry through the transduction channel. The transduction channel is open fully at t=0 and remains open throughout the simulation. The calcium concentrations are taken from cylindrical compartments centered at the distances shown on the plot. V_{hold}=-80 mV, $[Ca^{+2}]_{ext}$=0.020 mM, $[fixed\ buffer]_{int}$=1 mM, $[EGTA]_{int}$=1 mM, calcium extrusion pumps turned on. The solid line traces are in a stereocilium from the second row with a transduction channel at the top. The distance on the plot refer to the distance down from the top of the stereocilium. The dotted lines are in a stereocilium from the third row, which does not have a transduction channel. The distances are taken with reference to the base of the stereocilium and at 800 nm increments. (**B**) Same configuration as in the previous panel but with adaptation changing the transduction current from 100% to 10% with two time constants of 3 msec and 15 msec.

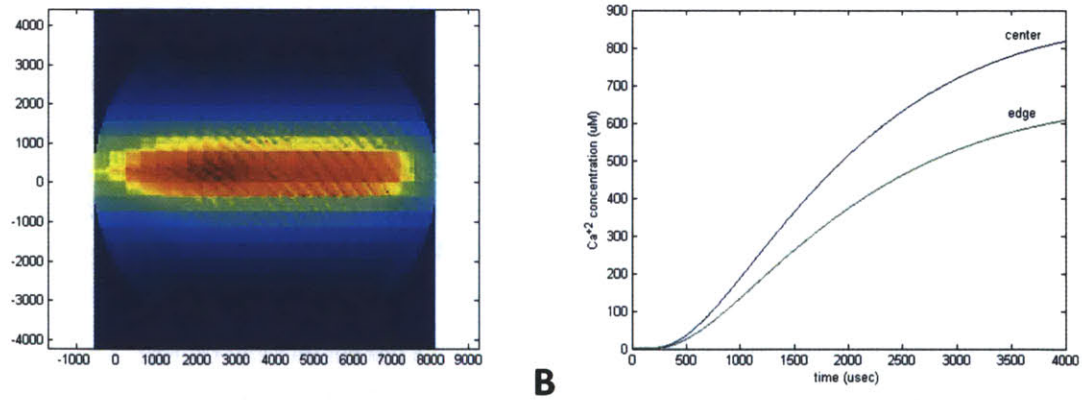

Figure 13: (**A**) Calcium concentration for an outer hair cell. The image is taken at the apical surface of the hair cell body, 200 nm from the surface. Red represents increased calcium whereas blue represents no calcium. The image is shown after the transduction channels were turned on for 4 msec. V_{hold}=-80 mV, $[Ca^{+2}]_{ext}$=1.5 mM, no buffers or pumps present. (**B**) Same simulation plotted as calcium concentration versus time where the calcium concentration is taken under the 2nd row of stereocilia either in the middle of the hair cell (blue) or under the 1st column (green)

Stochastic Modeling of Calcium Diffusion in a Hair Bundle at Rest

As mentioned in the prior sections, the calcium concentrations are not uniform across stereocilia. Hair cells have an asymmetrical tip link which produces the source of calcium for myosin motor modulation to come from transduction channels attached to different tip links. In outer hair cells, stereocilia influence the calcium concentration in adjacent stereocilia which establishes a calcium gradient across both dimensions of the hair bundle. The key question is how the calcium is distributed in a hair bundle where the transduction channels operate stochastically and the myosin motors weaken in the presence of calcium?

To answer this question, simulations were run with a calcium feedback parameter on the myosin motors. This weakens the overall myosin strength based on the local calcium concentration near that particular myosin motor. The feedback parameter was adjusted so that the resting transduction current settled around 10% for the entire hair bundle in a bullfrog saccular hair cell. The transduction channels were force gated by the force in the tip link, and the stereocilia were free to move. Figure 14 demonstrates the calcium pattern that develops under these conditions. The bundle takes around 100 msec to settle to a base position. The bundle then displays an alternating calcium pattern. There are no transduction channels present in the tallest stereocilium, therefore the myosin motor in that stereocilium are not weakened by calcium and the connected transduction channels have increased force gating them open more often. These transduction channels are located in the second tallest stereocilium which therefore contains a lot of calcium. This weakens the myosin motor contained in that stereocilium which is connected to the next smallest stereocilium. This pattern continues down the column so that the calcium concentration alternates for each stereocilium. The 3rd tallest stereocilium still has more calcium than the tallest stereocilium, so the pattern damps towards the smallest stereocilium in a column. This can be seen in panel B of figure 14. Stereocilium 5 and 6, towards the smaller end of the hair bundle, have more similar calcium concentrations than stereocilium 2 and 3, towards the taller end of the hair bundle. In general, this pattern will always form in this manner in some aspect. As the external calcium concentration is reduced, then the overall effect becomes weaker and the pattern averages out faster. Also, if random tip links are destroyed during the dissection, then the pattern resets because a channel with a missing tip link acts in the same manner as a channel that has a very weak tip link pulling on it.

In rodent outer hair cells, there are only three stereocilia per column and therefore two tip links per column. Based on the saccular results, this would suggest an alternating calcium pattern for three stereocilia. However, the situation is a bit more complicated because the calcium also diffuses much faster into the hair cell body and up into the stereocilia. For the simulation shown in figure 15, an alternating pattern does indeed form. However, the calcium concentration in the tallest stereocilium is actually higher than in the shortest stereocilium. In addition, the calcium concentration in the middle stereocilium occasionally spikes and then quickly drops back down. The transduction channel in the middle stereocilium is originally strongly gated, much in the same manner that the second tallest stereocilia in the bullfrog saccular bundle are. The difference in the outer hair cell bundle is that enough

of the free calcium diffuses back up into the tallest stereocilium. This weakens the myosin motor that regulates the tension on the transduction channels in the middle stereocilium, which produces less calcium in the middle stereocilium. The peak calcium concentration in the middle stereocilium leads the peak calcium concentration in the tallest stereocilium by around 5 msec. This delay means that the calcium concentration will never reach a steady state but will always have stochastic spikes in this manner. Each spike will also affect stereocilia from adjacent columns, which creates a very complicated calcium concentration pattern. When the calcium concentration is lowered, then this complicated effect disappears, and a small alternating pattern begins to appear. This pattern also depends on the feedback parameter that determines how much calcium weakens the myosin motor force. If the feedback parameter is lowered, then the spiking pattern also disappears. This spiking pattern probably does not occur *in vivo*, but could exist if myosin-1C is modified either genetically or chemically.

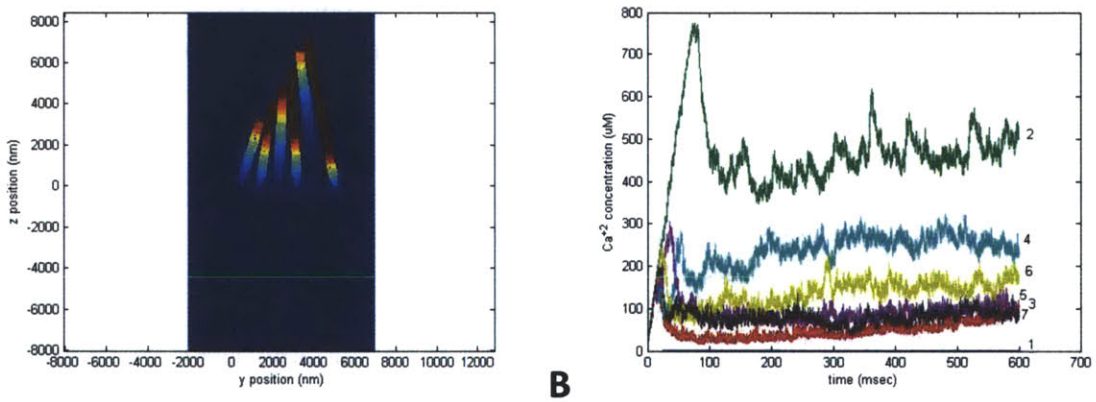

Figure 14: (**A**) Calcium concentration for a bullfrog saccular hair bundle after 600 msec of simulation with two transduction channels at the lower insertion point of each tip link. Red represents increased calcium whereas blue represents no calcium. The hair bundle is a cross section taken through the middle column in the hair bundle. There are 7 stereocilia in the column but the tallest stereocilium has very little calcium and is therefore not visible. (**B**) Calcium concentration taken 225 nm from the tip of each stereocilium versus time. The stereocilia are arranged from tallest to smallest as: 1. Blue, 2. Green, 3. Red, 4. Cyan, 5. Magenta, 6. Yellow, 7. Black.

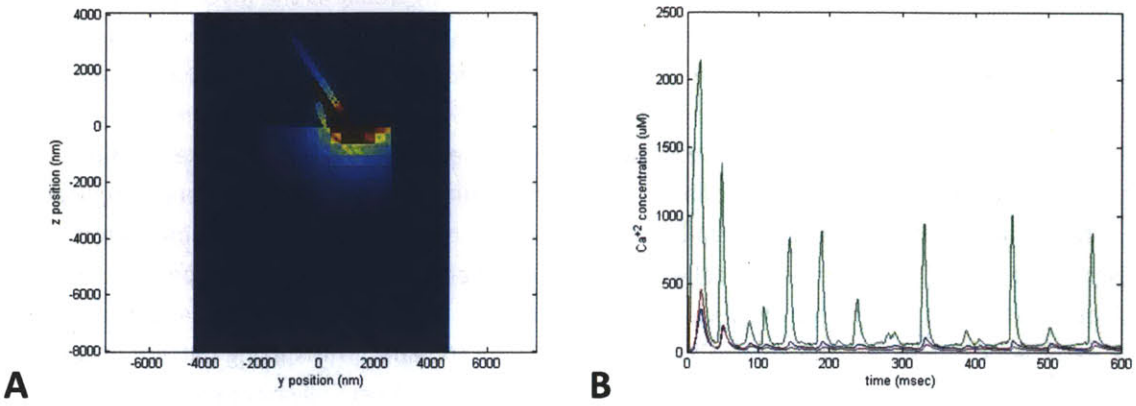

Figure 15: (**A**) Calcium concentration for an outer hair cell bundle after 500 msec of simulation. Red represents increased calcium whereas blue represents no calcium. The hair bundle is a cross section taken through the middle column in the hair bundle. (**B**) Calcium concentration taken 225 nm from the tip of each stereocilium versus time. The stereocilia are arranged from tallest to smallest as: 1. Blue, 2. Green, 3. Red.

The alternating pattern of calcium concentration arises because the transduction channels are only believed to be at the lower insertion point but the myosin motors are at the upper insertion point. This idea comes from calcium imaging work in which the tallest stereocilia did not show increased calcium fluorescence following a deflection of the hair bundle. Configurations in which a transduction channel is at both ends of the tip link and when two are present at the upper insertion point were also simulated to examine how the calcium profile would appear in these cases. This data creates a useful comparison for calcium imaging experiments to confirm the more recent result that transduction channels are only present at the lower ends of tip links. Figure 16 looks at the case in which a channel is at both ends of the tip link. As expected, the calcium concentration is weakest for the tallest stereocilium and smallest stereocilium in a column, which each only have one transduction channel. The average calcium concentration appears similar to the calcium concentration that the alternating pattern approaches in the case where there are only channels at the lower insertion point.

Figure 17 shows the case where there are two transduction channels at the upper insertion point. As expected, the smallest stereocilium does not show any calcium concentration. The average calcium concentration for this case is smaller than the other two cases. The transduction channels are all directly neighboring a myosin motor complex, therefore all of the myosin motors are weakened. This scenario would cause extremely rapid feedback by calcium on the myosin motors, which would also be expected to quickly affect adaptation after a deflection of the hair bundle.

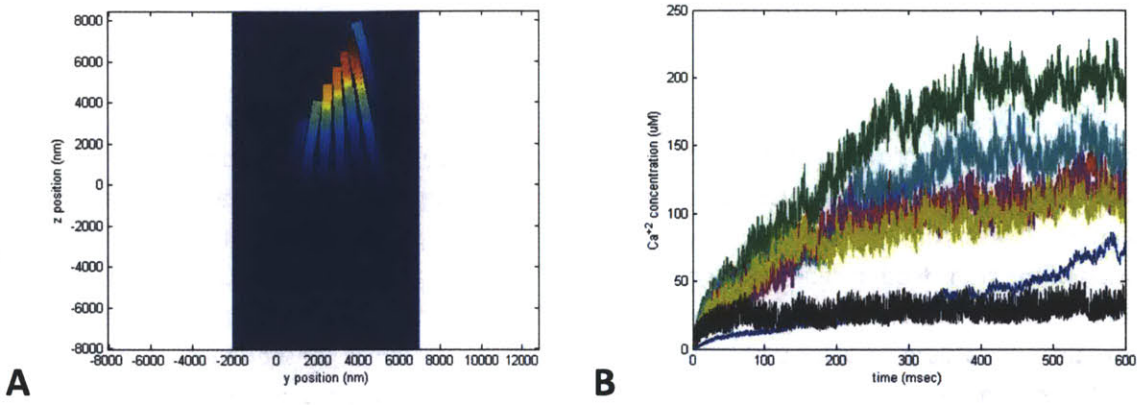

Figure 16: (**A**) Calcium concentration for a bullfrog saccular hair bundle after 500 msec of simulation with one transduction channel at the upper insertion point and another at the lower insertion point of each tip link. Red represents increased calcium whereas blue represents no calcium. The hair bundle is a cross section taken through the middle column in the hair bundle. (**B**) Calcium concentration taken 225 nm from the tip of each stereocilium versus time. The stereocilia are arranged from tallest to smallest as: 1. Blue, 2. Green, 3. Red, 4. Cyan, 5. Magenta, 6. Yellow, 7. Black.

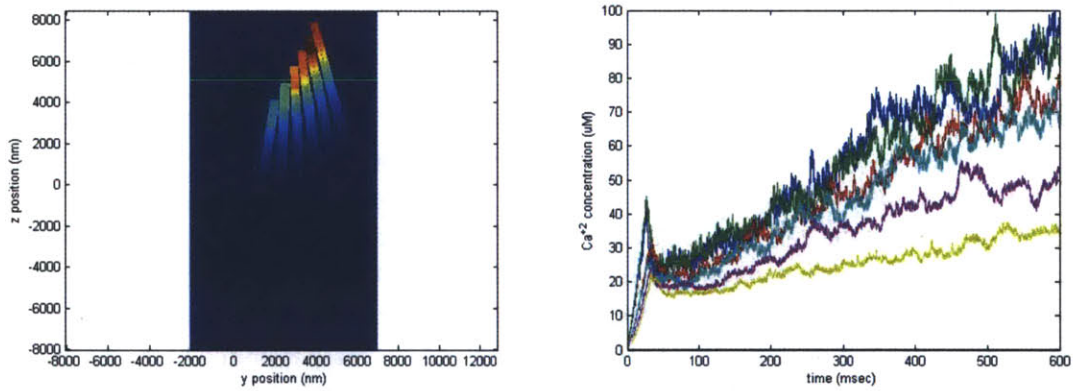

Figure 17: (**A**) Calcium concentration for a bullfrog saccular hair bundle after 500 msec of simulation with two transduction channels at the upper insertion point of each tip link. Red represents increased calcium whereas blue represents no calcium. The hair bundle is a cross section taken through the middle column in the hair bundle. There are 7 stereocilia in the column but the smallest stereocilium has very little calcium and is therefore not visible. (**B**) Calcium concentration taken 225 nm from the tip of each stereocilium versus time. The stereocilia are arranged from tallest to smallest as: 1. Blue, 2. Green, 3. Red, 4. Cyan, 5. Magenta, 6. Yellow, 7. Black.

Calcium Imaging Experiments

This work tries to accomplish several things with regards to calcium diffusion within hair bundles. First, it seeks to provide exact quantitative values for the calcium concentration within the stereocilia. The resolution for these values can be quite small, on the order of a few nanometers, which makes it impossible to confirm experimentally. Secondly, it seeks to provide a means for determining the location of the transduction channels with respect to the tip link. The expected result is that only the lower insertion points of tip links contain transduction channels. As has been shown, this creates a complex pattern of calcium diffusion within the stereocilia. This pattern has consequences for the strength of myosin motors that will have a large effect on how transduction occurs within the hair bundle. For this reason, it is important to confirm that this alternating pattern actually exists.

Confirming this result requires that a calcium indicator dye is used while using a confocal microscope. It is easiest to image stereocilia from the top of the cell which means that confocal cross sections will be made at the same height along adjacent stereocilia, as measured from the apical surface of the hair cell body. Because of the staircase formation in the hair bundle, the distance from the transduction channels varies for each stereocilium. This becomes a problem when comparing the calcium concentration across stereocilia. The calcium concentration is always largest close to the transduction channels. If an alternating pattern of calcium diffusion is to be observed, then the calcium concentration must be obtained near the transduction channels for each stereocilia.

A confocal microscope is a wonderful instrument that can obtain optical cross sections which reject out of focus light. However, it can only obtain a single cross section at a time and cannot obtain information about the whole hair bundle at once. This limits the knowledge that one can get about the calcium concentration within the hair bundle. Luckily, the most important prediction from this work involves measuring the calcium concentration of a hair bundle at rest. This means that optical cross sections of the hair bundle can be made systematically from the apical surface of the hair cell body up until the tallest stereocilia. The resting calcium concentration should increase from the base up to the tip of each stereocilium in stereocilium that have active transduction channels. The maximum calcium concentration for each stereocilium should be used as the calcium concentration for that particular stereocilium. Along an excitatory column, this value would be expected to alternate if the transduction channels are indeed only at the lower insertion point of the tip link. Furthermore, missing tip links should produce stereocilium with very little calcium signal. The neighboring stereocilium along the column towards the smaller end of the hair bundle should have a relatively large calcium signal. This observation would confirm that transduction channels only exist at the lower insertion point of tip links and that a complex calcium gradient does indeed exist within stereocilia. The latter result has strong implications on the resting strength of myosin motor complexes at rest.

An additional interest of any calcium imaging experiment should be to determine the calcium concentration pattern within stereocilia after a mechanical deflection. This experiment has the complication that the same deflection needs to be repeatedly performed while the confocal microscope is focused on different image planes. In principle, each deflection should produce a similar pattern of

calcium diffusion, so each confocal plane can be used to obtain an overall better understanding of the calcium concentration within the entire hair cell. In theory, stereocilia with weak resting calcium signals should also be harder to produce a calcium signal from stimulation because their myosin motor complexes are weaker. This would confirm the idea that all of the tip links within a hair bundle operate at different initial setpoints arising from calcium modulation. Additionally, one can use the average calcium response to a family of mechanical deflections to estimate the individual current versus displacement curve for each tip link. This is experimentally tricky but can provide evidence as to the initial offset of each tip link which is impossible to obtain from just examining the transduction current. This experiment would provide insight into the gating energy for each tip link.

Interpreting the Results of the Initial Calcium Imaging Experiment

The calcium imaging paper from 1995 (Denk *et. al.*) produced the result that transduction channels are at both ends of the tip link. This is in contrast to the more recent paper from 2009 (Beurg *et. al.*) that claims that transduction channels only exist at the lower insertion point of the tip link. Many theories have been explored to explain the discrepancy between the two results. Some of these theories are examined more closely in an attempt to validate the current results as well as understand the pitfalls of calcium imaging experiments.

The 1995 paper used bullfrog saccular hair cells for their experimental model while the 2009 paper utilized outer hair cells from the rat cochlea for their experimental model. The easy conclusion is that the two systems are different. This seems unlikely to be the case. Hair cells from both systems have similar morphological arrangements and function. The components in the tip link that associate with the transduction channel would also have to be different to accommodate a different location of the transduction channel between the two systems. This does not seem likely given that the tip link is believed to be made up of protocadherin-15 and cadherin-23. In fact, the asymmetrical nature of the tip link would argue for an asymmetrical arrangement for the placement of the transduction channels as well. Although one cannot exclude this argument, it is not very likely that bullfrog saccular hair bundles and rat outer hair cell bundles differ in this manner.

The paper from 1995 claimed that calcium was entering into the tallest stereocilia in the excitatory columns of the hair bundle. Without electron micrographs, it is impossible to determine which adjacent stereocilia are connected by tip links. It is therefore entirely possible that the tallest stereocilia were not properly identified. In this scenario, calcium would not have entered into the tallest stereocilia but these stereocilia were ignored because they did not have a significant calcium signal. This is certainly a possible explanation for the discrepancy but it is difficult to determine one way or another if this actually occurred during those experiments.

An additional possibility arises from limitations of the experimental equipment for the original paper. It took 0.5 seconds to complete an entire cross sectional image of the hair bundle. Additionally, calcium green was used as the calcium indicator dye, which has a relatively high affinity for calcium.

This means that even for very small changes in the free calcium concentration, calcium green would display an increase in fluorescence, indicating the presence of an increase in calcium concentration. Figure 18 displays two simulated confocal cross sections taken 800 nm above the apical surface of the hair cell body for similar bullfrog saccular hair bundles. Panel A utilizes calcium-green as the calcium indicator dye whereas panel B uses fluro-4. Both images are taken after 0.5 seconds with adaptation to 14% of the peak current present in the simulation. One can clearly make out the seventh and final row of stereocilia in panel A while one might assume that there is only a small amount of fluorescence in panel B. The fluorescence in row 7 of panel A is less, but during an actual experiment it would be difficult to notice the difference from one row to another. An experimenter would most likely interpret the hair bundle in panel A as having transduction channels in the tallest stereocilia and interpret the hair bundle in panel B as having transduction channels only at the lower end of tip links. The high affinity of calcium green to bind free calcium means that it produces more of a fluorescent signal for small free calcium concentrations. Free calcium can diffuse down the second tallest stereocilia and back up into the tallest stereocilia and produce a fluorescent signal even in small concentrations. And perhaps even more significant, the bound form of calcium green can also diffuse down and back up into the tallest stereocilia in this manner. This issue likely causes the interpretation that transduction channels exist at both ends of the tip link in the 1995 paper.

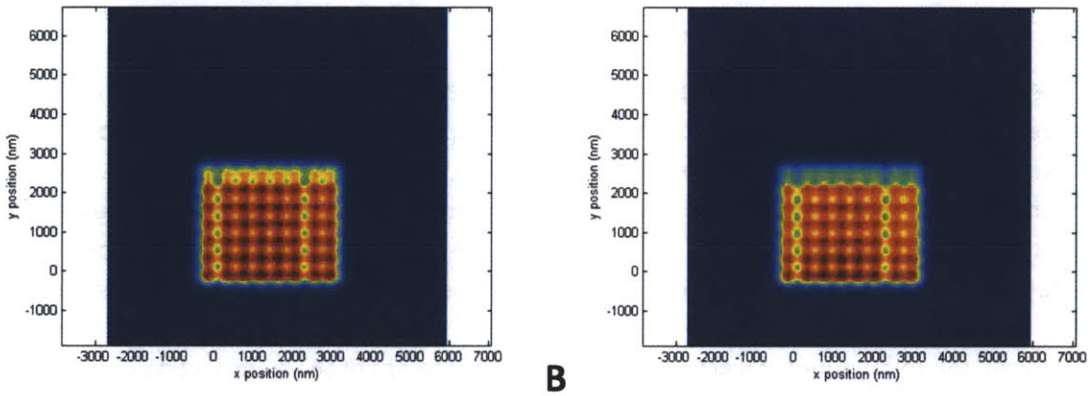

Figure 18: Calcium diffusion for confocal sections taken 800 from the apical surface of the hair cell body. V_{hold}=-80 mV, $[Ca^{+2}]_{ext}$=1.5 mM, $[\text{fixed buffer}]_{int}$=1 mM, $[EGTA]_{int}$=1 mM, calcium extrusion pumps turned on. Florescence is normalized to the peak intensity in the image. Adaptation is present with time constants of 3 msec and 15 msec that reduce the current to 14% of the peak current. (**A**) 250 μM calcium-green as the indicator dye. (**B**) 250 μM fluro-4 as the indicator dye.

Conclusion

This chapter described simulations that specifically examined how various constraints affect the intracellular calcium concentration. It was shown that the calcium concentration near transduction channels quickly reaches elevated values in a few microseconds. The concentration increase takes longer and is smaller near the myosin motors, and depends on the intracellular buffer concentrations as well as the external calcium concentration. More work is needed on studying exactly how calcium changes the force produced by myosin motors to determine the significance of these calcium concentrations.

In outer hair cells, the decreased stereocilia diameter greatly increases the calcium concentration within the stereocilia. This, combined with the smaller height of outer hair cell bundles, allows for diffusion of calcium into the hair cell body and up into adjacent stereocilia. This creates a calcium gradient across rows and columns in outer hair cells.

Finally, an alternating calcium pattern was observed in simulated hair bundles that arises because of the calcium feedback on myosin motors. The alternating calcium pattern has strong implications for the transduction response of individual transduction units within a hair bundle. Each transduction apparatus should have different open probabilities at rest because of the alternating calcium modulation. Confirming this result by using a calcium indicator dye is the most important future direction driven from this work.

Chapter 4

Adaptation in Bullfrog Saccular Hair Cells

Introduction

The bullfrog saccule organ seems like a strange experimental model for studying hair cell physiology. One would naturally assume that most experiments would be performed on mammalian cochlear hair cells in order to get a better understanding of how hair cells contribute to human hearing. However, the bullfrog saccule offers many experimental advantages that have made it a popular choice for experiments. Saccules from adult bullfrogs can be easily dissected, whereas dissecting a mouse cochlea becomes very difficult after the mouse is older than one week, a period when hearing is still developing in the mouse. In addition, bullfrog saccular hair cells have wider and taller stereocilia than in mouse cochlear hair cells. This makes them much easier to stimulate precisely, allowing for a better understanding of hair cell physiology. For these reasons, much of the pioneering work done on hair bundles is based on bullfrog saccullar hair bundles. The initial characterization of the speed of transduction (Corey & Hudspeth, 1979a; Corey & Hudspeth, 1979b; Corey & Hudspeth, 1983b), the rates and completeness of adaptation (Eatock, Corey, & Hudspeth, 1987; Shepherd & Corey, 1994), as well as the mechanical behavior of hair bundles to compliant probes (Howard & Hudspeth, 1987; Howard & Hudspeth, 1988; Martin, Mehta, & Hudspeth, 2000) have all been studied in bullfrog saccular hair cells. For better or worse, researchers tend to understand hair cell physiology based on how bullfrog saccullar hair bundles behave.

This chapter aims to use the basic knowledge gained from bullfrog saccular hair cells in order to better understand transduction and adaptation. Transduction is first examined with just its most basic components: a gating spring and transduction channels. Following this, the adaptation motor is added, initially without calcium diffusion and feedback and then allowing this. For each step, the implications of adding additional elements are discussed. This approach is used to build to a rational understanding of auditory transduction. The overall goal is to understand transduction better by focusing on the specific elements as well as to make predictions that can be used during future experiments. The most important aspect of this goal is to create theories that can be distinguished from other theories through experiments.

Stimulating Transduction Channels Directly

Transduction *in vivo* is not entirely straight forward. When the hair bundle is deflected, adjacent stereocilia, along an excitatory column, shear relative to each other. This shearing effect increases the stretch of elements associated with the tip link. The increased stretch is turned into a force via a gating spring which gates two transduction channels at the lower end of the tip link (Corey & Hudspeth, 1979b). Each tip link is attached to myosin motors at the upper end (Garcia *et. al.*, 1998), which act very rapidly to reduce the tension in the tip link. The tension in the tip links also changes the position of the hair bundle which in turn causes a shearing stretch on the other tip links. Altogether, these complications mean that it is very difficult to ascertain what is occurring precisely at a single tip link during an experiment in which the whole hair bundle is studied. The best that can be done is to

generalize the whole hair bundle results as arising from a population of tip links that share similar properties. This may not necessarily be the case; in addition, results from calcium diffusion studies indicate that myosin motor complexes operate with different forces, even within the same hair bundle (see calcium chapter).

Channel Open Probability

The open probability of a transduction channel versus the stretch applied across the gating spring is defined by the sigmoidal equation:

$$P(x) = \frac{1}{1+\exp\left(-k_g d\left(\frac{x-x_0}{kT}\right)\right)} \quad \text{(eq. 1)}$$

Where P(x) is the open probability, k_g is the stiffness of a single gating spring, d is the swing of the gate, x is the stretch of the gating spring, x_0 is the stretch of the gating spring that produces an open probability of 0.5, kT is Boltzman's constant and temperature in Kelvin. The x term in the equation takes some special consideration. Shear increases the distance from the upper insertion point to the lower insertion point. The tip link is believed to be much stiffer than the gating spring (Sotomayor *et. al.*, 2010). Because of this, the tip link acts like a stiff rope that pulls on a spring element in series. For this reason, most of the extension occurs at the gating spring when the end of the tip link is displaced. For clarity, I define the overall stretch on the whole tip link as the tip link stretch whereas the extension of the gating spring and channel is termed stretch. When the channel opens, the extension on the gating spring decreases by the distance of the gate swing, d, but the upper end of the tip link does not move during the conformational change. This allows an additional term to be defined, the gating spring stretch, which is simply the stimulus-induced stretch minus the gate swing if the channel is open. If the channel is closed then the stretch and gating spring stretch are identical. If the x term in the open probability equation is defined as the stretch term, which is typically the case, then the equation needs to be rewritten for the closed and open states of the channel:

$$P_{closed}(x) = \frac{1}{1+\exp\left(-k_g d\left(\frac{x-x_0}{kT}\right)\right)} \quad \text{(eq. 2)}$$

$$P_{open}(x) = \frac{1}{1+\exp\left(-k_g d\left(\frac{x-d-x_0}{kT}\right)\right)} \quad \text{(eq. 3)}$$

Where the open form of the equation is simply the closed form shifted by the gate swing.

Having separate forms of the open probability equation brings up an interesting point that the transduction channel has negative cooperativity with itself. Every time that the transduction channel opens, the relaxation of tension makes it more likely that it will close again. The important case to understand is the overall open probability of a transduction channel based on the stretch, x. This is difficult to determine based strictly on the open probability. The proper way to determine the combined open probability is to determine how long the channel stays in either state, which necessitates knowing the rates of the conformational changes. R_{co} is the rate at which the channel transitions from closed to open and R_{oc} is the rate at which the channel transitions from open to closed. The overall open probability is then:

$$P(x) = \frac{R_{co}\,(x)}{Rco(x) + R_{oc}(x)} \qquad \text{(eq. 4)}$$

The rates depend on the exponential terms in the open probabilities. Specifically, they can be written as:

$$R_{co}(x) = K_F \exp\left[\mu k_g d\left(\frac{x - x_0}{kT}\right)\right] \qquad \text{(eq. 5)}$$

$$R_{oc}(x) = K_R \exp\left[-1 * (1 - \mu) k_g d\left(\frac{x - x_0 - d}{kT}\right)\right] \qquad \text{(eq. 6)}$$

K_F and K_R are the rate constants for the forward and reverse transitions and μ is a constant between 0 and 1 that biases the rates towards the open or closed state, with a value of 0.5 meaning that neither state is preferred. If one assumes that the forward and reverse rate constants are the same and μ is 0.5, then the probability equation becomes:

$$P(x) = \frac{\exp\left[0.5 k_g d\left(\frac{x - x_0}{kT}\right)\right]}{\exp\left[0.5 k_g d\left(\frac{x - x_0}{kT}\right)\right] + \exp\left[-0.5 k_g d\left(\frac{x - x_0 - d}{kT}\right)\right]} \qquad \text{(eq. 7)}$$

Dividing the numerator and denominator by the term in the numerator and adding the exponential terms together yields:

$$P(x) = \frac{1}{1 + \exp\left[-k_g d\left(\frac{x - x_0 - \frac{d}{2}}{kT}\right)\right]} \quad \text{(eq. 8)}$$

This turns out to be the open probability of the transduction channel if the gate is always viewed as half open. One can create a new offset term $x_0'=x_0+d/2$ which recreates the original form of the equation. Deriving the equation in this manner is useful in understanding how the gate swing contributes to the offset of the channel open probability and can be utilized to better understand channel gating.

Direct Channel Stimulation

To get a good insight into transduction, simulations were performed where the tip link was pulled directly. Each tip link is believed to have two transduction channels attached to it, with each transduction channel having its own gating spring. This method of stimulation bypasses myosin-based adaptation, which allows a direct measurement of the gating spring stiffness and gate swing. These results are important for understanding how a single channel responds to force.

The actual experiments are feasible. Using laser tweezers, researchers have studied the force when myosin moves on actin (Molloy *et. al.*, 1994; Batters *et. al.*, 2004). A similar approach could be used for pulling directly on a single tip link. The tip links could be treated with a calcium chelator. Recent structural evidence suggests that this weakens the connection between protocadherin-15 and cadherin-23 which comprise the lower and upper portions of the tip link, respectively (Sotomayor *et. al.*, in press). A bead could be coated with fragments of cadherin-23 and moved to the tips of stereocilia, where it might bind to protocadherin-15. This would allow a direct force to be applied to the lower portion of the tip link, which should still be attached to its associated transduction channels. The results from these simulations serve as predictions for this future experiment.

For the simulations, the tip link was pulled with a steady velocity over 300 msec. During the ramp displacement, the channels are allowed to open and close stochastically based on the force provided from the gating springs, which is a function of the stretch applied from the tip link displacement. The current from this stimulus is very insightful. The current occurs in 3 distinct groups, corresponding to 0 channels open, 1 channel open or 2 channels open. From this information, the single channel conductance of the transduction channel is easily determined. For the simulation, the conductance is set as a parameter. For the real experiment, there is a chance that the two channels might have different single channel conductances. For this case, the current will form 4 peaks in the distribution. This kind of experiment would be the only way to ever determine the individual conductance of two channels that are both attached to the same tip link.

Figure 1 demonstrates how the open probability is the average probability between the closed and open forms of the P(x) curves. The cyan trace was made by using a moving average on the current as a ramp deflection was applied to the tip link. The average current was then used to estimate the open probability of the channel versus stretch on the gating spring. The open probability follows the predicted curve in which the offset term is $d/2+ x_0$. The noise of the simulated open probability curve happens to span directly between the open and closed form of the curves which is completely coincidental. Panel B demonstrates the theoretical open probability curves at P=0.5. This value occurs at x_0 for the closed form of the P(x) curve, $d+x_0$for the open form of the curve, and $d/2+ x_0$ for the actual form of the curve. This result confirms the derivation from the previous section.

Figure 2 compares open probability curves that were made with two different sets of parameters using the same moving average technique as in figure 1. For the blue trace, k_g=0.2 pN/nm, d=5nm, and x_0=15 nm whereas the green trace has k_g=1 pN/nm, d=1nm, and x_0=17 nm. The curves overlap each other and one could not determine the actual gating parameters from the curves as they are displayed. This demonstrates a problem with just observing the current in order to ascertain gating parameters. The steepness of the open probability curve is determined by the gating force, which is the product of the gating spring stiffness and gate swing. Without further information, the open probability curve represents a family of solutions that all have the same gating force but different offsets.

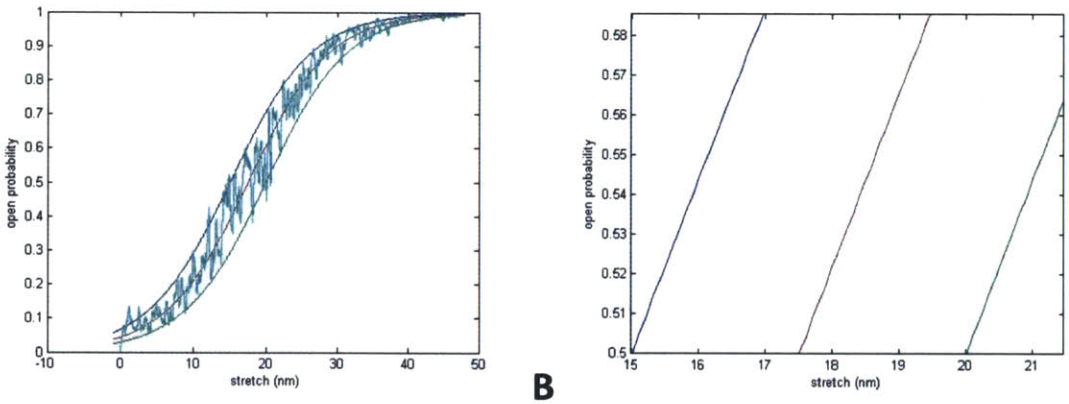

A B

Figure 1. (A) Displays the predicted open probability versus gating spring stretch P(stretch) for the following parameters: k_g=0.2 pN/nm, d=5 nm, x_0 =15 nm. The same parameters used in a simulation in which the gating spring was stretched over 0.5 sec. The open probability was filtered using a moving average filter with a width of 10 msec. Blue : P(stretch) for channel closed, Green: P(stretch) for channel open, Red: P(stretch) for combined rates, Cyan: P(stretch) from simulation. **(B)** Magnification of predicted probabilities.

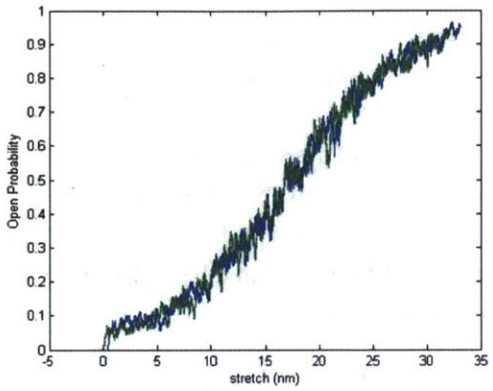

Figure 2. P(stretch) from simulations using two sets of parameters. The gating spring was stretched over 0.5 sec. The open probability was filtered using a moving average filter with a width of 10 msec. Blue: k_g =0.2 pN/nm, d=5 nm, x_0 =15 nm, Green: k_g=1 pN/nm, d=1 nm, x_0 =17 nm.

To determine the exact gating spring stiffness and gate swing, the most precise technique is to measure the force produced along the tip link axis. For an experiment using laser tweezers, where the apparatus has an effective stiffness based on the beam intensity and bead material, small motions of the stimulating bead correspond to changes in force from the gating spring. For the simulations, the gating spring force is an intrinsic property of the model. While the tip link is slowly pulled, the transduction channels are constantly opening and closing. Figure 3A displays the constant flickering of the force that occurs within the tip link when the stretch is near 4 nm. The force, like the single tip link current, occurs in three discrete levels. The jump from one force to another can represent the single channel gating force. This is still a product of the gating spring stiffness and gate swing and does not inherently define the individual parameters. Panel A only shows a magnified version of the whole trace. For this example, the force jumps in ever increasing values until it reaches a peak in the discrete step size when the stretch is 8 nm. This transition point represents the actual gate swing for the transduction channels. For stretch values smaller than this, the gate opens more than the extension on the associated gating spring which provides slack in the gating spring. By determining the gate swing in this manner, then the gating spring stiffness is simply the gating force that is measured for stretch values above the gate swing divided by the gate swing.

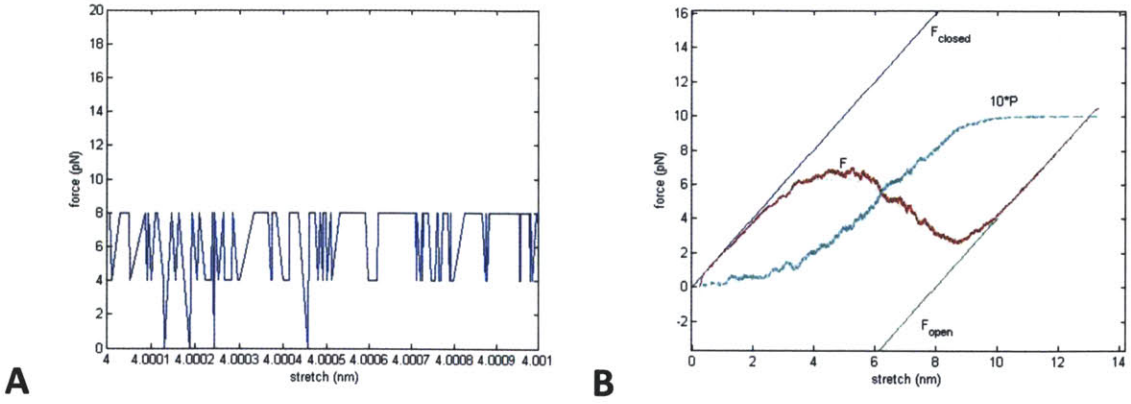

Figure 3. (A) Direct force measurements obtained near a stretch of 4 nm for k_g=1 pN/nm, d=8 nm, x_0 =3 nm. **(B)** Force profile. The gating spring was stretched over 0.3 sec. The force acting on the tip link was filtered using a moving average filter with a width of 5 msec. Blue (F_{closed}): Predicted force if channels are always closed, Green (F_{open}): Predicted force if channels are always open, Red(F): tension in the tip link from simulation, Cyan(10P): 10 times the open probability shown for reference.

An alternative approach to determining the gating parameters is to look at the average force as the tip link is stretched. This is done in a similar manner as the estimated open probability curve. A moving average filter was applied to the instantaneous force measurements to obtain a smooth curve that represents the average force while the tip link is being stretched. This is displayed as the red trace in figure 3B. The theoretical force if the channels are always closed is shown in blue with the label F_{closed} and the force if the channels are always open is shown in green with the label F_{open}. For small extensions of the tip link, the force curve follows the curve in which the channels are always closed. For larger stretch values, the force curve follows the curve in which the channels are always open. This fact alone provides very useful information. The slopes of both of these curves are the same; they only differ by an offset along the x axis. The underlying assumption is that two transduction channels are present in parallel at the lower insertion point of the tip link. The parallel arrangement means that the stiffness from each gating spring adds to the overall stiffness. Therefore, the slope of the linear portion of the curve represents twice the stiffness of the gating spring. The offset from one linear region of the curve to another is a direct measurement of the gate swing. With this technique, the stiffness and gate swing can be measured from a force versus stretch curve. The result should yield the same answer as the prior technique.

The force curve displays a very important behavior in that the stiffness of the curve becomes negative as it transitions between the two linear slopes. A negative stiffness region is interesting because increasing the stretch leads to decreased tension in the gating springs. This situation is made possible because of the compliance produced when transduction channels transition from closed configurations to open configurations. Figure 3B also displays the scaled open probability for this tip link. It can easily be seen that the midpoint of the negative stiffness occurs near the 50% open

probability point. This confirms that the negative stiffness arises at the greatest increase in open probability.

Hair bundles displaying a region of negative stiffness have been reported previously (Martin *et. al.*, 2000). However, while most hair bundles display a region of decreased stiffness, not every hair bundle displays a region of negative stiffness. It therefore becomes important to discuss the constraints on the parameters that allow a negative stiffness region to arise. Figure 4 examines force versus stretch curves for various gating parameters. Panel A varies the gating swing while panel B uses the same gating forces but varies the gating spring stiffness. Panel A shows a robust negative stiffness when k_g=1 pN/nm and d=8 nm while panel B does not display a negative stiffness even for k_g=8 pN/nm and d=1nm which has the same gating force as the negative compliant curve in panel A. This indicates the importance of the gate swing term in creating a negative stiffness region.

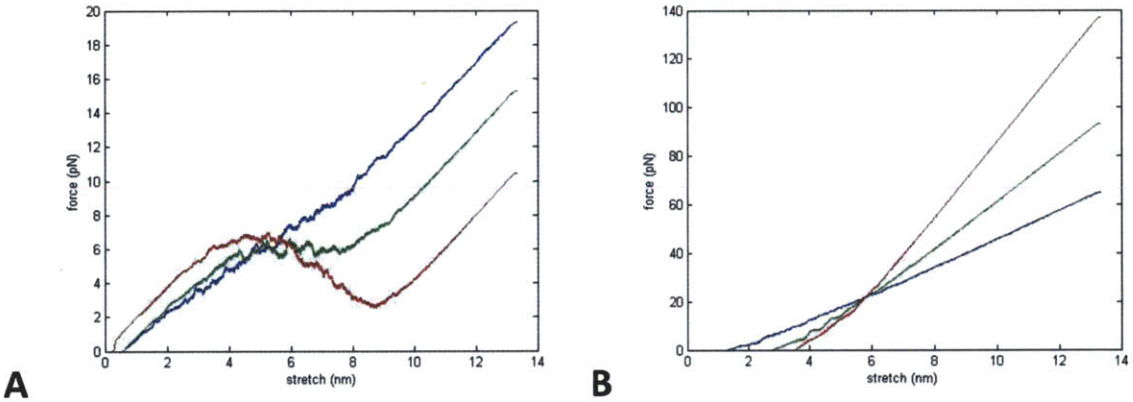

A **B**

Figure 4. Force profiles for various conditions. The gating spring was stretched over 0.3 sec. The force acting on the tip link was filtered using a moving average filter with a width of 5 msec. f_0=3 pN for all. **(A)** Blue: k_g=1 pN/nm, d=3 nm, Green: k_g=1 pN/nm, d=5 nm, Red: k_g=1 pN/nm, d=8 nm. **(B)** Blue: k_g=3 pN/nm, d=1 nm, Green: k_g=5 pN/nm, d=1 nm, Red: k_g=8 pN/nm, d=1 nm.

In order to determine when a negative stiffness region occurs, the force on the tip link needs to be defined. This term is dependent on the open probability with the stiffness being reduced by an offset of d when the channels are open. It follows that

$$F(x) = 2k_g x[1 - P(x)] + 2k_g[x - d]P(x) \quad \text{(eq. 9)}$$

Where a factor of two is necessary to account for two transduction channels per tip link. This simplifies to

$$F(x) = 2k_g x - 2k_g dP(x) \quad \text{(eq. 10)}$$

A local maximum of the force curve indicates where a negative stiffness region occurs. A local maximum occurs when the derivative is zero:

$$\frac{dF}{dx}(x) = 2k_g - 2k_g d\frac{dP}{dx}(x) = 0$$

(eq. 11)

This simplifies to $\frac{dP}{dx}(x) = \frac{1}{d}$. From equation 8, the open probability is

$$P(x) = \frac{1}{1 + \exp\left[-k_g d\left(\frac{x - x_0 - \frac{d}{2}}{kT}\right)\right]}$$

(eq. 12)

Taking the derivative of this term and equating it to $\frac{1}{d}$ gives:

$$\frac{k_g d}{kT}\frac{\exp\left[-k_g d\left(\frac{x - x_0 - \frac{d}{2}}{kT}\right)\right]}{\left[1 + \exp\left[-k_g d\left(\frac{x - x_0 - \frac{d}{2}}{kT}\right)\right]\right]^2} = \frac{1}{d}$$

(eq. 13)

Expanding the squared term and dividing by the numerator makes the equation:

$$\frac{1}{\frac{1}{\exp\left[-k_g d\left(\frac{x - x_0 - \frac{d}{2}}{kT}\right)\right]} + \exp\left[-k_g d\left(\frac{x - x_0 - \frac{d}{2}}{kT}\right)\right] + 2} = \frac{kT}{k_g d^2}$$

(eq. 14)

The exponential terms can be combined as hyperbolic cosine, and when terms are rearranged the result is:

$$k_g d^2 = 2kT\left[\cosh\left(-k_g d\left(\frac{x - x_0 - \frac{d}{2}}{kT}\right)\right) + 1\right]$$

(eq. 15)

The minimum term for hyperbolic cosine is 1. So, for a single tip link, a negative stiffness region is present if:

$$k_g d^2 > 4kT$$

(eq. 16)

This result explains the findings displayed in figure 4. The presence of a negative stiffness region varies linearly with k_g but with the square of the gate swing. This result is important in that it defines a constraint on parameters that determine a negative stiffness region when viewing the average tension in a single tip link. The same result was determined previously by deriving the final equation from the stiffness of the entire hair bundle (Markin & Hudspeth, 1995; Hudspeth *et. al.*, 2000). The derivation was performed in this manner to emphasize the importance of the gate swing in reducing the tension along a single tip link. The criteria established by equation 16 deviate if the myosin motors produce different forces for different tip links, which will be examined later. The values typically used for the gate swing term are large compared to typical values for protein conformational changes. It seems likely that evolution produced a large gate swing in order to create a negative stiffness region.

The prior simulations all assumed that the transduction channels are gated strictly based on the force applied via the gating springs. This assumes that the transduction channels do not directly adapt to the force. However, many theories suggest that the transduction channels can directly adapt without the aid of myosin motors. This is a calcium dependent process, presumably with calcium binding directly to the channel. Many mechanisms have been proposed as to how calcium biases the transduction channel towards the closed configuration. Cheung & Corey (2006) found that channel-based adaptation is most consistent with a mechanism in which calcium binding increases the force needed to open the channel. This is equivalent to increasing the x_0 term in the open probability equation when calcium is bound to the channel. Without knowing the identity of the transduction channel, it is difficult to determine exactly how calcium binds to the channel. For the model, four calcium binding locations are included. When calcium binds to each of the binding locations, it increases the force needed to open the transduction channel by an amount termed $F_{calcium}$.

How does calcium binding to the channel affect the open probability curve and F-x curve when the tip link is stimulated directly? During normal hair cell physiology experiments, myosin-based adaptation is also present, which makes it more difficult to distinguish channel-based adaptation from myosin-based adaptation. Figure 5 shows the open probability and F-x curve for $F_{calcium}$ varying from 0

pN to 2 pN. As $F_{calcium}$ is increased, there is a distinct trend in which the probability curve becomes less steep for lower open probabilities only. After enough force is applied to the transduction channels, then the open probability curve resumes steepness similar to the case in which calcium cannot promote channel re-closure. For the most part, the F-x curve appears to simply be shifted along the abscissa.

In this model, calcium can enter through the transduction channel and bind to the channel in a matter of a few microseconds. This allows calcium to have an immediate effect on the open probability of the transduction channel. Therefore, as the open probability is increased, more calcium is allowed to enter through the channel which will immediately reduce the open probability. The consequence of this rapid feedback is that the slope of the open probability curve appears as if the channel has a smaller gating force, at least for smaller stretches. For larger extensions of the gating springs, calcium binding to the channel has reached a saturation point that can no longer rapidly shift the open probability curve. Beyond this transition point, the open probability curve appears to have the same gating force as the situation in which calcium does not bind to the transduction channels. This is less apparent when one examines the F-x curve. The negative stiffness region in the F-x curve generally forms near the greatest change of open probability. $F_{calcium}$ holds the open probability low until the transition point, after which there is a much larger change in the open probability. This causes the F-x curve to appear fairly normal but shifted along the x axis.

The open probability curve displays a distinct biphasic nature when calcium is allowed to bind to the channel and promote channel re-closure. This distinct transition is never seen when the whole hair cell bundle is stimulated. The most obvious interpretation is that myosin adaptation obscures this effect in a whole hair cell bundle by producing additional adaptation.

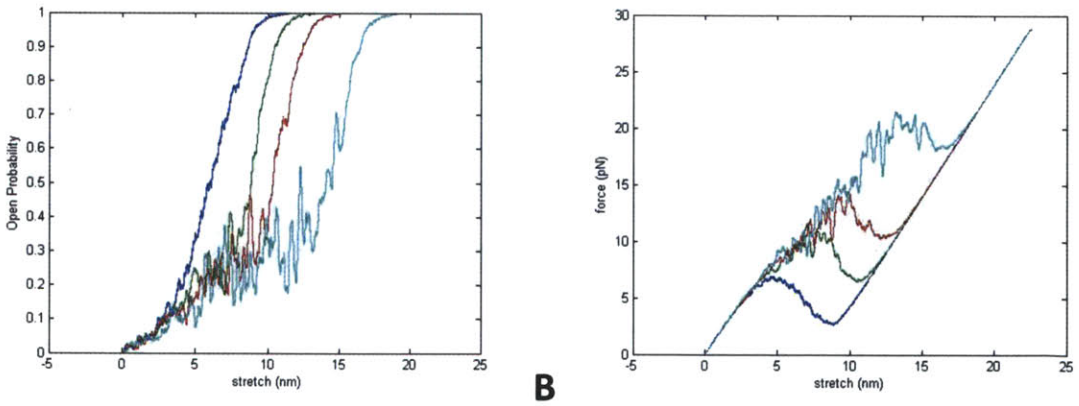

Figure 5. Open probability and force profiles for various channel re-closure force on the channel, $F_{closure}$ with calcium bound. The gating spring was stretched over 0.3 sec. The force acting on the tip link was filtered using a moving average filter with a width of 5 msec. k_g=1 pN/nm, d=8 nm, x_0 =3 nm for all, $[Ca^{+2}]_{ext}$=1.5 mM. Blue: $F_{closure}$ =0 pN, green: $F_{closure}$ =0.5 pN, red: $F_{closure}$ =1 pN, cyan: $F_{closure}$ =2 pN. **(A)** Open probability versus stretch. **(B)** Force versus stretch.

A better experiment for probing this mechanism is to pull on the tip link directly with laser tweezers for various calcium conditions. Increasing the external calcium concentration should shift the transition point to the right on the I-X curve. This experiment bypasses myosin adaptation; therefore, any shift in the I-X curve with increased calcium would be based strictly on a channel-based adaptation. Figure 6 shows an expected result for such an experiment. As expected, increasing the external calcium concentration shifts the transition point in the I-X curve to the right. This can be seen in both the current traces and force traces. This experiment would serve as direct evidence of channel-based adaptation that is sensitive to calcium. Such an experiment can also be used to determine the affinity of calcium for the transduction channel, if the intracellular calcium is controlled, as well as the change in force needed to open the channel after calcium binds. Alternatively, no shift in the I-X curve might be seen for changing calcium concentrations. This would be strong evidence against channel-based adaptation. This direct experiment is the best way to distinguish between channel-based adaptation and myosin-based adaptation, as other experiments that look to disrupt the myosin motors can have potential complications that make the result confusing.

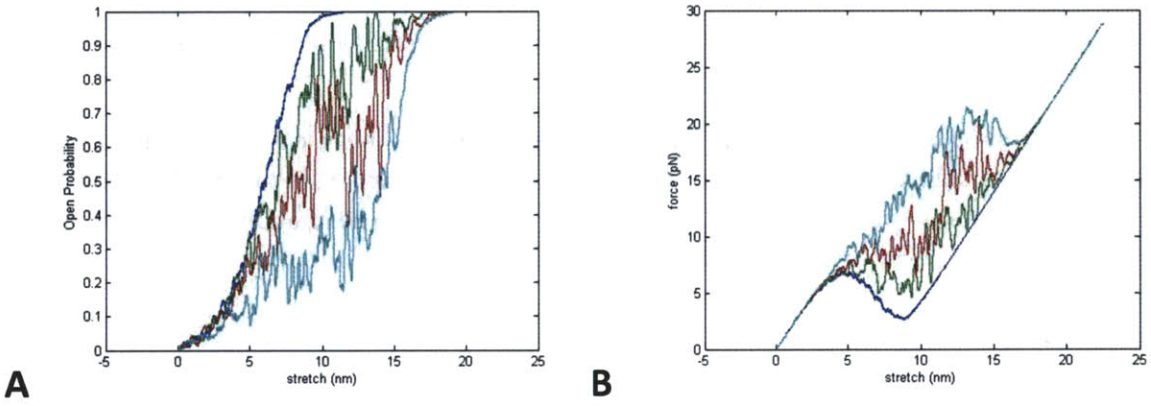

Figure 6. Average open time and force profiles for various external calcium concentrations. The gating spring was stretched over 0.3 sec. The force acting on the tip link was filtered using a moving average filter with a width of 5 msec. k_g=1 pN/nm, d=8 nm, x_0 =3 nm, and $F_{closure}$ =2 pN for all. Blue: $[Ca^{+2}]_{ext}$ =0 mM, green: $[Ca^{+2}]_{ext}$ =0.25 mM, red: $[Ca^{+2}]_{ext}$ =0.5 mM, cyan: $[Ca^{+2}]_{ext}$ =1.5 mM **(A)** Average open time versus stretch. **(B)** Force versus stretch.

Direct Channel Stimulation with Myosin Adaptation Present

The previous section examined an experiment in which the stretch applied to the tip link was directly controlled. Analyzing the gating mechanisms in this manner is not only important to build a conceptual foundation of transduction but also describes conceivable experiments to perform using laser tweezers. *In vivo*, there is strong evidence that adaptation occurs by the means of myosin-1C at the upper end of the tip link. Myosin adaptation relaxes the stretch applied to the tip links. Ideally, one would like to perform a similar experiment in which the myosin motor complex is intact at the end of a

tip link, the myosin motors are displaced and allowed to move naturally. Laser tweezers have been used to study the binding force of myosin-1C to actin attached to a silica bead. One could suppose that a bead under laser tweezer control containing actin could provide a deflection to the upper end of the tip link. If the bead position is maintained within a few nanometers, then the adaptation rate of myosin attached to a tip link could be measured. In practical terms, this would be nearly impossible to perform, because the myosin is normally intracellular and the bead is extracellular. Nonetheless, simulations examining this experimental setup provide a good insight into how myosin-based adaptation works. This can simplify the *in vivo* case which measures the current and force from a whole bundle containing adaptation.

The simple explanation of how myosin-1C causes adaptation in hair cells is that a complex of myosin-1C motors continually attempts to climb towards the tallest end of a stereocilium. Without tension in the tip link, the motor complex would eventually climb up the actin core and reach the top of the stereocilium. When the motor complex is attached to a tip link, the force that develops from the gating springs is directed to pull the motor complex down the actin core. The action of the myosin motors is modeled with two key parameters: F_{myosin}, which is the force that the motors are capable of exerting, and β_{myosin}, which is the drag coefficient of the motors with the actin core. A high drag coefficient can be thought of as the motors binding strongly and for longer duration to the actin core of a stereocilium. Calcium near the myosin motors has the effect of reducing F_{myosin} and β_{myosin}. Decreasing the drag coefficient implies that the motors will respond quickly to any change in tension by climbing or slipping, subsequent to a negative or positive deflection, respectively.

One would think that the action of the adaptation motors should be easy to predict. Increasing the stretch on the gating springs increases the force which pulls the adaptation motors down the actin. Decreasing the stretch on the gating springs decreases the overall force which allows the motors to climb up the actin core. However, as was shown in the previous section, the opening of transduction channels reduces the overall force in the tip link. This gating compliance affects the force felt by the adaptation motors as well as the overall force in the hair bundle. For a single tip link with two transduction channels at the lower insertion point, the downward force on the myosin motor complex would be reduced by a factor of $k_g d$ or $2k_g d$, which can be 10 pN or more, when one channel or two channels are in the open configuration, respectively. This can have a profound effect on the tension on the adaptation motors and their slipping or climbing rate.

Panels A and B of Figure 7 display an I-X curve and F-X curve created without myosin motors, in the same manner as the previous section. Panel B shows that this particular set of parameters creates a region of negative compliance. Using these gating parameters, active myosin adaptation was added. F_{myosin} and β_{myosin} were initially set at 5.5 pN and 5000 pN-μsec/nm respectively for this simulation. The value for F_{myosin} is very important in how myosin motors behave at rest. Panel 7B shows that the dip in the stiffness occurs at values higher than 5.5 pN. Therefore, the myosin motors do not have enough force to pull the tip link over this hill and to stretch the gating springs past the region of negative stiffness at rest. Instead, they maintain a resting stretch of around 4 nm, given the myosin motor force.

For this simulation, the tip link was quickly stretched to an initial displacement and the myosin motors were then allowed to respond to the force and readjust the tension in the gating springs. Panel C of Figure 7 shows how the myosin motors react to the force following an initial stretch plotted on the abscissa. In this case, a negative myosin velocity refers to the myosin climbing up the actin. For large positive steps the motors respond by moving down the actin core. For steps that move the myosin complex to have less tension than the baseline value, the myosin climbs up the actin core. These are the simple cases that respond exactly how one would expect. However, the myosin velocity curve also contains a region that dips below zero for initial stretches near 7 nm. This region corresponds to the local minimum on the F-X curve. This implies that when the tip link is stretched further than at rest, the myosin motors respond, over a particular region, by climbing up the actin core which increases the stretch even further. They can do this because the channels open, reducing tip link tension.

The consequence of this effect can be seen in panel D of Figure 7. Here, the stretch after the indicated amount of time is plotted versus the initial stretch. As can be seen, the myosin motors settle around two distinct stable positions. For initial stretch values above 7 nm, the post-adaptation stretch ends up near 7.5 nm. For deflections below 7 nm, the post-adaptation stretch ends up settling around 4 nm, which is the stable position at rest. The second stable position occurs at a position in which both transduction channels are biased to be open. This means that the overall stretch can be increased by around the length of the gate swing to create the same tension in the tip link as in the first stable location, in which both transduction channels are likely to be closed the majority of the time. The distance between the two stable points is not exactly the gate swing because the two locations do not correspond to 0% open probability and 100% open probability. In reality, these two locations correspond to 25% and 85% open probability, which is why the distance between the two stable points is actually 3.5 nm and not the gate swing distance of 5.5 nm.

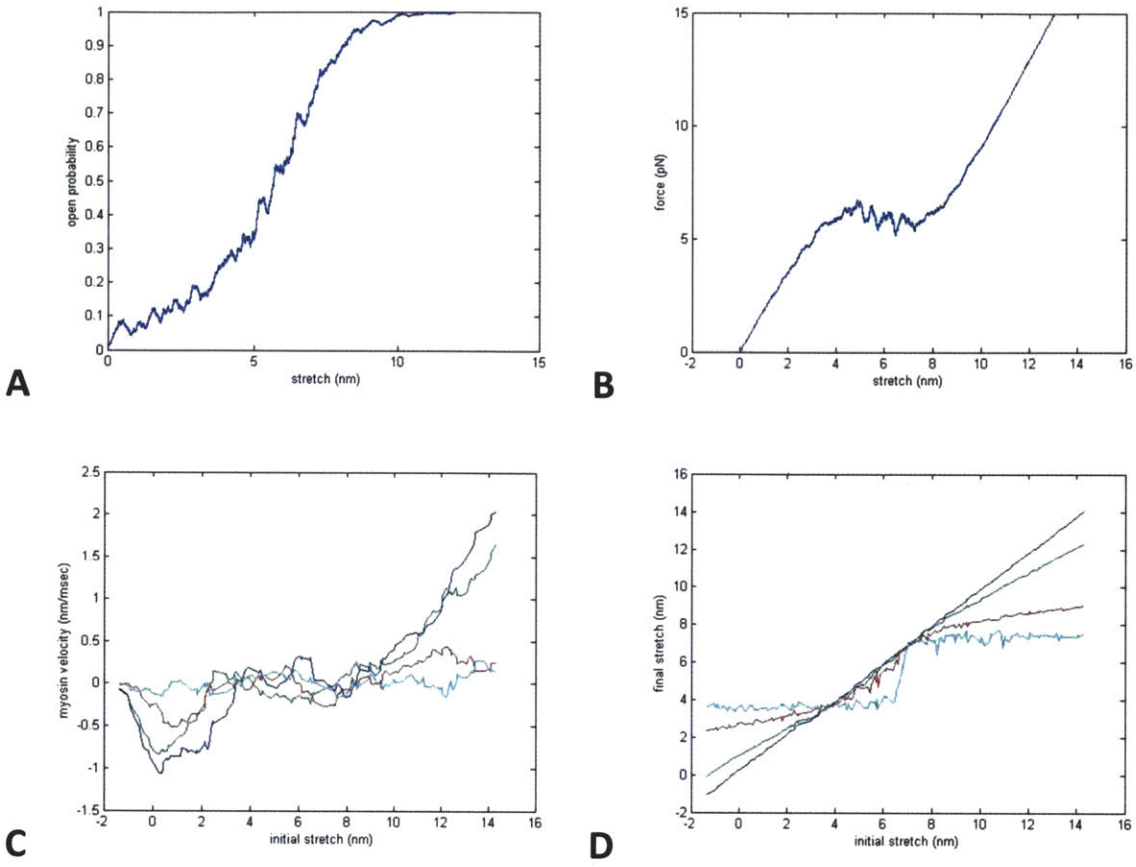

Figure 7. Myosin response to tension along the tip link. K_g=1 pN/nm, d=5.5 nm, x_0 =3 nm. **(A)** Estimated open probability curve without myosin motors. **(B)** Force curve for same simulation. **(C)** Myosin velocity with negative values interpreted as traveling up the stereocilium with F_{myosin}=5.5 pN and β_{myosin}=5000 pN-μsec/nm, blue: 0.1 msec, green: 1 msec, red: 5 msec, cyan: 20 msec. **(D)** Average stretch after myosin motion for a given amount of time using the same colors as in panel C.

To determine the open probability for the given myosin position, the values from panel 7D were evaluated using the I-X curve displayed in Panel 7A. This allows the current versus initial stretch curve to be created for various times after the initial stretch of the tip link. The result is displayed in Figure 8A. The initial curve is very similar to the I-X curve from figure 7A which is to be expected because the myosin motors have not had enough time to adapt at this point. At 20 msec post stimulus, the I-X curve has essentially become tighter. For this particular set of gating parameters, the myosin motors act to move the current to one of two values.

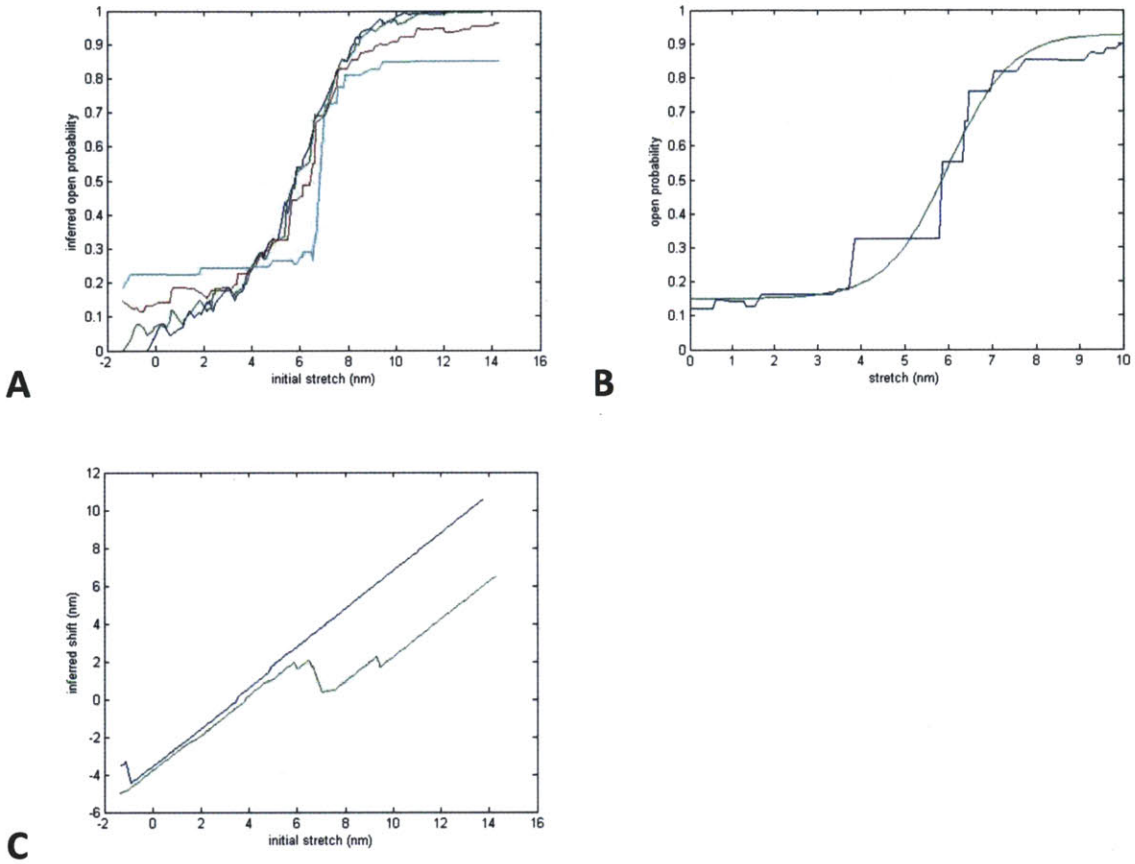

Figure 8. (A) Stretch positions from figure 7C evaluated using the open probability curve of figure 7A, F_{myosin}=5.5 pN and β_{myosin}=5000 pN-μsec/nm. Blue: 0.1 msec, green: 1 msec, red: 5 msec, cyan: 20 msec. **(B)** F_{myosin}=4.3 pN and β_{myosin}=400 pN-μsec/nm, blue: open probability made from the stretch positions evaluated using figure 7A, green: I-X curve made using equation 8 with k_g=1 pN/nm and d=8 nm. **(C)** Inferred shift of I-x curve at 20 msec. Ordinate displays the amount that the stretch changed after 20 msec from the initial stretch with positive values representing shifts in the negative direction. Blue: high calcium equivalent (F_{myosin}=4.3 pN and β_{myosin}=1000 pN-μsec/nm); green: low calcium equivalent (F_{myosin}=5.5 pN and β_{myosin}=5000 pN-μsec/nm).

The tightening of the I-X curve could explain an interesting result seen in physiological experiments: manipulations that reduce the stall force of the myosin motors, such as reducing the external calcium concentration, oftentimes causes the I-X curve to appear broader (Assad, Hacohen, & Corey, 1989; Crawford, Evans, & Fettiplace, 1991). One would traditionally think that adaptation should make the I-X curve look broader as adaptation shifts the curve during a stimulus. However, this example shows that if two stable points exist for the force curve, then the current will move to two different values which appear as a very steep I-X curve when measured. The speed at which this occurs depends on the rate at which myosin motors adapt. As the myosin drag coefficient is reduced, such as when calcium is present, then the current moves to the two discrete stable points faster.

Figure 8B was made with the gating parameters used previously but with myosin parameters arising from an environment in which a high external calcium concentration is present. For this simulation, F_{myosin}=4.3 pN and β_{myosin} =300 pN-μsec/nm. The blue trace represents the inferred probability using the stretch values 0.1 msec post-deflection. This time point was chosen to represent the delay that one might see during an actual physiological experiment when the peak transduction current is measured. The peak current can be delayed by the drag of the deflection as well as by the membrane time constant created by the capacitance of the cell membrane. Even though the blue curve was created using k_g=1 pN/nm and d=5.5 nm, a curve was fit by using equation 8 with k_g=1 pN/nm and d=8 nm and scaling for less current. This shows how adaptation can make it difficult to accurately measure the gating parameters.

The behavior discussed here is not in line with the traditional view that myosin adaptation always acts to return the transduction current to the baseline level. Much of this has to do with the choice of gating parameters and myosin parameters. Within a single hair bundle there is no reason to suspect that the gating spring stiffness or gate swing vary from channel to channel. The values are most likely very similar although they could vary slightly from channel to channel. Along the same line of reasoning, each tip link is most likely constructed in a similar manner with the myosin motor complex being relatively similar at the upper insertion point of the tip link. However, myosin is regulated by calcium and the intracellular calcium concentration varies from stereocilium to stereocilium. This creates a variety of myosin motor strengths and drag coefficients within a single hair bundle.

Typically, the inferred shift method can be used to determine the amount of adaptation that occurred (Sheperd & Corey, 1994). This technique involves shifting the I-X curve along the abscissa in order to account for adaptation. The underlying assumption is that the shape of the I-X curve does not change during adaptation but simply slides along the abscissa. This technique was utilized in Panel C of Figure 8 for simulations run with two sets of myosin parameters. The blue trace was made with F_{myosin}=4.3 pN and β_{myosin}=1000 pN-μsec/nm and the green trace with F_{myosin}=5.5 pN and β_{myosin}=5000 pN-μsec/nm. These essentially represent myosins in high and low calcium concentrations, respectively. The curves represent the amount of adaptation shift after 20 msec. The blue trace is completely linear which indicates that adaptation was complete for this case; the offset stems from the initial resting position of the tip link. Conversely, the green trace is not a straight line but is made up of two parallel line segments with the same slope. The line segment on the right represents incomplete adaptation and is made possible by the strength of the myosin motors for this particular simulation.

These traces were made from individual tip links. Typically, when the inferred shift method is used, the shift does not produce complete adaptation but has a percentage of current that does not adapt. Traditionally, the view point was that all myosin motors within a stereocilia adapt in the same manner. Therefore, all of the myosin motors would adapt slightly incompletely. Here, an alternative viewpoint is raised. The overall current for a hair cell is a composite from many tip links and transduction channels within the hair bundle. Depending on the local calcium concentration, some of the tip links may be attached to strong myosin motors and some may be attached to weak myosin motors. After a deflection, the weak myosin motors are likely to adapt fully back to their positions at rest in which both attached transduction channels are likely to be in the "mostly closed" state, whereas

the strong myosin motors will maintain enough force so that they can balance the force where both transduction channels are in the "mostly open" state. The terms mostly closed state and mostly open state will now be used to refer to the two stable positions in which the open probability is closer to 0 or 1, respectively. The measured shift of adaptation in a real physiological experiment would therefore be a weighted average of tip links that end up in the mostly open state and the mostly closed state.

This idea gives an explanation to the incompleteness of adaptation that has previously been described but where a proper mechanism has never been given (Shepherd & Corey, 1994). It utilizes the function of myosin motors, which are well documented, and does not necessitate an additional mechanism. It simply requires a negative region of stiffness for an individual tip link. Ideally, having a spectrum of different myosin motor strengths also creates diversity throughout the hair bundle. However, each transduction channel behaves stochastically, responding to thermal fluctuations in the surrounding fluid. Therefore, for two tip links with identical gating parameters and myosin parameters one could be stuck in the mostly open position while the other is stable in the mostly closed position. In fact, the myosin motor complex is constantly climbing or slipping based on the number of channels that are open at a given instant. When both channels are closed, the myosin motors maintain a stretch that biases the transduction channels to stay mostly closed, therefore this position is relatively stable. The same is true for when both channels are mostly open. It is difficult to maintain a stretch that keeps only one transduction channel open and not the other. The channels probably have the same gating spring tension and will flicker open and closed at the fifty percent open probability point. Each time a channel closes, the tension increases and the myosin motors respond by sliding down actin which decreases the open probability for both channels, and every time a channel opens the myosin motors respond by climbing which increases the open probability for both channels. For this reason, a half open state is inherently unstable.

Even without any force on the channel, thermal noise can occasionally cause a transduction channel to transition from the closed conformation to the open conformation. If both transduction channels attached to a tip link are open long enough, then the myosin motor complex has enough time to climb up the actin and reach the mostly open stable position for the tip link. The same can be said for the reverse process, a prolonged period of channel closure pulls the myosin motor complex towards the mostly closed state. For a given set of gating parameters, the rate at which this occurs depends on the myosin motor force and drag coefficient. A higher motor force increases the likelihood that the complex will end up in the mostly open state. A low drag coefficient creates more transitions from one state to another, as the motors can respond quickly to rapid channel fluctuations.

Figure 9 shows the rate at which transitions occur from these two stable positions. For these simulations, the transduction parameters and myosin parameters were set at K_g=1 pN/nm, d=6.5 nm, x_0 =3 nm for a single tip link. The myosin motor complex was allowed to move freely in response to the force and from the gating springs. Initially, β_{myosin} was set at 100 pN-μsec/nm, which is quite low for myosin-1C. The calcium concentration near the myosin motors decreases the drag coefficient, making an exact value difficult to ascertain. In high calcium concentration, the myosin drag rate has been estimated as 34000 pN-usec/nm (Gillespie & Cyr, 2004) and as low as 500 pN-usec/nm (Tinevez *et. al.*, 2007). The value used here is very low but was chosen so that many transitions would occur in 1 second

of simulation. Later, reasoning will be given as to why this value may actually be lower than previously speculated.

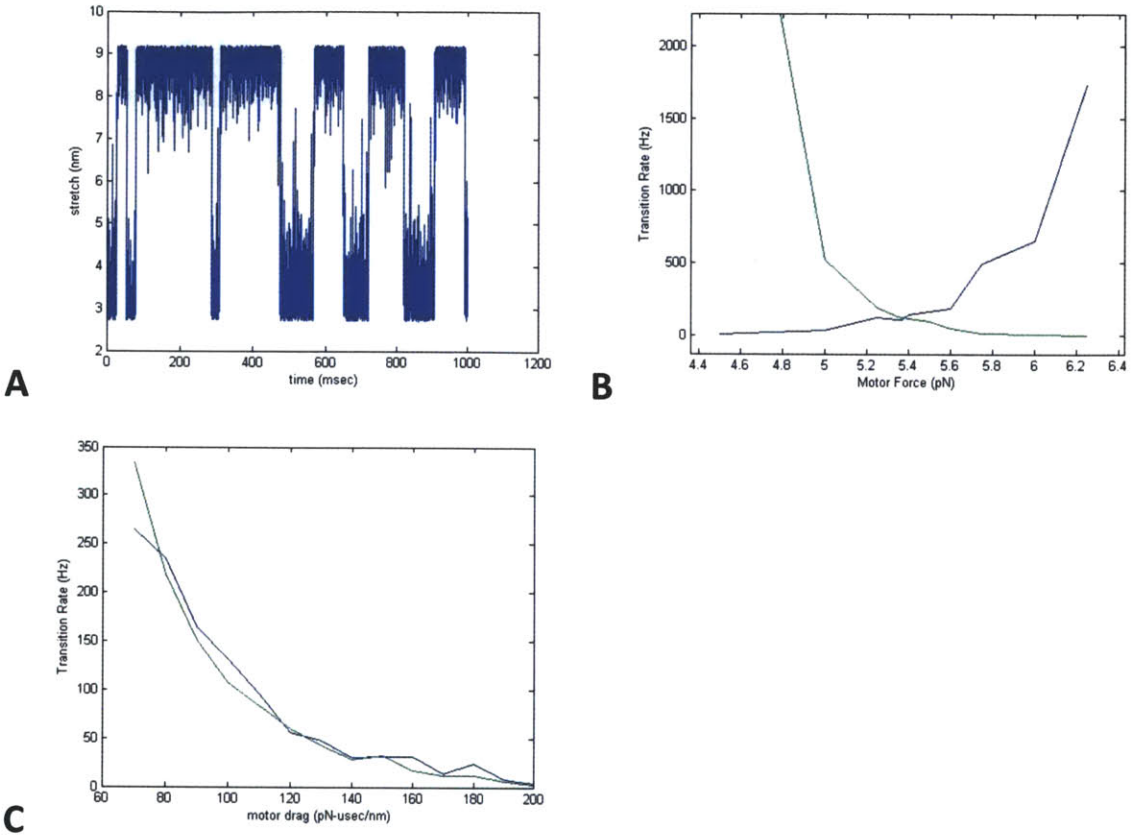

Figure 9. Measurement of stretch on gating spring for an un-stimulated tip link attached to a myosin motor. K_g=1 pN/nm, d=6.5 nm, x_0 =3 nm for all. **(A)** Stretch versus time for F_{myosin}=5.38 pN and β_{myosin}=180 pN-usec/nm. **(B)** Measurement of transition rate from low to high stretch (blue) and high to low stretch (green). B_{myosin}=100 pN-μsec/nm for all but F_{myosin} varies for different simulations. **(C)** High to low transition (blue) and low to high transition (green) with F_{myosin}=5.38 pN for all, but β_{motor} varies for different simulations.

Examining Panel A of figure 9 shows a typical simulation in which the myosin motor jumps back and forth between two stable positions. A subroutine was used to analyze the data. A "low-to-high transition" from the mostly closed state to the mostly open state was said to have occurred only when the stretch passed above 75% of the maximum stretch for the simulation. A "high-to-low transition" only occurs when the stretch position dropped below 25% of the maximum stretch. This technique creates hysteresis to prevent counting transitions that did not actually occur. The average time before a transition occurred was used to calculate the low-to-high and high-to-low transition rates. This simulation was performed for a range of myosin forces and the results are displayed in panel B of figure 9. As expected, lower myosin forces tend to bias the system towards the mostly closed state, so the high-to-low transition rate is very fast while the low-to-high transition rate is comparatively very low.

The converse is true for higher myosin forces, which tend to bias the system towards being stable in the mostly open state. The rates are balanced around 5.38 pN of myosin force which is between the local maxima and local minima that define the negative stiffness region for this F-X curve. The force minimum occurs at 4.5 pN and the force maximum at 7.5 pN. One might expect the rate midpoint to occur at the midpoint between the forces which is 6 pN. However, the stable positions actually occur in a range. Panel A shows how the distribution is tighter towards the mostly open state. This makes the open to closed transition less likely to occur. Therefore, at 6 pN the system is balanced towards the mostly open configuration. For this reason, the balanced point for the rates occurs below the midpoint of the force maxima and minima. In this case, that value occurs at 5.38 pN. An exponential fit was made for both the low-high and high-low transition rates. There are:

$$Transition\ Rate_{Low-High} = 2e-6\exp\left[3.3165F_{myosin}\right](Hz) \quad \text{(eq. 17)}$$

$$Transition\ Rate_{High-Low} = 1e12\exp\left[-4.2652F_{myosin}\right](Hz) \quad \text{(eq. 18)}$$

To test how the rates vary with the myosin drag coefficient, the myosin force was maintained at 5.38 pN while the drag coefficient was varied. As panel C shows, both the low-to-high and high-to-low transition rates vary at the same rate with the drag coefficient. The average of the curves was fit with an exponential for these particular gating parameters and myosin motor force of the form:

$$Transition\ Rate = 2256\exp\left[-0.0291\beta_{\mathrm{myosin}}\right](Hz) \quad \text{(eq. 19)}$$

This equation predicts the change in the transition rate for both the low to high and high to low transitions as they vary with the myosin motor drag for the same motor force. A product of exponentials was used to predict the transition rate when both the motor drag and motor force terms are independent variables. These equations are:

$$Transisition\ Rate_{Low-High} = 3.85e-5\exp\left[3.3165F_{myosin}\right]\exp\left[-0.0291\beta_{myosin}\right](Hz) \quad \text{(eq. 20)}$$

$$Transition\ Rate_{High-Low} = 1.96e13\exp\left[-4.2652F_{myosin}\right]\exp\left[-0.0291\beta_{myosin}\right](Hz) \quad \text{(eq. 21)}$$

These equations do a good job of predicting the transition rate for a range of myosin motor forces and drag coefficients for the given gating parameters.

Ideally, one would like to use these equations to predict how long adaptation will take to restore the transduction current to the baseline level after a deflection. This involves a population of tip links all

with their own myosin motors. For a real hair bundle, each myosin motor complex will have its own parameters. For this analysis, they are assumed to be the same. In this case, each complex will have the transition rates and the mean time that it takes for all of myosin complexes to transition back to the baseline level is the net time that it takes for one complex to transition to the low stable point. This involves taking the difference between the transition rates:

$$Full\ Adaptation\ Rate = Transition\ Rate_{High-Low} - Transition\ Rate_{Low-High} \quad \text{(eq. 22)}$$

$$Full\ Adaptation\ Rate = \exp[-0.0291\beta_{myosin}]\,[1.96e13\exp[-4.265F_{myosin}] - 3.85e-5\exp[3.317F_{myosin}]] \quad \text{(eq 23)}$$

This equation determines the time that a myosin complex takes to go from the high stable point to the low stable point while taking into consideration the transitions in the reverse direction. It should be noted that complete adaptation will never occur if the myosin force is too high. In this case, the system is biased towards the mostly open stable point. For these equations, this point occurs at F_{myosin}=5.25 pN which is close to the value of 5.38 pN that was found directly from the simulations. This equation is valid only for myosin parameters close to those used for the simulation. Using this equation, one can test the complete adaptation time for various myosin parameters, which is just the inverse of this equation. For example, if F_{myosin}=4.8 pN then the tip links are in the mostly closed configuration at rest. However, after a deflection the adaptation rate depends on β_{myosin}. For a motor drag coefficient of 400 pN-μsec/nm, adaptation should be complete in 4.5 seconds. This is a rather large amount of time for a physiological experiment but is still feasible to test. If β_{myosin} has a value of 600 pN-usec/nm, then complete adaptation should take 25 minutes. This essentially means that the adaptation will never be complete for this particular tip link. This points out how sensitive this effect is to the actual myosin drag coefficient. Calcium can affect the value of this parameter and can change a tip link from one that does not adapt completely to one that does adapt completely.

As mentioned earlier, these values for the myosin drag coefficient are quite low compared to the expected values. Previous values have been calculated by measuring the rate of adaptation in a hair bundle (Gillespie & Cyr, 2004). The assertion here is that this value actually takes into account all of the myosin motors which is rather complicated. Some of the myosin motor complexes will get stuck in the mostly open state while others will adapt back down to the mostly closed state. By measuring the rate of adaptation, experimenters are actually measuring the adaptation rate as defined in equation 20. Any measurement of the myosin drag coefficient will therefore greatly overestimate this parameter. A proper determination of this parameter could be done using laser tweezers. For such an experiment, force should be applied to myosin-1C while the motors are allowed to bind and climb up actin. The calcium modulation can also be determined during such an experiment.

The endolymphatic extracellular calcium concentration in mammalian cochlea is very low, around 20 μM (Bosher & Warren, 1978). This means that the myosin drag coefficient should be quite high in mammalian cochlear hair cells *in vivo*. Therefore, adaptation is not likely to be complete unless there are other factors that regulate this myosin's motility. It seems strange that myosin-1C is an

essential component of the transduction apparatus in hair cells but provides very poor adaptation in the mammalian cochlea. In the vestibular system, myosin-1C provides nearly complete adaptation. The difference in the two systems is in the nature of the native stimulus. In the vestibular system, the stimulus can deflect the hair bundles in a step-like manner. Therefore, myosin-1C must adapt completely to prepare the hair bundle for additional stimuli. This is accomplished by keeping the myosin drag coefficient low. By contrast, mammalian cochlear hair cells need to respond very rapidly to sinusoidal stimuli. Therefore, adaptation does not need to be complete; the negative half cycle of the sinusoidal stimulus will quickly close the transduction channels. In the mammalian cochlea, myosin-1C serves less as an adaptation motor but acts to ensure that the tip link is positioned in the most sensitive region of the I-X curve. In addition, it may serve to increase the sensitivity of the hair bundle by quickly moving to the mostly closed stable position for negative deflections and the mostly open stable position for positive deflections.

Transduction in Whole Hair Bundles without Calcium Feedback

Most models of hair cell transduction assume that all the transduction complexes within a hair bundle are essentially identical in their response to stimulation. Top links keep the tips of stereocilia together during a deflection which means that each tip link receives the same amount of shearing from the hair bundle deflection. In addition, most models equate adaptation to a shifting of the I-X curve as a whole. This implicitly assumes that adaptation, works in a similar manner across the whole hair bundle. The work presented in this thesis on calcium diffusion (see calcium chapter) suggests that the calcium concentration near each myosin motor complex is unique. Furthermore, even identical myosin motor complexes will behave differently from each other based on the stochastic nature of the transduction channels. Most models of adaptation assume that calcium influx through transduction channels is important for establishing the rate of fast and slow adaptation following a stimulus. However, calcium can take a few milliseconds to diffuse down to the adaptation motor complex, which is slower than the action of adaptation.

In the previous section, it was shown that myosin motors behave depending on the force acting on them from the gating springs, delivered by the tip link. Calcium clearly modulates the force that the myosin motors can deliver but the system is still active even without calcium modulation. The model structure of a bullfrog saccular hair bundle consists of 48 tip-links each with two transduction channels at the lower insertion point. Each tip link applies force to the hair bundle as a whole which changes how the hair bundle responds to force. Also, the combined current from 96 transduction channels creates whole bundle transduction currents that mimic physiological currents, even without feedback from calcium. To explore this notion, model hair cells without calcium feedback are simulated for this section. For these hair cells, each tip link is essentially identical. The gating parameters and myosin motor parameters are the same throughout the entire hair bundle. This technique is utilized to determine what characteristics of hair cell physiology can be explained without the presence of calcium.

The origin of slow adaptation is commonly believed to stem from the action of myosin-1C. For a positive deflection, the tip links are stretched due to the shearing action of the stereocilia. The increase in stretch increases the force in the gating springs which in turn increases the open probability of the transduction channels. Myosin-1C responds to the increase in force by slipping down the actin core of the stereocilia. As was shown in the previous section, the force acting down on the myosin motor complexes can be quite complicated, due to the nonlinear force curve created by the gating compliance of the transduction channels. This means that the adaptation motors can move with different velocities as they adapt to a stimulus, or even get stuck so that the transduction channels are mostly open.

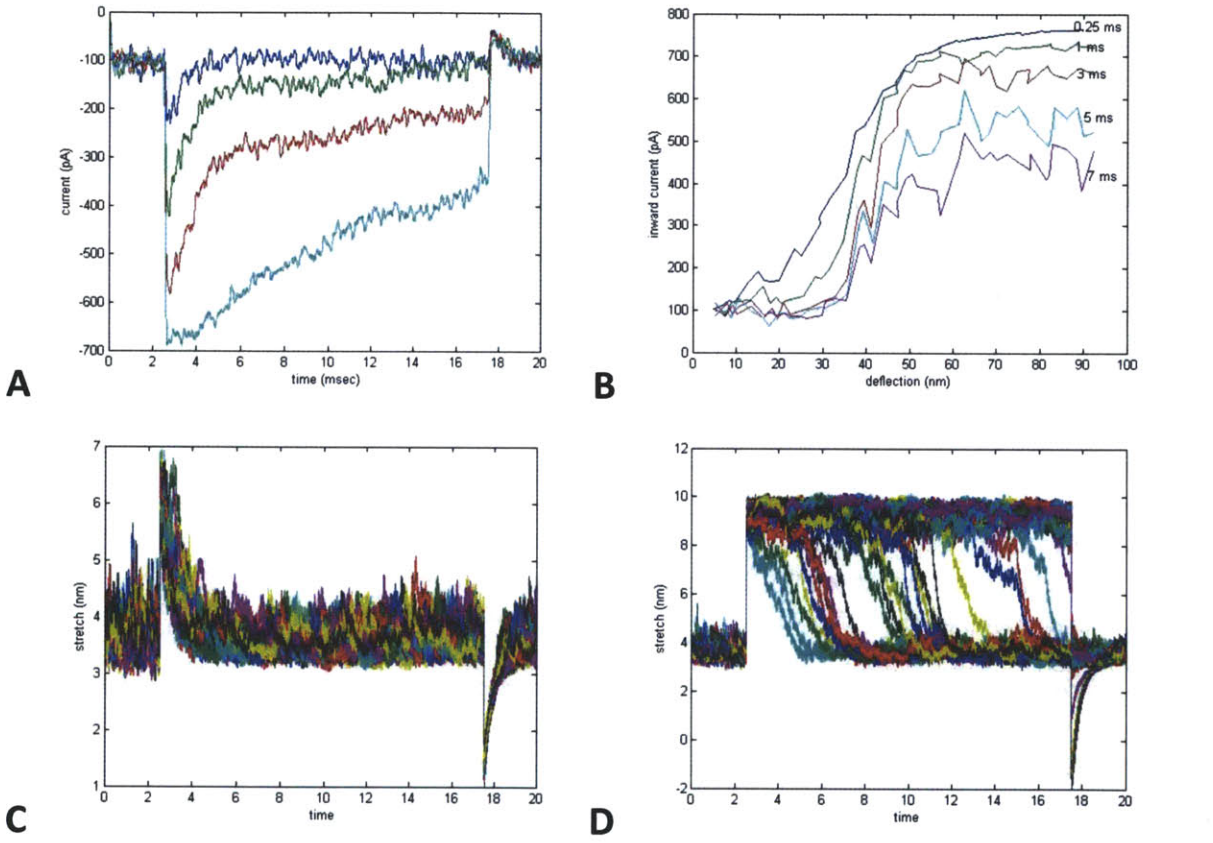

Figure 10. Transduction in a whole hair bundle deflected with a stiff probe (k_{probe}=50 pN/nm) with every tip link containing the same parameters. K_g=0.8 pN/nm, d=7 nm, x_0 =3 nm, F_{myosin}=5 pN, and β_{myosin}=500 pN-μsec/nm for all. **(A)** Transduction currents for 20 nm (blue), 30 nm (green), 40 nm (red), and 50 nm (cyan) deflections. **(B)** I-X curve taken from panel A at various times following the deflection as displayed on the figure. **(C)** Stretch for 42 of the tip links during the 20 nm deflection. **(D)** Stretch for 42 of the tip links during the 50 nm deflection.

To examine how the current adapts to displacement steps, the hair bundle was deflected with a relatively stiff probe with a stiffness of 50 pN/nm. A stiff probe controls the hair bundle and prevents active bundle movements from complicating the recorded transduction current. K_g=0.8 pN/nm and d=7 nm to approximate values for a bullfrog saccular hair cell and create a region of negative stiffness. The

myosin parameters were set at F_{myosin}=5 pN and β_{myosin}=500 pN-μsec/nm to approximate the myosin values that one might see during an experiment performed with typical external calcium concentration. The resultant filtered transduction current is displayed in figure 10A. The displayed current shows many key features of transduction current. For small deflections, the current adapts quickly and completely. For slightly larger deflections fast adaptation is still present, but an additional component of slow adaptation also exists and adaptation is not complete. For an even larger stimulus, adaptation is dominated by slow adaptation and the adaptation is even less complete.

This result is remarkable in that it reproduces key features of adaptation without many of the elements typically used in modeling hair cell transduction. Fast adaptation is present without including a mechanism that allows calcium to bind to the channel to promote channel closure. Slow adaptation is present without allowing calcium influx to promote slippage of myosin-1C down the actin core under tension. Finally, incomplete adaptation is present without creating a mechanism that prevents myosin-1C from adapting completely. Previously, no physiological mechanism had been theorized to explain why slow adaptation is not complete. This model predicts incomplete adaptation consistently.

The mechanism for fast adaptation for this simulation occurs when the myosin motors slip down actin due to the increased force produced from the gating springs. In order for myosin-1C to produce fast adaptation, the myosin drag coefficient must be set lower than most researchers speculate for its value. However, even with a lower drag coefficient, slow adaptation still proceeds with a slower time course. By just looking at the rate of slow adaptation from the current trace, one would estimate that the motor drag coefficient should be 50 times higher than the value of 500 pN-μsec/nm used for this simulation. This value of 25000 pN-μsec/nm is more in line with the value that has been previously cited (Gillespie & Cyr, 2004). If adaptation proceeds so quickly directly following a stimulus, why does it occur so slowly following fast adaptation? The mechanism for slow adaptation and incomplete adaptation require further examination.

Figure 10B displays the I-X curve for this particular hair bundle for various times. Figure 10A illustrates a very common feature of adaptation: for small deflections, the current quickly drops back to the baseline level completely. But, for larger deflections the current takes longer to adapt and adapts incompletely. Put simply, small deflections are dominated by fast adaptation and large deflections are dominated by slow adaptation. Can the same mechanism really explain this difference in behavior?

As was discussed in the section examining single tip links with myosin motors, a myosin motor complex attached to a single tip link will tend to be stable at two distinct locations along the F-X curve: a mostly open state and a mostly closed state. A tip link that is not stretched sufficiently will not reach the mostly open state and will therefore quickly settle back in the mostly closed configuration. Figure 10C shows the stretch associated with 42 of the tip links within the hair bundle during the 20 nm step. This shows that all of the tip links quickly settle back down to the mostly closed state around 4 nm of stretch. This explains why small deflections are dominated by fast adaptation. For larger deflections, most myosin motor complexes will settle in the mostly open state. Then, due to the stochastic nature of channel opening and closing, each tip link has a chance of having its myosin motor complex resettle in the mostly closed state. Figure 10D shows the stretch of the tip links during the 50 nm step. Tip links

with a stretch around 10 nm are in the mostly open state. This figure shows a steady drop of myosin motor complexes down into the mostly closed state. This is reflected in panel A, which shows a decline in the current that is equivalent to the percentage of myosin motor complexes that have dropped down to the mostly closed state. After 15 msecs of simulation, which is a typical duration for a physiological experiment, roughly half of the motor complexes have dropped to the mostly closed state. This accounts for the adaptation being only roughly half complete for this duration of stimulus.

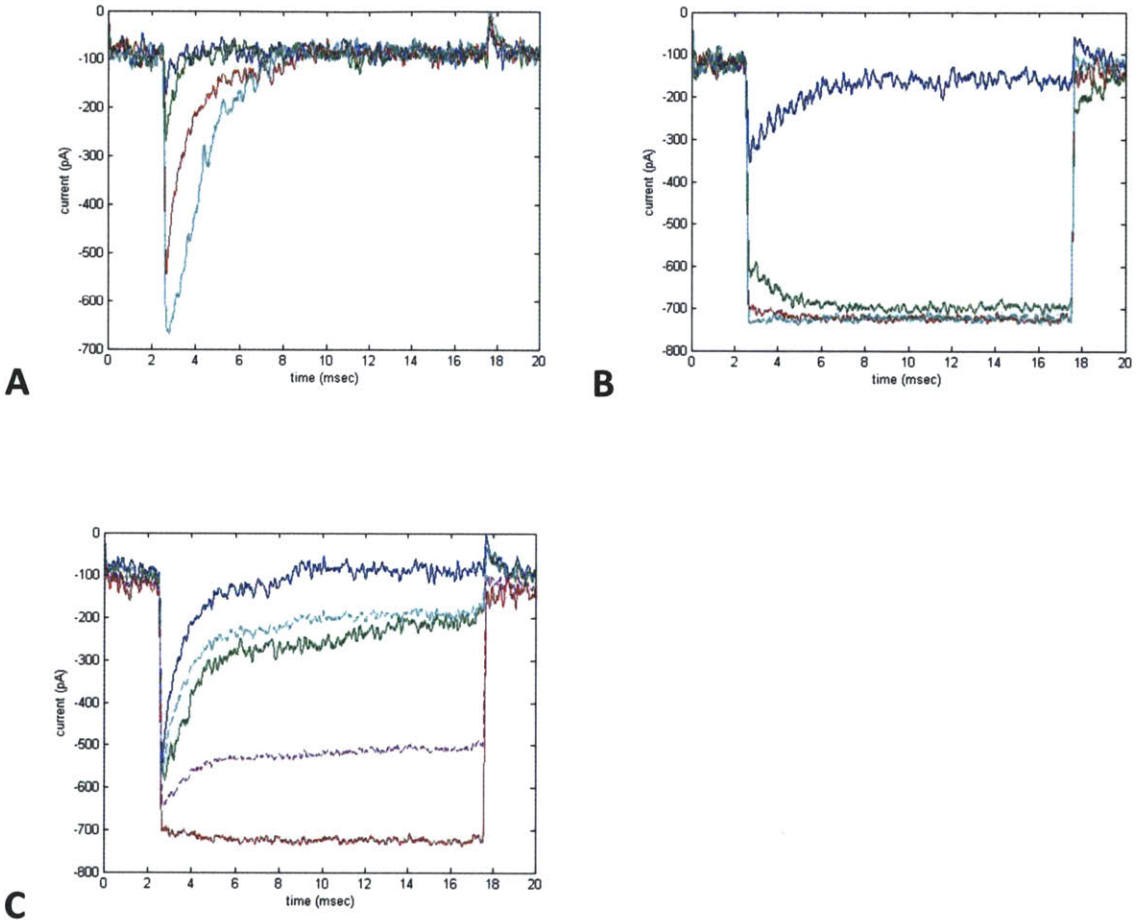

Figure 11. Transduction in a whole hair bundle deflected with a stiff probe (k_{probe}=50 pN/nm) with every tip link containing the same parameters. K_g=0.8 pN/nm, d=7 nm, x_0 =3 nm for all. **(A)** Transduction currents for 20 nm (blue), 30 nm (green), 40 nm (red), and 50 nm (cyan) deflections with F_{myosin}=4.6 pN and β_{myosin}=300 pN-μsec/nm. **(B)** Transduction currents with F_{myosin}=5.6 pN and β_{myosin}=1000 pN-μsec/nm using the same key as in A. **(C)** Transduction currents from 40 nm currents for the conditions used in 11A (blue), 10A (green), and 11B (red). Dashed curves represent weighted averages of the solid curves. Cyan: 60% blue, 30% green, 10% red, magenta: 10% blue, 30% green, 60% red.

This interpretation of adaptation means that slow adaptation originates from the fact that adaptation is incomplete rather than incomplete adaptation being caused by an unknown additional mechanism. This has the added benefit that the incompleteness of adaptation is calcium dependent,

which physiological experiments show is indeed the case. Increasing the calcium concentration is equivalent to decreasing the myosin force and drag values for this version of the model that does not incorporate calcium feedback directly. For a "high calcium" case, F_{myosin}=4.6 pN and β_{myosin}=300 pN-μsec/nm. Under these conditions, the current adapts quickly back to the baseline even for larger deflections, as shown in figure 11A. By contrast, if F_{myosin}=5.6 pN and β_{myosin} =1000 pN-μsec/nm, then the adaptation is very incomplete, as shown in figure 11B. This condition is meant to mimic a low calcium condition. In reality, the myosin motor force is set higher than it probably ever reaches *in vivo*, but is set this high in the model to demonstrate how a change in the myosin force greatly changes the behavior of adaptation.

Changing the properties of the myosin motor complexes not only changes the rate of adaptation but also changes the completeness of adaptation. *In vivo*, these changes are brought about by differences in the local calcium concentration near myosin motor complexes. In a real hair bundle, the local calcium concentration is not the same for all of the myosin motor complexes. The concentration changes based on the open probability of transduction channels located in the same stereocilium but not attached to the same tip link. Damage to tip links during dissection, or variable number of intact tip links *in vivo*, would therefore greatly change how the intracellular calcium concentration varies from hair cell to hair cell, and even more so from stereocilium to stereocilium. In addition, it is currently not known how the number of myosin molecules per tip link is regulated. Given the importance of this factor, one assumes that this would be tightly regulated in hair bundles. However, it could that some tip links have additional myosin-1C molecules added at the upper insertion point. This would likely increase the myosin motor force and drag coefficient. Overall, the transduction current within a single hair bundle is the sum of all of the transduction currents from all of the active tip links within the hair bundle. This means that the overall current appears as a combination of the currents made using different myosin parameters for the whole hair bundle. As an example of this, figure 11C shows filtered transduction currents from the three myosin conditions from figures 10A, 11A and 11B obtained from 40 nm deflections in solid lines. The rate of adaptation and completeness of adaptation clearly differs from trace to trace. The dashed traces represent weighted averages of the solid traces. Both dashed traces include 30% from the green trace, but the cyan trace includes 60% from the blue trace and 10% from the red trace while the magenta line includes the opposite contribution. This figure is meant to show an example of what one might measure during an actual experiment. The combined traces appear very similar to the traces made from single myosin parameters. One might therefore easily model the transduction current as originating from a hair bundle that only contains myosin motors with the same parameters. This explains why simpler models that lump the myosin parameters as uniform throughout the hair bundle produce fairly accurate results. In reality, the current could be coming from tip links with myosin motors that have very different parameters.

The point made here is that the output of the hair bundle does not provide information about the status of individual transduction channels. Only the average current from all of the transduction channels within in a hair bundle can be known. It is impossible to distinguish between a case in which two channels both have a 50% open probability and the case where one channel has a 0% open probability and another channel has a 100% open probability. The former case is the traditional view of

how hair bundle deflection affects transduction channels (Karavitaki & Corey, 2010) whereas a less extreme version of the latter case is supported in this work.

When a hair bundle is deflected with a probe with a stiffness that is relatively close or below that of the hair bundle, then the bundle has more freedom of motion. This allows active movements of the bundle that stem from internal changes of stiffness to be measured in terms of how the bundle moves. Mechanical correlates of adaptation have been observed using this technique. Slow adaptation tends to produce a slow movement of the hair bundle in the same direction that the stimulus is applied. This motion is much slower than what would be expected from the fluid drag of the hair bundle and is clearly an effect associated with a changing stiffness within the hair bundle. The correlate of fast adaptation is a "twitch" in the direction opposite of the stimulus. This motion is usually not larger than a few nanometers. The time course of both of these motions changes with the calcium concentration in the same way that the current adaptation time course changes which lends further proof to the claim that they are different measures of the same phenomena.

The idea behind the slow creep forward of the hair bundle is that as the myosin motors slip down actin, they reduce the force in the tip links. This is certainly a good explanation for this behavior but it also gets a bit tricky. As has been thoroughly discussed, each tip link can be producing roughly the same amount of force from the gating springs in a position that holds the transduction channels in either a mostly closed or mostly open configuration. As myosin complexes transition from a mostly open configuration to a mostly closed configuration, there is no actual net change in the force being produced by the gating springs in the tip link. Because of this, the myosin motors should always be pulled towards a lower force state, but this should occur at a faster rate than the current reaches a post-adaptation level. This, at least, is what one would expect without the addition of calcium influx through the transduction channels. An increase in the intracellular calcium concentration will decrease the myosin motor force throughout the entire hair bundle. The time course of this decrease in force is dependent on the time course of the calcium influx, which is indeed well correlated with the transduction current.

Current thinking about the twitch is that channel reclosure increases the force produced in the gating springs in the same way that the opening of channels decreases the force. The correlation with fast adaptation almost certainly implies that the twitch does indeed come from this increase of force associated with channels closing. The more interesting question is what causes the channels to close. For adaptation of the current, a theory was presented that explains fast adaptation through the slipping of myosin-1C. But, the twitch is also rather fickle. It does not occur for all deflections that produce fast adaptation. The twitch generally only happens for small deflections and always occurs quickly after the stimulus.

Figure 12A shows the position of a hair bundle when pushed with a stimulus probe with a stiffness of 2 pN/nm. The hair bundle has the same transduction parameters that were used in figures 10 and 11, with the myosin parameters being set to those for the high calcium condition, which produces weak myosin force. Under these conditions, the hair bundle displays very robust twitches for the larger deflections but not for the smaller deflections. Another interesting aspect about the twitches

is that the twitch near 60 nm is the largest and occurs fastest after the deflection. The larger deflections produce twitches with a delay following the deflection, are slightly smaller in magnitude, and have less of a smooth appearance.

The corresponding current in figure 12B helps explain the results about the twitch. For the two smallest deflections, there is an insignificant amount of current, which quickly adapts. For these deflections, the transduction channels don't open very much so there is not a major effect of gating compliance. Therefore, when the myosin motors adapt, there is simply a decrease in tension in the tip links. A decrease in tension results in the bundle moving slightly forward and cannot produce a twitch. For the deflection near 60 nanometers, most of the transduction channels have opened so the overall tension in the hair bundle is immediately reduced due to the gating compliance. But, the myosin motors are so weak under these conditions that they cannot stay in the mostly open configuration for long. Therefore, the motors are pulled down the actin of the stereocilia. This reduces the open probability of the transduction channels resulting in reduced transduction current. An overall increase in force happens for each individual tip link as the stretch decreases along F-X curves with regions of negative stiffness. Because all of the tip links contain myosin motor complexes with the same parameters, all of the transitions from the mostly open configuration to the mostly closed configuration occur at roughly the same time. The coherence of the transitions means that there is an overall increase in force throughout the entire hair bundle which produces a very strong twitch immediately following the stimulus. For larger deflections, the current reaches a peak that is near 100% open probability for all of the transduction channels. This means that the adaptation motors will initially create a net decrease in tension as they slip down the actin. When the stretch reaches a local minimum on the F-X curves, then the tension begins to increase as the myosin motors continue to slip. This has the additional effect of increasing the rate of slipping down actin. The delay in the twitch is present because it takes considerable time for the local minima to be reached. Even for identical myosin motor complexes, the time that it takes to reach this point is different for each tip link, based on the stochastic nature of channel gating. Each myosin motor complex will move through the region of increased tension with slightly different timing. The longer the delay to this point, the less of a chance of coherence between the individual myosin motor complexes. This results in twitches that have less magnitude and a less smooth appearance than for smaller deflections.

A completely different mechanical behavior occurs if the myosin motors are strong, mimicking the condition of very low calcium in the extracellular solution. This is displayed in figure 12C for the position and figure 12D for the current. For this condition, a twitch is never present. For the two smallest deflections, the position slowly creeps forward and the current adapts back down to the baseline level rapidly. For these deflections, the stretch of none of the myosin motor complexes was large enough to make it beyond the local maxima on the F-X curves. Therefore, tension pulled all of the myosin motors back down actin which reduced the tension in the tip links. For the trace shown in red, the deflection was just able to stretch the tip links past the local maxima on the F-X curves. Because of the negative stiffness regions, the myosin motor complexes paradoxically climb up the actin to reduce the tension in the tip link. This opens more transduction channels and has an overall effect of quickly reducing the overall tension in the bundle. This occurs very quickly after the deflection; essentially the

myosin motors act to enhance the gating compliance effect or produce a twitch in the positive direction. After the initial climbing of myosin motors, the stretch reaches local minima on the F-X curves. At this point, the myosin motors can still produce enough force to continue climbing up the actin until a balance of force is established at the mostly open configuration. As this happens, the tension in the tip links again begins to slowly increase. This results in the bundle slowly moving in the negative direction. For larger deflections, the tip links are stretched past the mostly open configuration. This means that the myosin motor complexes all slip down the actin until they reach this state. As they slip down, the tension is reduced. This produces a slow movement forward of the bundle for larger deflections.

A condition where the myosin motor parameters are set in between the two extremes just discussed is displayed in figure 12E for the position and figure 12F for the current. For this condition, a very typical twitch occurs for the cyan trace around 30 nm. This corresponds with what one typically calls fast adaptation of the current. For the next largest deflection, the myosin-enhanced-gating-compliance effect occurs again directly following the stimulus. The bundle then moves in the negative direction when the current quickly adapts. The next two largest deflections show the variability that can occur for this condition. The myosin motor force is balanced so that the myosin motor complexes will just slightly be biased towards moving to the mostly closed state. This increases the variability in the traces. The negative bundle motion may occur at various times during the trace, even if the exact same simulation is run repeatedly. If an average of the position was done over multiple runs, then no negative motion would actually be seen.

This section took an unusual approach of setting the myosin motors to be all the same throughout the hair bundle. This would be difficult or impossible to actually implement for a real physiological experiment. Nonetheless, these simulations provide a reasonable explanation for many of the features involved in adaptation. Some of the behaviors seem strange but represent how the hair bundle would behave under extreme conditions. In general, a true hair bundle would combine these behaviors to produce a composite response, once calcium is allowed to modulate the strength of myosin-1C.

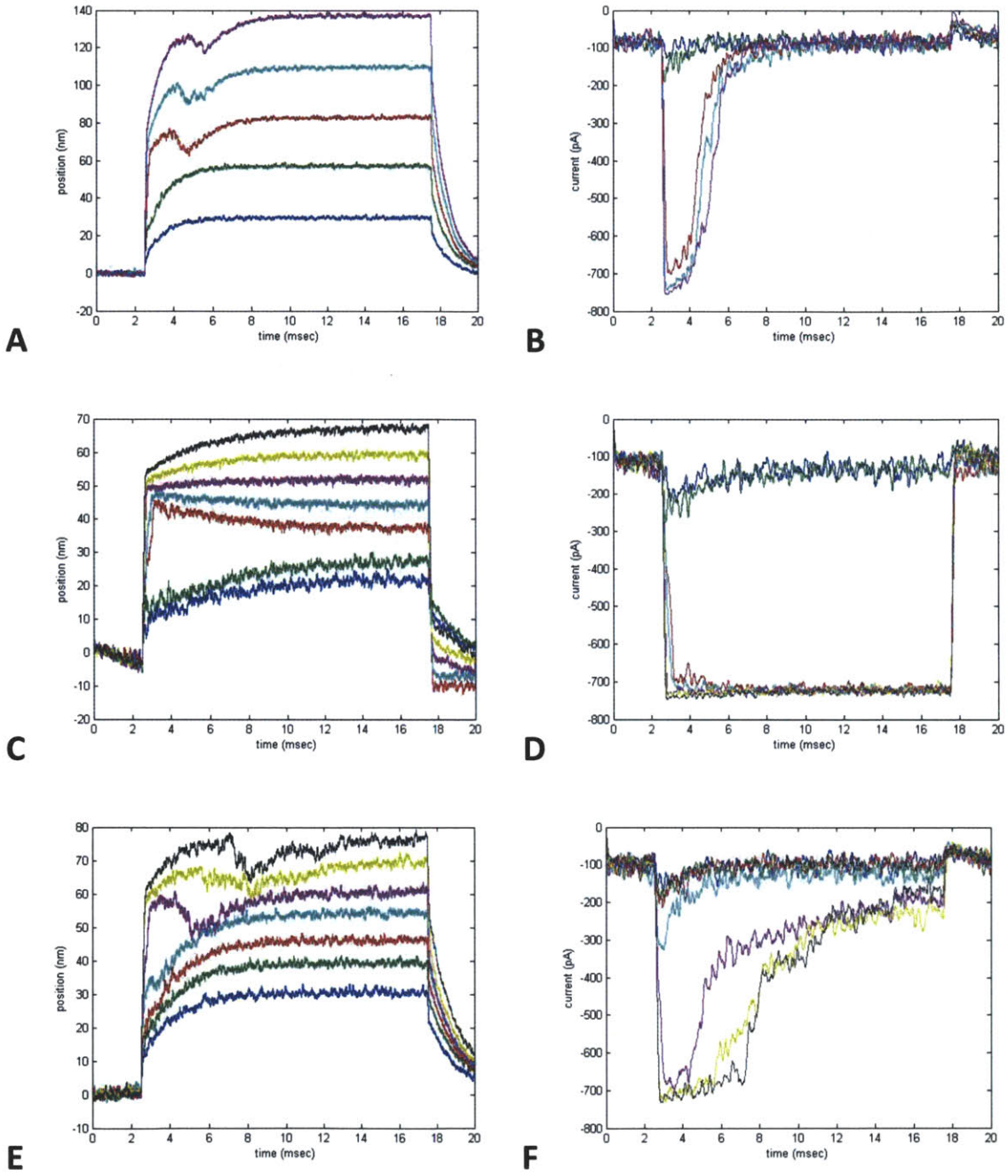

Figure 12. Position and transduction in a whole hair bundle deflected with a compliant probe (k_{probe}=2 pN/nm) with every tip link containing the same parameters. K_g=0.8 pN/nm, d=7 nm, x_0 =3 nm for all. **(A)** Position traces with F_{myosin}=4.6 pN and β_{myosin}=300 pN-μsec/nm. **(B)** Transduction currents for the same simulation as in A. **(C)** Position traces with F_{myosin}=5.6 pN and β_{myosin}=1000 pN-μsec/nm. **(D)** Transduction currents for the same simulation as in C. **(E)** Position traces with F_{myosin}=5.0 pN and β_{myosin}=500 pN-μsec/nm. **(F)** Transduction currents for the same simulation as in C.

Transduction in Whole Hair Bundles with Calcium Feedback

The previous section showed that much of the features of adaptation are present even without direct feedback from calcium through the transduction channels after a deflection. It has been shown repeatedly that calcium has a direct effect on the rate of adaptation. In the prior section, the myosin motor force and drag coefficient were modified before a stimulus to mimic the effect that calcium has on myosin-1C. Calcium entry through transduction channels should produce a range of myosin motor forces throughout the entire hair bundle. Changes in the external calcium concentration should change the range of myosin motor forces prior to stimulation due to the resting open probability of channels. But, is this change capable of completely explaining the effects of calcium concentration on adaptation? And, what role does influx through transduction channels after a deflection play in shaping the response of the hair bundle. To answer these questions, the diffusion portion of the model is used together with the mechanical portion of the model in this section. This allows the model to predict the response of the hair bundle as calcium diffuses down the stereocilia.

When all of the myosin motors have the same strength, the F-X curve for each transduction channel is essentially the same. This means that a region of negative stiffness is present for the whole hair bundle according to equation 14. However, if calcium modulates the strength of the myosin motors, then offsets exists amongst the individual F-X curves. This will tend to average out the negative stiffness region for the whole bundle. This effect has been seen for physiological experiments when the external calcium concentration is changed (Tinevez, Jülicher, & Martin, 2007). To examine exactly when a negative stiffness region is present for the whole bundle, equation 14 needs to be re-derived for the general case in which multiple independent tip links and motors are present.

The overall probability equation for the whole bundle becomes the average probability of all the individual tip links; for n tip links this becomes:

$$P(x) = \frac{1}{n}\sum_{k=1}^{n} P_k(x - x_{k0})$$

(eq. 24)

In this case, each probability term has the same structure and x deflection term, but a different offset to account for the difference in set point established by the myosin motors, x_{k0}.The minimum in the force curve occurs at a zero in the derivative of force, which again occurs at $\frac{dP}{dx}(x) = \frac{1}{d}$. The solution for the multi-tip-link case therefore utilizes the sum of derivatives. For simplicity, a shorthand is defined:

$$p_k(x) = \exp\left[-k_g d\left(\frac{x - x_{k0}}{kT}\right)\right]$$

(eq. 25)

The minimum then occurs when:

$$\sum_{k=1}^{n} \frac{p_k}{1 + 2p_k + p_k^2} = \frac{nkT}{k_g d^2}$$

(eq. 26)

The left side of the equation can be simplified in terms of hyperbolic cosine and the terms rearranged:

$$k_g d^2 = \frac{2nkT}{\sum_{k=1}^{n} \cosh\left(\frac{-k_g d}{kT}(x - x_{k0})\right) + 1}$$

(eq. 27)

The x term is the same for all of the tip links. The overall minimum for the equation must occur at the mean of the offsets which is $\overline{x_{k0}} = \frac{1}{n}\sum_{k=1}^{n} x_{k0}$. Therefore, a negative stiffness region occurs if:

$$k_g d^2 >= \frac{2nkT}{\sum_{k=1}^{n} \cosh\left(\frac{k_g d}{kT}(x_{k0} - \overline{x_{k0}})\right) + 1}$$

(eq. 28)

A solution to this equation requires that one know the individual offset terms established by all of the myosin motors. This term is based on the resting tension provided in the tip link, which is a function of the calcium concentration near the motor. This equation points out that a negative stiffness region in the overall F-X curve can only occur when there is a very small distribution in the myosin motor force. When the variance increases in the myosin motor force, then the negative stiffness region will disappear. This gives a mathematical explanation as to why increases in calcium tend to flatten the negative stiffness region.

Calcium will setup a gradient of myosin motor forces throughout the entire hair bundle. This will make the hair bundle respond as a summation of the behaviors explored in the previous section. For these simulations, the gating parameters are set to the same as before, k_g=0.8 pN/nm and d=7nm. The myosin motor parameters are set as F_{myosin}=5.2 pN and β_{myosin}=600 pN-μsec/nm. Two additional parameters that adjust how calcium affects myosin-1C are calcium_force_slope=0.001 and calcium_drag_slope=0.015. These values affect the myosin motor force and drag respectively as:

$$Post\ Calcium\ Value = \frac{Pre\ Calcium\ Value}{1 + [Ca^{+2}]calcium_{slope}}$$

(eq. 29)

This general formula is used for both the motor force and drag. The calcium concentration used is the internal calcium concentration immediately adjacent to the myosin motor complex for that particular stereocilium. Initially, the external calcium concentration was set at 1.5 mM. Once calcium was allowed to settle for 1 second of simulation, the myosin motor forces were established along the first excitatory column as 5.06 pN, 5.05 pN, 4.95 pN, 5.00 pN, 4.76 pN, and 5.20 pN, going from shortest to tallest stereocilium. This was similar for all of the columns, so only the values from the first are shown here. The tallest myosin motor complex never has calcium feedback because there is no channel associated with this complex. The second tallest myosin motor complex is always infused with the most calcium, which makes it the weakest. From the previous section, the myosin motors from the tallest stereocilia should adapt slowly compared to the second tallest stereocilia, which should adapt very quickly. The actual response is shown in figure 13A. The response is very similar to those obtained without calcium feedback. Fast adaptation is dominant for the smallest deflection whereas slow adaptation is dominant for the larger deflections. Adaptation is not complete but also depends proportionally on the size of the stimulus.

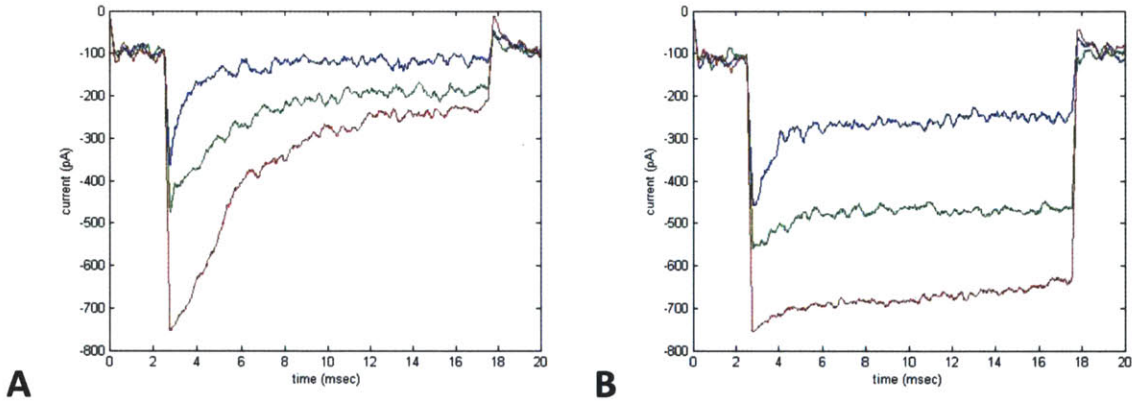

Figure 13. Transduction in a whole hair bundle deflected with a stiff probe (k_{probe}=50 pN/nm) with active calcium diffusion affecting myosin-1C. K_g=0.8 pN/nm, d=7 nm, x_0 =3 nm, $F_{myosin,max}$=5.2 pN, $\beta_{myosin,max}$=600 pN-μsec/nm, calcium_slope_force=0.004 and calcium_slope_drag=0.02 for all. **(A)** Current with $[Ca^{+2}]_{ext}$=1.5 mM for 35 nm (blue), 55 nm (green), 75 nm (red). **(B)** Current with $[Ca^{+2}]_{ext}$=0.1 mM using the same key as A.

When the external calcium concentration is dropped to 100 μM, the motor forces along the first excitatory column are 5.18 pN, 5.17 pN, 5.15 pN, 5.16 pN, 5.11 pN, and 5.20pN. Decreasing the external calcium concentration not only increases the motor force across the entire bundle but also decreases the variance of these forces. This makes the tip links act more coherently and creates a negative stiffness region for the whole hair bundle. The current for this simulation is displayed in figure 13B. In agreement with physiological results, the rates of adaptation have slowed and adaptation is less complete in this case.

Calcium is definitely important in changing the myosin motor force prior to a deflection of the hair bundle. To examine what role calcium influx through the transduction channels after a deflection

plays in shaping the adaptation response, the calcium concentration can be fixed for a simulation. This keeps the myosin gradient that develops from calcium diffusion at rest but does not allow additional diffusion to alter the myosin parameters. The results of this simulation are displayed in figure 14. The figure compares the transduction current in 1.5 mM external calcium for 55nm and 85 nm deflections. The blue and green traces allow calcium diffusion while the red and cyan traces do not allow for additional calcium diffusion throughout the simulation. The smaller deflections appear near identical for both cases. This makes intuitive sense. For a small deflection, the transduction channels do not open as much. Therefore, there is not a large increase in the intracellular calcium concentration. For the larger deflections, the green trace adapts faster than the cyan trace. The increased rate of adaptation arises from the additional influx of calcium through the transduction channels. In addition, adaptation is more complete for the case in which calcium is allowed to diffuse through the transduction channels.

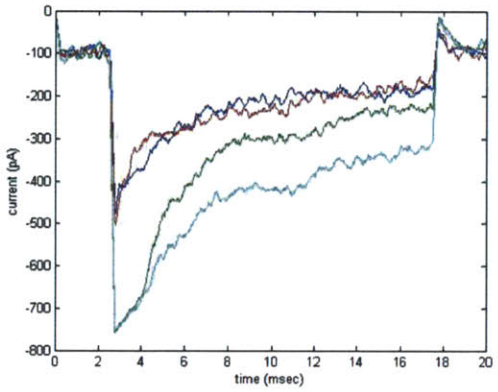

Figure 14. Transduction in a whole hair bundle deflected with a stiff probe (k_{probe}=50 pN/nm) for $[Ca^{+2}]_{ext}$=1.5 mM K_g=0.8 pN/nm, d=7 nm, x_0 =3 nm, $F_{myosin,max}$=5.2 pN, $\beta_{myosin,max}$=600 pN-μsec/nm, calcium_slope_force=0.004 and calcium_slope_drag=0.02. Calcium diffusion is either turned on or the calcium concentration is held fixed for the simulation depending on the trace. Blue: 55 nm deflection with calcium diffusion, green: 85 nm deflection with calcium diffusion, red: 55 nm deflection without calcium diffusion, cyan: 85 nm deflection without calcium diffusion.

Even for the larger deflections, the transduction current does not appear that different for the two cases in which calcium is allowed to diffuse through the transduction channels and when it is not allowed. This provides an answer to a recently proposed mystery: if the transduction channels are not adjacent to the myosin-1C motor complexes, then how does calcium influx through the channels provide rapid feedback to modulate the myosin motors? The answer appears to be that rapid feedback is not actually necessary: the majority of calcium's effect comes from changing the force produced at rest by the myosin motors. The change in force for the myosin motors that comes from calcium influx after a mechanical deflection does not play a significant role in shaping the adaptation behavior. This solution maintains the importance that calcium plays in modulating the adaptation time constant, while coming to terms with the fact that myosin motors and transduction channels are separated by hundreds of nanometers in a stereocilium.

The previous section gave an explanation for the mechanical twitch that occurs just following a stimulus with a flexible fiber. For hair bundles in which the myosin motor force was very weak, the twitch was very robust, a characteristic which is not always true for real hair cells. Figure 15A shows the position of the hair bundle in response to mechanical deflection with a flexible fiber and figure 15B shows the corresponding current. For these simulations, calcium diffusion and myosin feedback are present. The position traces display behavior that is more consistent with typical physiological experiments. A small negative twitch is visible just following the initial deflection of the hair bundle. The current shows that adaptation is still present. The twitch will occur when myosin motors slip down actin, which reduces the open probability for the attached transduction channels, and when there is a net increase in force. A net increase in force happens when myosin motors move through the steepest portion of the I-X curve, and it is a consequence of the transduction channels closing. When all of the myosin motors have the same initial offset, then they all move through this region at roughly the same time. For this simulation, the myosin motors all have different offsets at rest. This means that different myosin complexes adapt through the region where force increases at different times. The lack of coherence amongst the myosin motor complexes means that the overall increase in force for the entire bundle only occurs for a very brief duration. This weakens the size and duration of the twitch. Under this theory, a strong twitch will only occur when all of the myosin motors are equally weak. This is not likely to occur because calcium weakens the myosin motor force but also increases the variation in the motor force throughout the hair bundle. Therefore, it is very difficult to obtain consistently large twitches in bullfrog saccular hair cells by simply changing the external calcium concentration (Cheung & Corey, 2006).

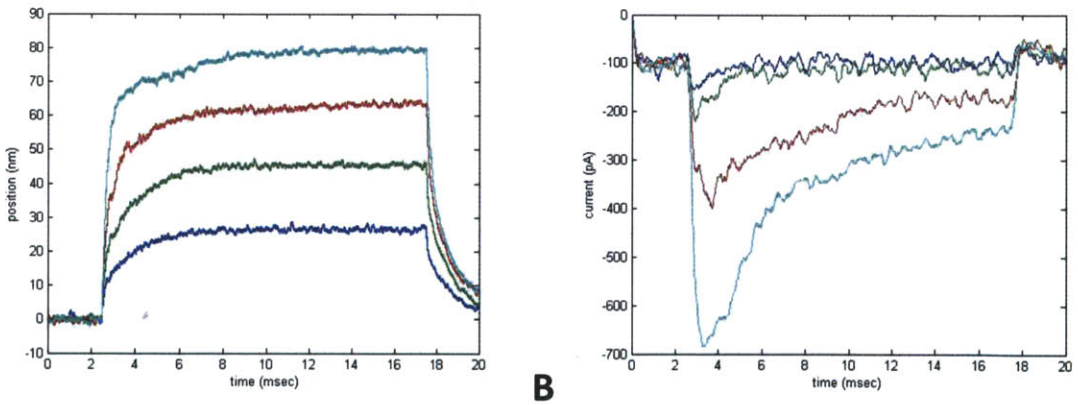

Figure 15. Position and transduction in a whole hair bundle deflected with a compliant probe (k_{probe}=2 pN/nm) for $[Ca^{+2}]_{ext}$=1.5 mM K_g=0.8 pN/nm, d=7 nm, x_0 =3 nm, $F_{myosin,max}$=5.2 pN, $\beta_{myosin,max}$=600 pN-μsec/nm, calcium_slope_force=0.004 and calcium_slope_drag=0.02 for all. **(A)** Position traces. **(B)** Transduction currents for the same simulation as in A.

Testing Mechanisms of Adaptation

This work has described a theory in which myosin-1C is necessary and sufficient to produce the twitch, fast adaptation and slow adaptation. This is contrary to the traditional theory in which calcium must bind to the transduction channel directly to promote channel closure. This work produces results that are similar to those seen physiologically while only requiring myosin-1C. This makes this theory attractive because it uses fewer elements to produce the same results as other models, but it does not necessarily make this model correct. Alternative models have been used for years that also produce results similar to those seen during experiments. In order to strengthen the arguments presented in this work, experiments will need to be performed that distinguish between this model and its alternatives. This section summarizes the principle claims made in this work and then presents experiments to be performed in bullfrog saccular hair cells that should test this model and alternative theories.

The theory presented in this thesis makes use of the negative stiffness region in the F-X curves. This idea is not new but the way in which it affects myosin-1C throughout adaptation is uniquely explored. The main assumption is that the calcium concentration is different for all of the stereocilia within a hair bundle. This idea has taken shape by modeling calcium diffusion and can be best confirmed through calcium imagining experiments. With regards to standard physiological experiments, the following characteristics are consequences of this model:

1. Myosin-1C has two potentially stable equilibrium positions, one in which the attached transduction channels are "mostly closed" and another in which the transduction channels are "mostly open" at rest. The force produced by the myosin motor complexes as well as the drag coefficient between myosin and actin determines the rate that myosin transitions from one state to another.
2. Fast adaptation and slow adaptation both arise from the behavior of myosin-1C. Fast adaptation is a consequence of the myosin motors quickly adapting back down to the mostly closed state. Slow adaptation is a consequence of the myosin motors occasionally transitioning from the mostly open state to the mostly closed state.
3. Calcium mostly affects the rate of adaptation by changing the myosin motor forces prior to a deflection. The calcium influx through the transduction channels following a deflection is less important in modifying this rate.
4. Incomplete adaptation is a direct result of how myosin-1C responds to a negative stiffness region and is predicted based on the rate at which myosin motors transition from the mostly open state to the mostly closed state. Incomplete adaptation is simply having a population of myosin motors stuck in the mostly open state.
5. Myosin-1C does not always reduce the transduction current but can actually climb up actin in response to gating compliance. This has the effect of steepening the measured I-X curve.
6. The twitch is a predicted consequence of adaptation from myosin-1C. It occurs most strongly when the myosin motors are weak and coherent in their timing of adaptation.

The main basis for all of these ideas is characteristic #1, which the foundation for slow adaptation. This idea is a simple mathematical conclusion from myosin-1C reacting to a negative stiffness region at the level of a single tip link. Therefore, it is easy to believe in the plausibility of this idea. Proving this concept requires examining the current from a single tip link. Recordings from a single tip link have been done in turtle cochlea (Ricci, Crawford, & Fettiplace, 2003) and rat cochlea (Beurg *et. al.*, 2006). In turtle cochlea, 0.05 mM external calcium biases the single channel current near the 50% open probability point. The open time for this calcium condition is 2.5 msec, which is 5 times longer than at 2.8 mM calcium. Additionally at +80 mV, adaptation is essentially non-existent and the single tip-link transduction current stays either in the open or closed configuration without flickering open and closed. Even if the open probability is low, one would still expect the channel to open and close stochastically and not be dependent on the amount of calcium affecting the myosin motor complex; but this is not the case. The 50% open probability in 0.05 mM calcium is unstable for the myosin motors. It is unlikely that the myosin motor complex is stably positioned to keep the channels biased at 50% open probability. What is more likely is that the myosin complex is transitioning between the two stable positions. This would give an explanation for why the apparent duration of the channel in the closed or open state increases as the calcium is reduced. The myosin drag coefficient goes up and the transition rate between the two stable positions decreases. This would also suggest that myosin motors have very little drag coefficient in turtle cochlear hair cells in the presence of even minimal calcium. This agrees with the fact that turtle cochlear hair cells tend to show relatively complete adaptation. By contrast, single tip link current from inner hair cells of the rat cochlea show currents that stay for prolonged periods of time in the open state or closed state. This would suggest that the myosin drag coefficient is higher in myosin motor complexes of rat inner hair cells. This is consistent with the fact that inner hair cells display very incomplete adaptation. The myosin drag coefficient is likely increased in inner hair cells by increasing the number of myosin motors per myosin motor complex on each tip link. This would increase the likelihood that a myosin motor is bound to actin at any given time.

This experiment indicates that calcium can change the amount of time that the transduction channels stay either open or closed. Here, the argument is presented that calcium is affecting the rate at which myosins transition from a position in which the attached transduction channels are mostly open to a position where the transduction channels are mostly closed. An alternative viewpoint is that calcium is interacting directly with the transduction channels and thus changing the duration that they stay either open or closed, by directly controlling the opening or closing rates. To test this possibility, single tip-link experiments need to be performed in which agents that only affect myosin-1C are introduced. SP-cAMPs are known to speed adaptation (Gillespie & Cyr, 2004), apparently reducing the myosin drag coefficient. This should decrease the duration that the single tip link transduction current stays in either the open state or closed state. Conversely, myosin-1C motors in Y61G mice bind tightly to actin when NMB-ADP is delivered through a patch pipette (Stauffer *et. al.*, 2005). This increases the myosin drag coefficient which should increase the duration that the single tip link transduction current stays in the open or closed configuration. If this is the case, then this would argue that the transitions in the single tip link current are not just spontaneous transitions for the transduction channel that is constantly biased at a particular open probability. Rather, the transitions are a result of the myosin motor complex moving between two stable positions that bias the transduction channels to be open

most of the time or closed most of the time. This would give strong support for characteristic #1, which creates a new way of understanding hair bundle mechanics and allows for the possibility of the other characteristics.

Finding an experiment that supports characteristic #2 is definitely tricky. The dominant theory in the field supports the idea that calcium binds to the transduction channel directly to cause fast adaptation. Figure 16 shows a hair cell that has $F_{closure}$= 0.25 pN. This means that 0.25 pN of extra force is needed to open the channel per each calcium ion that binds to the transduction channel (with 4 calcium ion binding locations). F_{myosin} has been set to 7.6 pN to compensate for this effect. Fast and slow adaptation are present for this simulation and it is impossible to support either theory over the other simply by pushing the hair bundle.

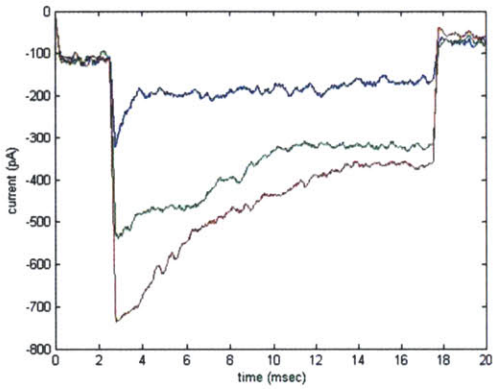

Figure 16. Transduction in a whole hair bundle deflected with a stiff probe (k_{probe}=50 pN/nm) for $[Ca^{+2}]_{ext}$=1.5 mM K_g=0.8 pN/nm, d=7 nm, x_0 =3 nm, $F_{myosin,max}$=7.6 pN, $\beta_{myosin,max}$=600 pN-μsec/nm, calcium_slope_force=0.004 and calcium_slope_drag=0.02, $F_{closure}$=0.25 pN. Deflections are 25 nm (blue), 40 nm (green), 55 nm (red).

To sort this situation out, it is helpful to realize that characteristic #2 and characteristic #3 are actually strongly related to each other. From the traditional viewpoint for fast adaptation, calcium must enter through open transduction channels, bind to the transduction channels, and promote closure of the channels. This viewpoint requires a source of calcium influx through the transduction channels to work successfully. Characteristic #3 supports the idea that the calcium concentration already within the stereocilia before a deflection is most important for changing the rate of adaptation. This idea can be tested while at the same time utilized to lend support to characteristic #2.

Transduction currents from a simulation that tests this idea are displayed in figure 17. For this simulation, a calcium concentration is established within the cell. The external calcium concentration is set to 1.5 mM and the holding potential of the cell is held at -80 mV. For 0.5 msec prior to a deflection, the holding potential is changed to +80 mV. This essentially eliminates the driving force of calcium ions into the cell through the transduction channels while at the same time preserving the calcium gradient within the cell. When the holding potential of the cell is inverted, the polarity of the transduction current is also inverted. Panel A displays transduction currents for the hair cell that does not contain a channel-based calcium binding mechanism. These currents behave rather typically. Both fast and slow

adaptation are present. It should be pointed out that prior work (Assad, Hacohen, & Corey, 1989) examined transduction current while the hair cell is held at +80 mV. For these experiments, the holding potential is changed well before the mechanical deflection is presented. That work did not show normal adaptation, presumably because the intracellular calcium concentration was severely lowered prior to the deflection.

Panel B displays the transduction current from the hair cell that does contain a channel-based calcium binding mechanism, for the same experimental protocol. This transduction current does not show significant adaptation. This cell required a combination of channel-based adaptation and myosin-based adaptation to reduce the transduction current. Without the additional calcium influx, the channel-based adaptation is not present, which essentially eliminates most of the adaptation.

In reality, this experiment will also have to deal with currents that result from changing the voltage as well as the transduction currents. If this is too difficult then calcium uncaging can be utilized to increase the intracellular calcium concentration prior to a mechanical stimulus. For this experiment, the cell is simply held at +80 mV, so there is no capacitive current. At 10 msec prior to the stimulus, calcium is uncaged which increases the intracellular calcium concentration while still preventing calcium influx through the transduction channel. This experiment is displayed for panel C with the same parameters used in panel A. Even without calcium influx through the channel, adaptation is still present, which argues against a channel-based calcium binding mechanism for fast adaptation.

This experiment makes use of the delay that calcium takes to diffuse down the stereocilia to reach the myosin motors, and is potentially a very powerful experiment. If the current appears similar to Panel A, then characteristics #2 and #3 are both strengthened. However, if the transduction current appears more similar to that in Panel B, then these two characteristics are both weakened and an argument in favor of a channel-based calcium binding mechanism is strengthened. Either way, a better understanding of adaptation is gained from this one experiment.

When examining characteristic #4, there really are not alternative theories proposed as to the extent of adaptation. Support for characteristic #1 forms a basis for characteristic #4, but proof must still be obtained to show that this occurs in the whole hair bundle. This idea can be broken down into two parts. The first idea is that some transduction channels within a hair bundle are open the majority of the time whereas other transduction channels are closed the majority of the time. The sum of all of these individual currents produces a whole-cell current that has incomplete adaptation. From just recording the whole cell transduction current, it is impossible to resolve the individual currents from every transduction channel. The only way to properly prove this idea is through calcium imaging. After a deflection, some stereocilia should maintain a calcium signal while others will quickly return to the baseline level of fluorescence. This is the only way to ascertain the state of individual transduction elements.

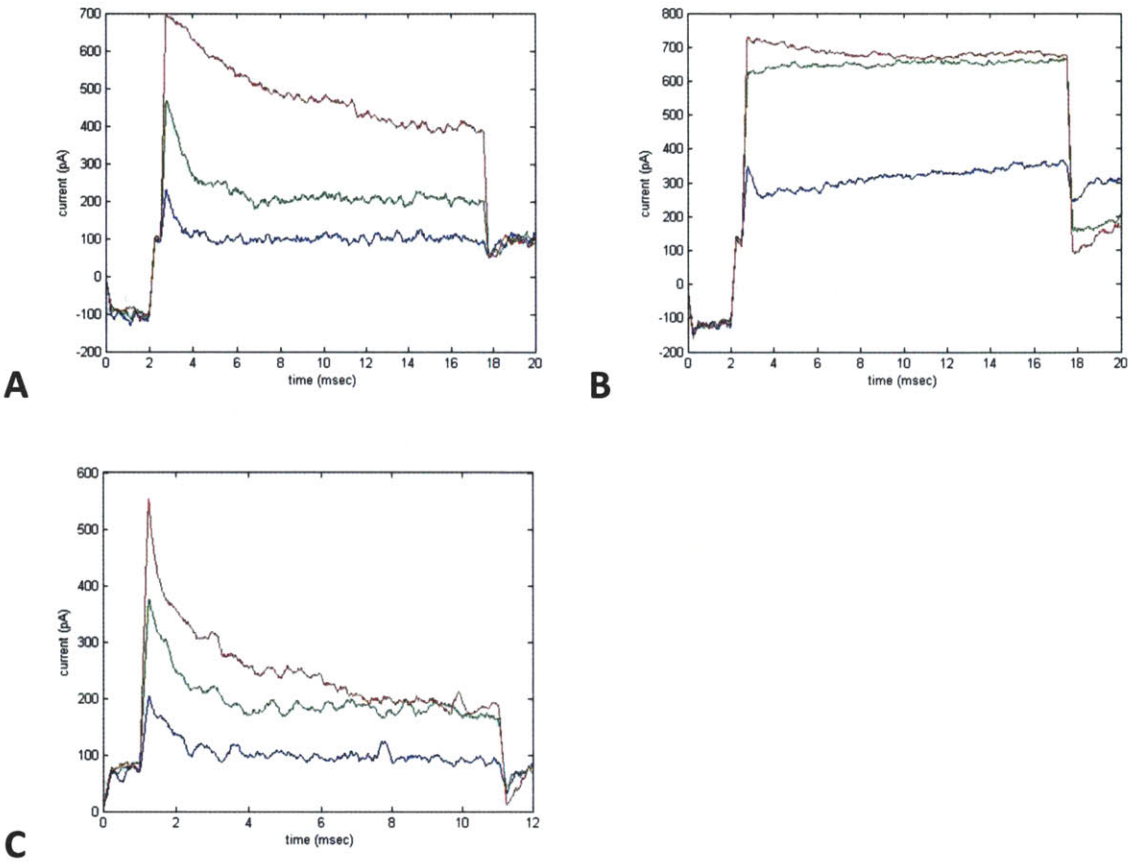

Figure 17. Transduction current in a whole hair bundle deflected with a stiff probe (k_{probe}=50 pN/nm) for $[Ca^{+2}]_{ext}$=1.5 mM K_g=0.8 pN/nm, d=7 nm, x_0 =3 nm, $\beta_{myosin,max}$=600 pN-μsec/nm, calcium_slope_force=0.004 and calcium_slope_drag=0.02. Deflections are 25 nm (blue), 40 nm (green), 55 nm (red). **(A)** The holding potential is switched from -80 mV to +80 mV 0.5 msec before the mechanical stimulus. $F_{myosin,max}$=5.2 pN $F_{closure}$=0 pN. **(B)** Same change in holding potential as in A. $F_{myosin,max}$=7.6 pN $F_{closure}$=0.25 pN. **(C)** Holding potential held at +80 msec. Calcium uncaged starting 10 msec before the mechanical deflection. $F_{myosin,max}$=5.2 pN $F_{closure}$=0 pN.

The second part of characteristic #4 is that incomplete adaptation is intimately linked with slow adaptation. This means that increasing the calcium concentration near every myosin motor should complete adaptation. This is actually difficult to do under normal circumstances. The tallest stereocilia do not have a transduction channel associated with them. For this reason, even increasing the external calcium concentration does little to actually affect the myosin motors within the tallest stereocilia. An alternative approach could be to release calcium within the stereocilia by uncaging calcium. Using this technique, calcium can have access to the myosin motors of even the tallest stereocilia. Figure 18 shows transduction currents for simulations using this idea. For these simulations, the extracellular calcium

concentration is set at 0.1 mM. The cell is loaded with 4 mM calcium cage preequilibrated with 3.5 mM intracellular calcium. At the start of the simulation, most of the calcium cage is bound to calcium, ready to be uncaged when it absorbs photons from the uncaging laser. Panel A displays the current from a hair cell without a channel-based calcium binding mechanism, without turning on the uncaging laser. The current displays adaptation but does not adapt completely. Panel B shows the current when the uncaging laser is turned on starting at 8 msec after the deflection of the hair bundle. As can be seen, adaptation is now complete. For this simulation, the uncaging laser is focused near the tallest stereocilia. When the laser is focused near the smallest stereocilia, then adaptation remains incomplete and looks very similar to the current shown in panel A. If this result is seen during a physiological experiment, it indicates that adaptation can be complete if enough calcium is present throughout the entire hair bundle. Specifically, it also indicates that incomplete adaptation is occurring primarily at the tallest end of the hair bundle. This strengthens the argument that the hair bundle has some transduction channels that are open the majority of the time with other transduction channels being closed the majority of the time.

The prior modeling experiment provides evidence that the completeness of adaptation is calcium dependent. It does not directly indicate the mechanism for the calcium dependence. One could still argue that the calcium dependence comes from calcium binding somewhere other than myosin-1C. To circumvent this argument, calcium uncaging can be used in conjunction with Y61G mice. These mice have a mutant copy of myosin-1C that binds tightly to actin in the presence of NMB-ADP. For simulations, this is modeled as increasing the maximum myosin drag coefficient from $6*10^2$ pN-μsec/nm to $6*10^7$ pN-μsec/nm. This essentially locks the myosin motors tightly in place. Panel C of figure 18 shows the transduction current for a hair cell with myosin-1C locked and uncaging pulses beginning at 8 msec following the deflection. Essentially, adaptation is not present at all. Increasing the intracellular calcium concentration still does not allow for myosin-1C to slide down actin; therefore, adaptation is still incomplete. This set of experiments provides evidence for the location of incomplete adaptation, shows that it is calcium dependent, and is additionally dependent on myosin-1C.

Characteristic #5 was discussed quite thoroughly in the section where just a tip link and myosin motors were present. Testing this hypothesis is easy to do experimently. The peak current versus displacement curve should be made repeatedly while the external calcium concentration is gradually lowered. Lowering the calcium concentration should increase the myosin drag coefficient. This should cause the measured I-X curve to appear broader over time. Alternatively, the I-X curve of hair cells from Y61G mice can be continuously measured while NMB-ADP diffuses from the patch pipette. This should gradually broaden the I-X curve as NMB-ADP makes its way up to the myosin motors.

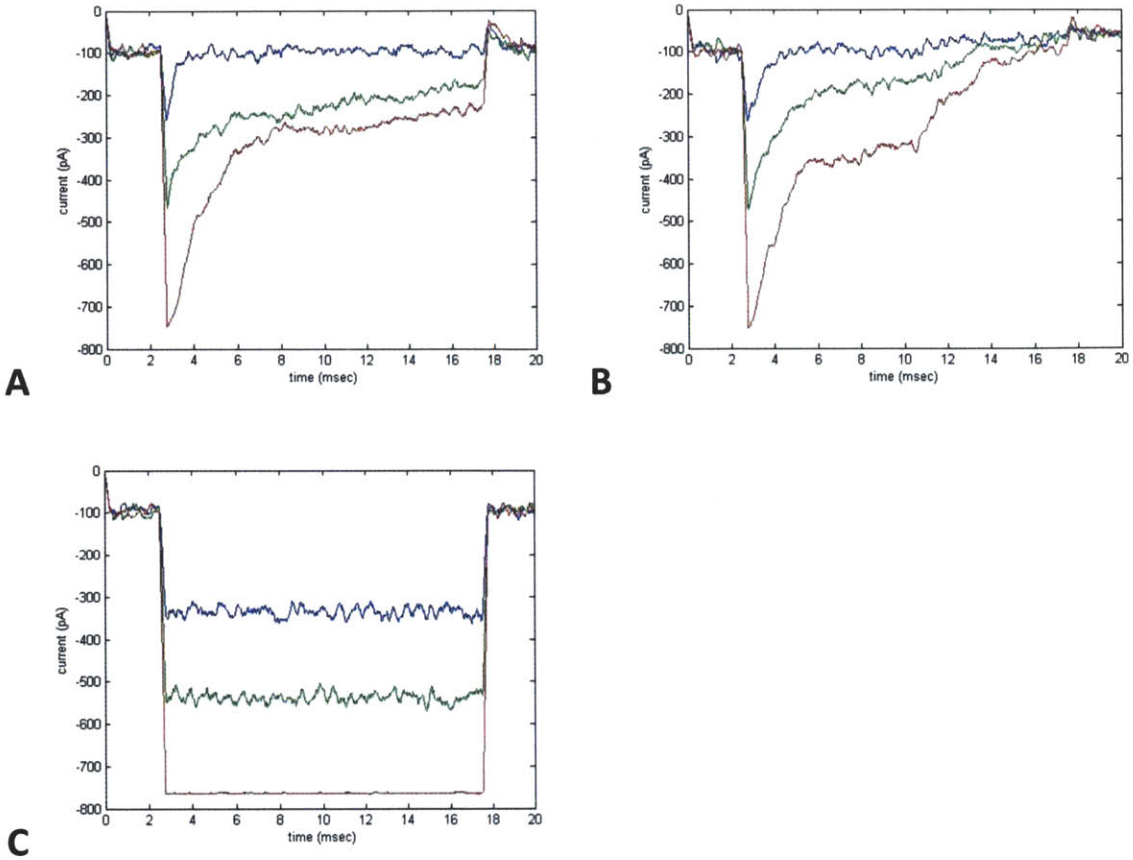

Figure 18. Transduction current in a whole hair bundle deflected with a stiff probe (k_{probe}=50 pN/nm) for $[Ca^{+2}]_{ext}$=0.1 mM K_g=0.8 pN/nm, d=7 nm, x_0 =3 nm, calcium_slope_force=0.004 and calcium_slope_drag=0.02, $F_{closure}$=0 pN. [Calcium Cage]=4 mM and $[Ca^{+2}]_{int}$=3.5 mM. Deflections are 15 nm (blue), 30 nm (green), 45 nm (red). **(A)** $\beta_{myosin,max}$=600 pN-μsec/nm and no calcium uncaging is present. **(B)** $\beta_{myosin,max}$=600 pN-μsec/nm and calcium uncaging is present beginning at 8 msec after the mechanical deflection. **(C)** $\beta_{myosin,max}$=60e6 pN-μsec/nm and calcium uncaging is present beginning at 8 msec after the mechanical deflection.

Overall, this characteristic slightly redefines how myosin-1C acts within the hair bundle. Myosin-1C simply reacts to the tension placed on it via the tip link. Because of gating compliance, this means that the motors will sometimes climb towards the mostly open state. Any argument that strengthens characteristic #5 will also lend support to characteristic #1, because two stable positions are required for this argument to make sense.

When examining characteristic #6, one has to think carefully about what needs to be proved. Every theory agrees that the negative motion comes about because of channel closure, and that it is closely linked with fast adaptation. The main issue is what causes the channel closure. Experiments described earlier to examine characteristic #2 should better determine the mechanism for fast adaptation. The remaining issue to be answered is why the twitch is not as robust as fast adaptation. For some experiments, fast adaptation may be present while the twitch is not. The explanation given

for the occasional lack of a twitch involved the coherence of myosin motor complexes. If all of the myosin motors are adapting at the same time, then a twitch should be present.

Testing this theory involves conditioning the myosin motors within a hair bundle with two key features: they should all have very similar strength and they should all be quite weak. Lowering the external calcium concentration makes all of the myosin motor complexes have similar strength, but they also become rather strong in this condition. High external calcium makes some of the myosin-1C complexes weak while others are less affected. Uncaging calcium is not a useful strategy as the narrow point spread function of the uncaging laser does not provide a uniform release of calcium throughout all of the stereocilia. The best experiment is to weaken the myosin motors through delivery of an agent through a patch pipette. High intracellular calcium within the patch pipette would cause additional effects within the hair cell. For this to work, a molecule that only affects myosin motors should be utilized. Including SP-cAMP, a potent and specific activator of cAMP-dependent protein kinase (Gillespie & Cyr, 2004), within the patch pipette should provide uniform access to all of the Myosin-1C molecules and weaken them. Under this environment, the hair bundle would expect to show displacement traces similar to those in figure 12A. This would give an explanation as to why the twitch is very difficult to find in some experiments as well as strengthen the idea that it originates from myosin-1C movement.

Conclusion

This work has presented a theory to describe how adaptation works in hair cells. It started with a very simple description of the transduction apparatus. Even a simple system of just a gating spring in series with a transduction channel produces a complicated nonlinear result. Elements were introduced individually so that overall ideas were developed logically into the theory that describes a complete hair cell. This theory can do an excellent job of explaining complex behaviors seen in hair cell recordings. Even so, understanding hair cells requires additional work that should come in two forms: better understanding of the proteins involved and better understanding of how the proteins create the observed physiology.

Recent work has been able to identify the some of the proteins used by hair cells, which also allows researchers to better understand how hereditary diseases affect hair cell function. In addition, protein knowledge allows one to better understand the physical parameters of the elements involved in transduction. The specific parameters are expected to change from one model system to another, but getting some measurement is better than guesswork. As this work has shown, even small changes to some of these parameters can greatly change how the hair bundle behaves. A better understanding of the physical parameters within a hair cell yield more accurate results during hair cell modeling.

Understanding hair cell physiology requires testing hypotheses that are developed through quantative modeling. Transduction and adaptation are too complicated to properly understand from intuition, even with simple models. To begin with, the theories presented in this chapter should be tested using the given protocols. These protocols will either confirm or reject the theories that are

presented. If these theories are confirmed, then this work will have explained many of the mysteries in hair cell physiology. New findings will undoubtedly complicate and refine the model. These results should be reincorporated into the model to produce new and testable hypotheses. Increased understanding of how hair cells behave ultimately leads to a better understanding of the vestibular and auditory systems as a whole.

Chapter 5

Adaptation and Amplification in Outer Hair Cells

Introduction

Outer hair cells seem to provide a unique role within the mammalian cochlea. They are sparsely innervated by unmyelinated type II spiral ganglion neurons which are not myelinated than the type I afferents that innervate inner hair cells (Brown, 1987a). By contrast, they are strongly innervated by medial olivocochlear myelinated efferent fibers (Brown, 1987b). Any change in the membrane potential works in concert with a remarkable protein, prestin (Zheng *et. al.*, 2000). Prestin changes its conformation in response to the membrane potential. This allows the cell body of outer hair cells to change in length in response to changes in the membrane potential. The membrane potential is changed directly upon stimulation of the hair bundle through the transduction current. In addition, changes in the membrane potential can be elicited directly by efferent stimulation. Cholinergic efferent fibers act on α9 and α10 nAChR channels that modulate the intracellular membrane potential (Elgoyhen *et. al.*, 1994). This changes the length of the hair cell body which in turn adjusts the voltage-to-length gain of the outer hair cells. Additionally, the efferent-mediated somatic length change could create a direct effect on the mechanical feedback by adjusting the resting position of the hair cell. This affects the degree to which the hair bundles are stimulated.

Overall, there is strong evidence that outer hair cells are used entirely for mechanical amplification within the cochlea. Deletion or functional disruption of prestin results in a loss of cochlear amplification (Liberman *et. al.*, 2002; Dallos *et. al.*, 2008). This results in the elevation of hearing thresholds as well as distortion product otoacoustic emissions, which are a trademark of active amplification within the cochlea.

The amplification has been theorized to occur in two different manners. The prestin-based somatic electromotility can move the hair cell in an axis parallel to the hair cell body. This increases or decreases the distance between the basilar membrane and tectorial membrane, which lie below and above the hair cells, respectively. The tectorial membrane also moves perpendicular to this axis which directly stimulates the stereocilia of outer hair cells. Non-mammalian species do not have prestin and their hair bundles have nonetheless displayed spontaneous oscillations (Le Goff, Bozovic, & Hudspeth, 2005). It is therefore likely that stereocilia have developed a form of amplification that increases motion along the excitatory axis of stereocilia. This would serve to increase the transduction current flowing through outer hair cells, which increases the amount of somatic electromotility as well as increase the motion of the tectorial membrane. Increasing the tectorial membrane motion along this axis should increase the stimulus to inner hair cells, which project myelinated afferent neurons to the central nervous system and are the cells responsible for primary auditory transduction.

Outer hair cells detect motion and provide an afferent signal but they have evolved to perform an entirely different function. They form a very precise arrangement of three rows within the cochlea. Outer hair cell bundles are typically very short, smaller in stereocilia diameter, and only have three rows of stereocilia in rodents. They are bathed in endolymph solution that has a very high extracellular potential of +80 mV, which reduces the overall extracellular calcium concentration (Bosher & Warren, 1978). In this environment, outer hair cells are open approximately 50% at rest (Johnson *et. al.*, 2011),

which is exceptionally high for any hair cell. The different structure, function, and environment mean that outer hair cells have to be examined from a different perspective than other hair cells.

This chapter specifically seeks to explore mechanical amplification performed by the stereocilia; amplification by the hair cell body is not included in this work. First, a simple three-stereocilia model is examined to determine how stereocilia respond to step deflections. Next, sinusoidal inputs are utilized for the same model system to better simulate the natural stimulus of outer hair cells. Following this, a more realistic outer hair cell model is used for high and low extracellular calcium conditions. This section utilizes changes in calcium to better understand outer hair cell bundle behavior.

Bundle Motion in a Simple Outer Hair Cell to Step Deflections

When a hair bundle is deflected in the positive direction with a flexible fiber, an external force is applied to the bundle that is equal to the product of the stiffness of the fiber and the net displacement of the fiber tip as compared to the base of the fiber. As the bundle moves in the positive direction, the net displacement of the fiber tip decreases and the external force of the fiber therefore also decreases. The bundle comes to an equilibrium position when the internal forces provided from the overall compliance of the stereocilia balance with the external fiber force. A positive deflection stretches the gating springs by providing shear via the tip links. Therefore, one would expect that the internal tension increases from the resting position of the bundle. This means that an equilibrium position is usually reached with a net deflection on the stimulus fiber.

In a scenario where adaptation is complete, the tension in the tip link should naturally be reduced back down to the same tension that was present in the resting hair bundle. Hair bundles generally have a slightly negative initial resting position. Therefore, a positive motion of the bundle tends to reduce the positive force provided by the rootlet springs. This reduction in force makes it necessary that an equilibrium position is reached while maintaining a deflection on the stimulus probe. Therefore, even when there is complete adaptation, implying a zero net increase in the tension in the gating springs, the bundle should still not move as far as the base of the stimulus probe.

With these facts in mind, it may seem surprising that outer hair cell bundles sometimes move further than the stimulus probe when deflected with a flexible fiber in the positive direction (Kennedy, Crawford, & Fettiplace, 2005). This is exceptional in that the hair bundle provides a positive force on the stimulus fiber. This occurs even when adaptation is incomplete. This means that there is a reduction in the positive force provided by the rootlet springs as well as in increased open probability of the transduction channels, which one usually interprets as necessitating increased tension in the gating springs. Strictly from a balance of forces point of view, it does not make intuitive sense that the hair bundle can move further than the mechanical stimulus.

The only possible solution to this problem is that there must be a reduction in tension from the gating springs to account for the bundle moving further than the stimulus. When transduction channels open, there is an associated reduction in tension called the gating compliance. This provides a

temporary reduction in the intrinsic force but myosin-1C should move along the actin core of the stereocilia to balance the tension along the tip link axis. Over a time period of more than a few milliseconds, the force in a tip link is the force provided by the myosin motor complex in that tip link. The overall conclusion is that there must be a reduction in the force that myosin-1C complexes can produce in order to explain the fact that hair bundles can move further than the stimulus.

To test this idea, simulations were performed using a model hair cell consisting of only three stereocilia. The heights of 1.1 μm, 1.6 μm and 3.5 μm for the stereocilia were chosen to represent the heights along a column in an outer hair cell. A typical outer hair cell bundle will have close to 30 columns. Only one column was chosen to decrease the computation time and simplify the analysis. In addition, stereocilia from outer hair cells are not strongly connected laterally to one another. This seems unnecessary because the tips of the tallest stereocilia are firmly embedded in the tectorial membrane. For this reason, it is believed that modeling a single column will produce similar results as modeling an entire set of columns.

Figure 1 displays the results of a single simulation performed in 20 μM external calcium concentration, using a compliant probe with a stiffness of 0.25 pN/nm. Panel A shows the position of the hair bundle to 2 displacements, with a solid line, as well as the base of the flexible stimulus probe with a dashed line. As can be seen, the bundle moves further than the stimulus probe over the course of a few milliseconds for the larger stimulus but does not move further than the stimulus for the smaller deflection. The discrepancies for the two deflections arise because of the amount of transduction current in the two cases. When there are three stereocilia in a column, there are only two tip links. The tip link connected to the tallest stereocilium, which will be referred to as tip link 2 from now on, does not have a direct source of calcium to modulate the strength of the myosin motor complex. By contrast, the tip link connected to the smallest stereocilium, tip link 1, receives a large calcium influx that modulates the strength of the myosin motor complex. For the smaller deflection, there is not enough shear created to make either channel set open most of the time. Therefore, there is not a considerable influx of calcium into the hair bundle. For the larger deflection, there is enough force from the gating springs to make both sets of transduction channels open most of the time. This provides a larger calcium influx into the two smaller stereocilia. The calcium influx is not important in the smallest stereocilium because there is no myosin motor complex. In the middle stereocilium, the calcium acts on the myosin motor complex attached to tip link 1 to weaken the stall force of the motors.

The force of the motor complexes is displayed in panel B for the larger of the two deflections. The force of the myosin motor complex attached to tip link 1 is shown in blue and the force of the myosin motor complex attached to tip link 2 is displayed in green. The calcium influx into the second tallest stereocilium reduces the force of the myosin motor complex for tip link 1. This reduces the overall tension in the tip link that pulls the hair bundle in the negative direction. Panel C displays the overall balance of force within the hair bundle. The sum of the force along the tip links is displayed in blue. This force acts to move the bundle in the negative direction but is plotted as a positive value to make it easier to compare to the other forces. The sum of the rootlet forces is shown in green and the external force is shown in red. It is easy to see that there is an overall drop in the tip link force which arises completely by a force reduction from tip link 1. As the bundle moves in the positive direction, the

rootlet force decreases but not by the same amount as the decrease in the gating spring force. Therefore, the external force continues to drop as the tip of the stimulus probe moves towards the base position of the stimulus probe. Eventually, the hair bundle moves past the base position of the stimulus probe and the stimulus force becomes negative.

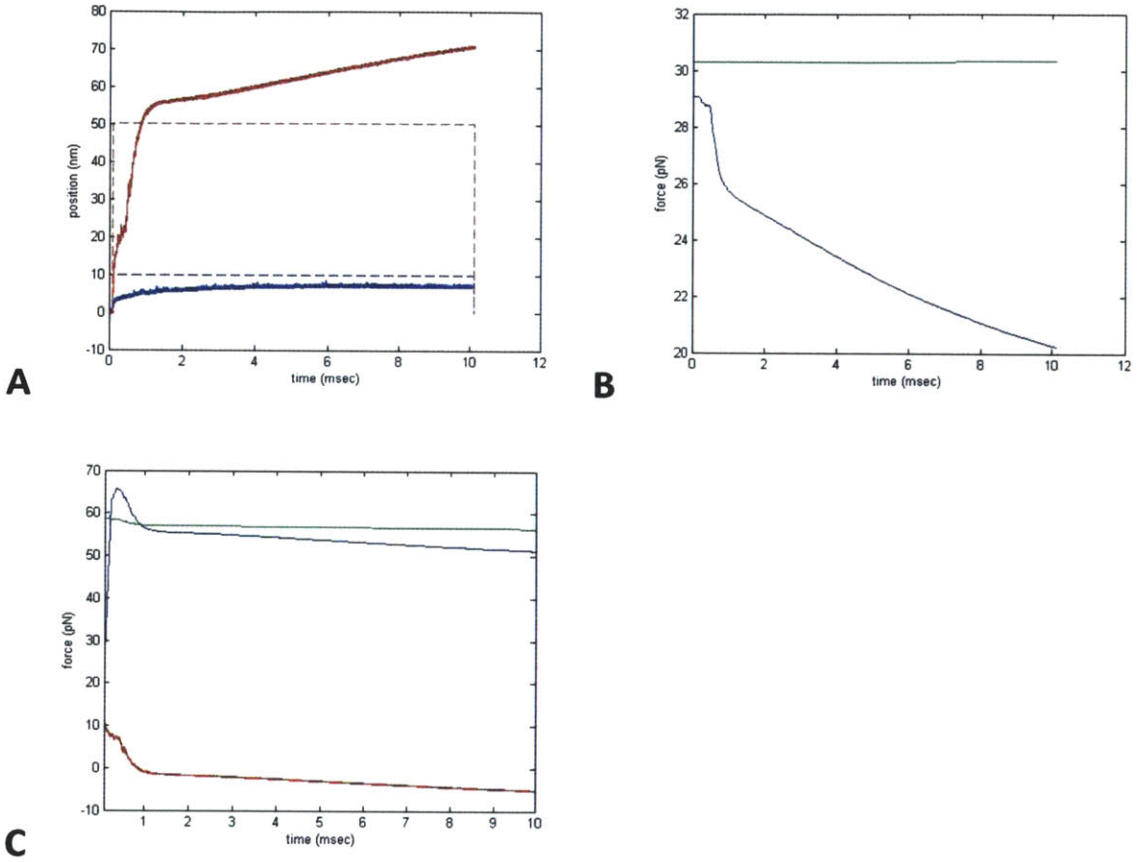

Figure 1. Response of a simple three stereocilia hair bundle to positive mechanical deflections with k_{probe}=0.25 pN/nm. **(A)** Position of the hair bundle (solid lines) and stimulus probe base (dashed lines) to two step deflections. **(B)** Myosin motor force of the myosin motor complexes attached to the two tip links for the 50 nm deflection. Tip link 1, referring to the tip link attached to the smallest stereocilium is in blue and tip link 2 is in green. **(C)** Forces acting on the hair bundle for the 50 nm deflection. Blue displays the sum of forces along the tip link averaged with a 0.5 msec wide moving average filter, green shows the sum of forces from the rootlet springs and red displays the force from the stimulus probe.

One might additionally wonder how the hair bundle responds to a negative deflection. For the positive case, the extra motion of the hair bundle relies on transduction channels attached to tip link 2 changing configuration from the closed to open state. If all of the transduction channels are mostly closed at rest, then there is not a significant change in the calcium influx to a negative deflection. However, if the transduction channels attached to tip link 2 are mostly open at rest, then a negative

deflection would close these channels and result in a significant decrease in the calcium influx into the hair bundle.

Figure 2A displays the response of the hair bundle to the same negative deflection but under these two different initial conditions. For the blue trace, the transduction channels attached to tip link 2 are mostly closed at rest whereas they are mostly open at rest for the green trace. The position of the base of the stimulus probe is displayed in black. The hair bundle pulls the tip of the stimulus fiber further than the base only for the green trace. For the blue trace, the hair bundle stops before the full motion of the base of the probe. This situation is essentially acting like the passive case without any calcium feedback on the myosin motors.

For the green trace from figure 2A, the calcium concentration in the second tallest stereocilium rapidly decreases as the transduction channels that are located in that stereocilium close. This causes an increase of the myosin motor force for myosins attached to tip link 1. The myosin motor force over time for this case is displayed in figure 2B. The force of myosins attached to tip link 1 is shown in blue and the myosin force of motors attached to tip link 2 is shown in green. This situation is essentially the reverse of the positive deflection. The reduction in calcium causes the myosin motor force for tip link 1 to increase. The increase in force pulls the bundle more negative than the negative stimulus.

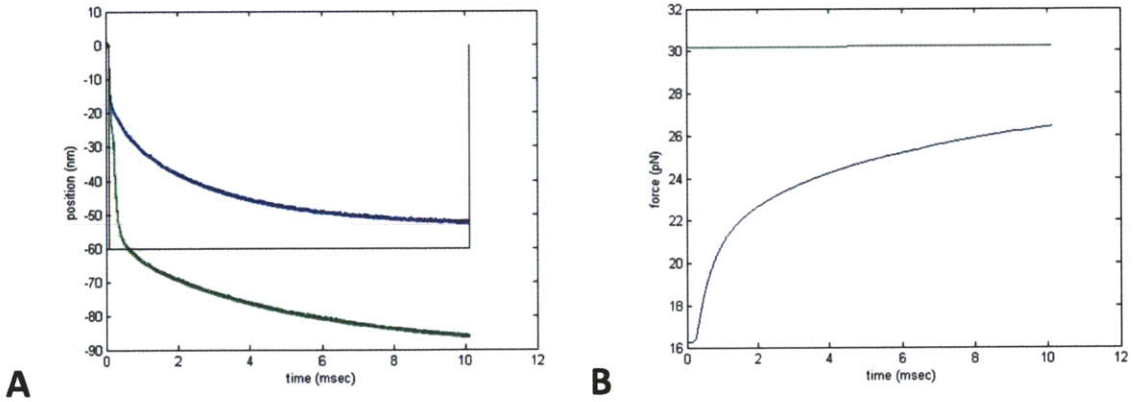

Figure 2. Response of a simple three stereocilia hair bundle to a negative mechanical deflection with k_{probe}=0.25 pN/nm. **(A)** Position of the hair bundle when the transduction channels attached to tip link 2 are closed at rest (blue) or open at rest (green) compared to the base position of the stimulus probe (black). **(B)** Myosin motor force of the myosin motor complexes attached to the two tip links for the green trace from panel A. Tip link 1 is displayed in blue and tip link 2 is displayed in green.

This simple explanation provides a mechanism for how outer hair cell bundles are capable of moving further than their stimulus. The arrangement of two tip links per column in rodent outer hair cells has most likely evolved so that small stimuli in either direction cause the hair bundle to react by moving further than the stimulus. This process depends on calcium to directly modulate the strength of the myosin motor complexes. This effect is also dependent on the specific external calcium concentration in the vicinity of the outer hair cell bundle and the feedback factor of calcium on the

myosin motor force. This reinforces the need to accurately determine these values. Furthermore, the degree to which the bundle moves past the stimulus depends on the state of the transduction channels prior to the deflection. This makes the prior history of the hair bundle very important in determining the amount that the hair bundle moves past the stimulus.

Sinusoidal Amplification in a Simple Outer Hair Cell

The previous section described a mechanism that allows hair bundles from outer hair cells to move further than the stimulus probe. That section utilized a step deflection which is not the typical stimulus for outer hair cell bundles. The cochlea provides a wonderful natural mechanism that creates distinct resonant frequencies throughout the length of the basilar membrane (von Bekesy, 1960). This means that any mechanical motion is band-passed filtered by the time it reaches the outer hair cells. Even broad-band noise should cause the basilar membrane to oscillate at the local resonant frequency. Therefore, the natural environment for an outer hair cell bundle is constant sinusoidal stimulation that is primarily at the resonant frequency for that section of basilar membrane. The only factor that changes is the amplitude of the vibration.

In order for the hair bundle to move further than the stimulus probe, the hair bundle must exhibit a negative stiffness region. This can arise because of gating compliance but this is a fast effect. The negative stiffness that is exhibited by outer hair cell bundles occurs over the course of many milliseconds and therefore does not arise from gating compliance. As was discussed in the previous section, this negative stiffness region occurs because of a calcium induced change in force for myosin motor complexes located in the second tallest stereocilia. This concept allows the hair bundle to move further than the stimulus in both the positive and negative direction which would theoretically amplify the stimulus on a cycle by cycle basis.

A negative stiffness region is defined as having a reduction in force for an increase in displacement. To determine when this situation occurs, it is important to examine the balance of forces within the tip links. The force acting on a myosin motor complex is balanced when the tension pulling the complex down is equal to the force allowing the complex to climb up actin. When the bundle is deflected there is an increase of extension along the tip link due to shear. For an incremental deflection of the bundle, Δx, there is a length increase along the tip link of $\gamma\Delta x$, where γ is the shear constant for that particular tip link. This value is often approximated as being the same throughout the entire hair bundle, but there are actually small differences across rows. For any time step, the myosin motor complex can also move an additional amount along actin. This motion will be represented with the variable, myo_{slide}, with positive motions being represented towards the tallest end of the stereocilium. Therefore, for an incremental increase in time, Δt, the increase in downward force is:

$$\Delta F_{down} = 2k_g\gamma\Delta x + 2k_g myo_{slide} \quad \text{(eq. 1)}$$

The factor of 2 is present because of the two transduction channels per tip link. The additional motion of the myosin motor complex creates a drag force which can be viewed as directed upward. The force produced by the myosin motor complex can also change due to calcium modulation. Combining these two terms:

$$\Delta F_{up} = \beta_{myosin}\frac{-myo_{slide}}{\Delta t} + \Delta F_{myosin} \quad \text{(eq. 2)}$$

For any given time step, these two terms must be equal to each other. Therefore:

$$2k_g\gamma\Delta x + 2k_g myo_{slide} = \beta_{myosin}\frac{-myo_{slide}}{\Delta t} + \Delta F_{myosin} \quad \text{(eq. 3)}$$

Solving for myo_{slide}:

$$myo_{slide} = \frac{\Delta F_{myosin} - 2k_g\gamma\Delta x}{2k_g + \frac{\beta_{myosin}}{\Delta t}} \quad \text{(eq. 4)}$$

This value determines how much the myosin motor complex moves in addition to the motion created from shear. It is important in determining the overall increase in tension along the tip links by inserting myo_{slide} back into equation 1:

$$\Delta F_{down} = 2k_g\gamma\Delta x + 2k_g\frac{\Delta F_{myosin} - 2k_g\gamma\Delta x}{2k_g + \frac{\beta_{myosin}}{\Delta t}} \quad \text{(eq. 5)}$$

For the model hair bundle being explored in this case, there are only 2 tip links that contribute to the force. For the remaining analysis, parameters associated with the tip link connected to the smallest stereocilium, tip link 1, will contain a subscript of 1 and parameters associated with tip link 2 will have a subscript of 2. There is a negative stiffness when $\Delta x>0$ and $\Delta F_{down}<0$ for the sum of forces from both tip links:

$$\Delta F_{down} = 2k_g\gamma_1\Delta x + 2k_g\frac{\Delta F_{myosin,1} - 2k_g\gamma_1\Delta x}{2k_g + \frac{\beta_{myosin,1}}{\Delta t}} + 2k_g\gamma_2\Delta x + 2k_g\frac{\Delta F_{myosin,2} - 2k_g\gamma_2\Delta x}{2k_g + \frac{\beta_{myosin,2}}{\Delta t}} < 0 \quad \text{(eq. 6)}$$

This is the situation for which a negative stiffness occurs. For sinusoidal stimuli there is not enough time for significant calcium to diffuse into the tallest stereocilium. Therefore, $\Delta F_{myosin,2}$ is approximately equal to 0. By removing this term, and simplifying the equation, the inequality is

$$\Delta F_{myosin,1} < \frac{-\Delta x}{\Delta t}\left[\gamma_1\beta_{myosin,1} + \gamma_2\beta_{myosin,2}\frac{2k_g\Delta t + \beta_{myosin,1}}{2k_g\Delta t + \beta_{myosin,2}}\right] \quad \text{(eq. 7)}$$

Δt can be made arbitrarily small so that $k_g\Delta t << \beta_{myosin}$. This allows the entire equation to be reduced further to

$$\Delta F_{myosin,1} < \frac{-\Delta x}{\Delta t}[\gamma_1\beta_{myosin,1} + \gamma_2\beta_{myosin,1}] \quad \text{(eq. 8)}$$

. Finally, γ_1 and γ_2 are approximately the same and can be set as equal. This gives a final form of

$$\Delta F_{myosin,1} < -2\gamma\beta_{myosin,1}\frac{\Delta x}{\Delta t}, if\ \Delta x > 0 \quad \text{(eq. 9)}$$

And for the case when $\Delta x < 0$:

$$\Delta F_{myosin,1} > -2\gamma\beta_{myosin,1}\frac{\Delta x}{\Delta t}, if\ \Delta x < 0 \quad \text{(eq. 10)}$$

This set of equations gives the criteria for determining when a deflection of the hair bundle will produce a negative stiffness from calcium modulation of the myosin motor force. As was shown in the prior section, a negative stiffness can occur if there is a significant change in the force production of the myosin motor complex in the second tallest stereocilium. For a positive step deflection, there is initially a fast deflection of the bundle followed by a slower motion. During the slower motion of the bundle, $\Delta x/\Delta t$ is very small but the calcium concentration near the myosin motor complex is still increasing which decreases the strength of the motor. Therefore, a negative stiffness region exists for such step deflections and the hair bundle may slowly move further than the stimulus probe.

Calcium has two effects on myosin motors. It reduces the myosin drag coefficient as well as the amount of force that the motors produce. As shown in equations 9 and 10, both of these effects contribute to producing a negative stiffness region. Reducing the myosin drag coefficient can be static. The steady state calcium concentration within the stereocilium should contribute to reducing this parameter. Ideally, to create a negative stiffness from calcium modulation, the myosin drag coefficient for tip link 1 should be very low but the drag coefficient for tip link 2 should be comparatively higher so

that that the connected transduction channels still respond to the stimulus and alter the calcium concentration on a cycle by cycle basis.

This situation potentially sets up two distinctly different roles for the two tip links along a single excitatory column. Tip link 2 has a traditional role of sensing the deflection of the hair bundle and producing transduction current in response. The transduction current acts to provide calcium for the myosin motor complex attached to tip link 1 as well as change the membrane potential to drive the somatic electromotility. Reducing the drag coefficient of the myosin motors attached to tip link 1 makes them less able to produce transduction current in response to a deflection but more capable of reducing the force that resists the stimulus. This makes this tip link more likely to provide amplification that deflects the hair bundle but less likely to contribute to amplification via electromotility.

Figure 3 examines the response of a simple outer hair cell bundle to sinusoidal stimulation at 250 Hz. This frequency is quite low compared to the range of frequencies detected by rodents, but it is used as a first example to ensure that the bundle has enough time to move past the stimulus. This simulated hair bundle has the transduction channels attached to tip link 2 open at rest. Therefore, the initial phase of stimulation begins with a negative deflection. Panel A compares the bundle position in blue with the base of the stimulus fiber in green. The bundle moves further than the stimulus probe in the negative direction but does not move further in the positive direction. Overall, this creates a baseline position shift of the hair bundle in the negative direction. A preference for the baseline to shift in the negative direction can be easily understood if one remembers that the bundle had one set of transduction channels open at rest. This biases the bundle to move in the negative direction.

After a few cycles, the bundle does not significantly change in amplitude. The peak to peak amplitude of the bundle motion is 70 nm and the peak to peak amplitude of the stimulus probe is 80 nm. This means that the bundle has a gain of 0.875. One might hope for this value to be larger than 1 if amplification is indeed present. To examine why this value is not larger then 1, the forces along the two tip links are plotted in panel B. A moving average is applied to remove the change in tension created by rapid channel opening and closing. The tension in tip link 1 is plotted in blue, the tension in tip link 2 is plotted in green and the average of the tension is shown in red. The tension in tip link 1 is easy to understand. The myosin drag coefficient is quite low for this myosin motor complex. The force simply changes in response to the local calcium concentration. It decreases when the transduction channels on tip link 2 are open and increases when the transduction channels on tip link 2 are closed. The tension in tip link 2 is slightly more complicated. The tension naturally increases due to shear when the bundle moves in the positive direction and decreases when the bundle moves in the negative direction. In addition, the tension decreases when the transduction channels open and increases when the channels close. The tension therefore jumps between two sinusoidal patterns that are shifted with respect to each other along the ordinate axis. The decrease in tension when the transduction channels open acts to offset the increase in tension from bundle shear. This negates some of the sinusoidal tension from tip link 2 for deflections close to threshold for the hair bundle. Examining the average of the two tensions shows that the overall tip link tension for this deflection is dominated by the tension in tip link 1.

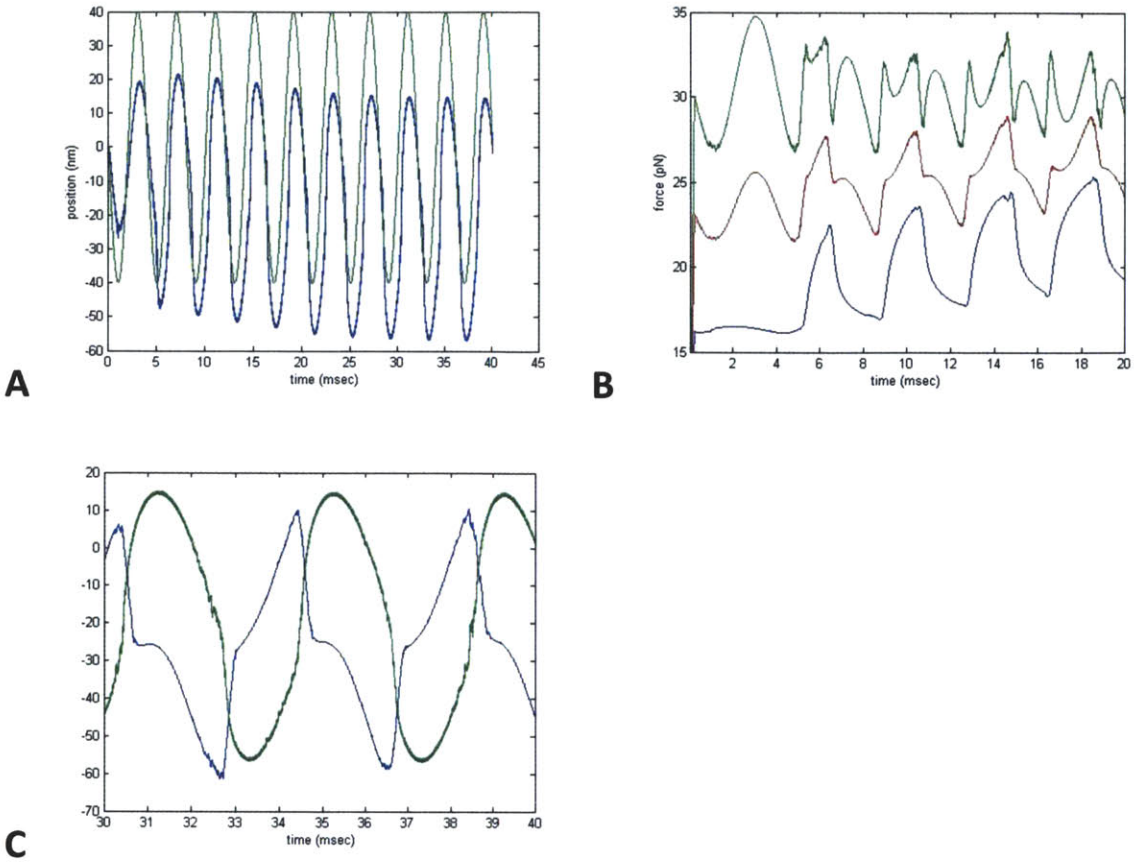

Figure 3. Response of a simple three stereocilia hair bundle to a sinusoidal stimulus at 250 Hz with k_{probe}=0.25 pN/nm. **(A)** Position of the hair bundle displayed in blue and the position of the base of the stimulus fiber is displayed in green. **(B)** Myosin motor forces for tip link 1 in blue, tip link 2 in green, and the average of the two displayed in red. **(C)** Close up view of the bundle position in green along with a scaled version of the sum of myosin motor forces used to compare the timing between the two.

For the deflection shown in figure 3, the overall tension in the tip links increases when the transduction channels attached to tip link 2 are open and increases when these channels close. This is consistent with the behavior that should produce amplification, so it may seem puzzling that this does not actually occur. The explanation as to why it does not occur can be seen in panel C of figure 3. This panel shows a close up view of the bundle position in green with the total tip link tension scaled and offset for easy comparison shown in blue. For the best amplification, the tension should be increasing when the bundle is moving in the negative direction and decreasing when the bundle is moving in the positive direction. This panel shows that there is about a $\pi/2$ phase shift from this ideal case. For about half of every cycle, the tension in the tip link is changing in the opposite manner that would create amplification. The delay comes from the time that it takes for the transduction channels to transition from one state to another as the bundle begins to change direction. Near the peak of the sinusoid, the

rate of deflection is very slow and does provide enough deflection for the channels to change state. Only near the peak velocity of the hair bundle do the transduction channels change state and thus assist in the motion of the hair bundle.

This panel brings to light an inherit problem with hair bundle amplification to a compliant fiber stimulus. Amplification in this manner can only occur when the bundle moves further than the stimulus. When a compliant probe is used, this naturally causes the stimulus to phase lead the position of the hair bundle. This means that the stimulus acts to oppose amplification in this manner. Ideally for amplification, the hair bundles should be able to exert a force on the stimulus that reshapes the stimulus pattern. This feedback between the stimulus and hair bundle is necessary to align the phase between the two mechanical elements. It is likely that this does occur within the organ of Corti with the interaction between a population of outer hair cells and the tectorial membrane. The tectorial membrane sits on the apical surface of many outer hair cells that all have a similar resonant frequency. These outer hair cells could combine their forces and cause a delay in the motion of the tectorial membrane, slightly altering the stimulus from a sinusoidal waveform. If this delay occurs on every half cycle of the sinusoidal stimulus, then a decrease in the resonant frequency of the tectorial membrane would be measured during bundle amplification. Interestingly, the tectorial membrane does display a resonant frequency half an octave lower than the resonant frequency of the basilar membrane (Gummer, Hemmert, Zenner, 1996).

Even though the simulated hair bundle never displays a gain of above 1 to sinusoidal stimulation, the gain still depends on the amplitude and frequency of the stimulus. For small stimuli, there is not enough shear to transition the transduction channels from one state to another. This means that the hair bundle behaves passively and does not exhibit any active compliance from transduction gating or calcium modulation of the myosin motor force. An example of this is shown in figure 4A. For this panel, the bundle is deflected with a 500 Hz stimulus with a peak to peak amplitude of 70 nm in blue and 80 nm in green. It is easy to see that the hair bundle moves with a much greater amplitude for the 80 nm deflection compared to the 70 nm deflection. The difference in these two cases is that the 80 nm deflection is large enough to open and close the transduction channels attached to tip link 2 on every cycle of the stimulus. This provides feedback from calcium and a reduction in tension from the gating compliance to allow the bundle to move further than the 70 nm case. For even larger deflections, the fraction of additional gain obtained from channel opening is less. Therefore, the gain approaches a more linear rate of increase for larger deflections. This means that small deflections are selectively amplified more than larger deflections, a situation that is ideal for amplifying quiet sounds but not loud sounds.

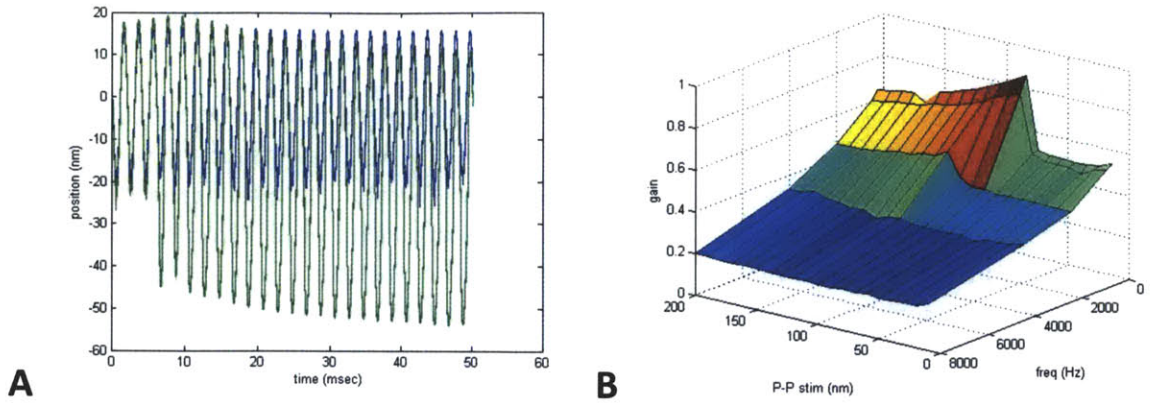

Figure 4. (A) Position of a simple three stereocilia hair bundle to sinusoidal stimuli at 500 Hz with k_{probe}=0.25 pN/nm. Blue displays the bundle position in response to a 70 nm peak to peak stimulus and green is the bundle position in response to a 80 nm peak to peak stimulus. **(B)** Bundle gain as defined as peak to peak bundle deflection divided by the peak to peak deflection of the base of the stimulus plotted versus stimulus frequency and amplitude.

The gain of the hair bundle motion also depends on the frequency of the stimulus. Increasing the frequency also increases the drag forces on the bundle as well as drag from the myosin motors, as evident in equations 9 and 10. Panel B of figure 4 shows the combined influence of amplitude and frequency on the gain of the hair bundle motion to sinusoidal stimulation. For lower frequencies, there is a distinct amplitude for which there is a sudden jump in the gain. This corresponds to the amplitude at which the transduction channels attached to tip link 2 open and close during every cycle. As the frequency increases, the passive gain decreases. This means that the stimulus has to move more to elicit a change in the transduction channel open probability. This shifts the transition point to larger amplitudes for higher frequencies. For higher frequencies, the transition point becomes nonexistent as the issue with the phase delay of the feedback becomes increasingly problematic.

Outer hair cells can be very difficult to work with. They have small hair bundles and are natively stimulated at very high frequencies. In addition, they are bathed in a low extracellular calcium concentration. This section explored the possibility that they can amplify a stimulus motion through calcium modulation of the myosin motors. For stimulation with a flexible fiber, many factors limit the ability of a single hair bundle to create amplification of the stimulus. It is possible that the combined efforts of many hair bundles make amplification possible by giving the hair cell more control over the stimulus. This idea makes outer hair cells even more difficult to study during experiments. A proper mechanical stimulus used during sinusoidal stimulation should likely require feedback with the position of the hair bundle. A stimulus with feedback would better mimic *in vivo* stimulation and be more likely to produce amplification.

Changes in Outer Hair Cell Behavior with Calcium Concentration

Traditionally, physiologically experiments on hair cells have involved using an extracellular solution with a calcium concentration higher than 1 mM. It is thought that divalents in the extracellular solution are helpful in establishing a seal for whole cell recordings. Therefore, a high external calcium concentration helps to make the experiments easier from a practical point of view. Typically, the extracellular concentration can be lowered with a separate profusion pipette in the vicinity of the hair cell or in the entire bath solution by using a profusion system. An extremely low external calcium concentration also has the potential to break the tip links, thus removing the transduction apparatus. Finally, a high external calcium concentration increases the rate and extent of adaptation. For these reasons, experiments on hair cells tend to utilize high external calcium concentrations.

Even given the prior reasons, a high external calcium concentration might not be the most ideal environment for studying outer hair cell physiology. The chapter on calcium diffusion showed that the decreased diameter of outer hair cells coupled with their smaller height drastically increases the amount of calcium that can diffuse into the hair cell body. This calcium can also make its way from the hair cell body back up into adjacent stereocilia. *In vivo*, the external calcium concentration is around 20 μM. For this calcium concentration, the intracellular calcium concentration does not greatly increase in the tallest stereocilia. This difference in intracellular calcium concentration should greatly change how outer hair cell bundles respond based on the external calcium concentration. This section explores how the calcium concentration changes outer hair cell behavior. These results from the model can be used to predict future experimental results.

The reported resting current in outer hair cells varies largely depending on the external calcium concentration. With 1.5 mM external calcium concentration, the resting current tends to be around 6 percent of the overall current (Johnson *et. al.*, 2011). In 20 μM external calcium concentration, the resting current also depends on the strength of the internal calcium buffer. For a calcium buffer with a high affinity for calcium such as BAPTA, the resting current is around 46 percent of the overall current. If the internal calcium buffer is weaker, then the resting current is near 6 percent of the overall current.

Calcium changes the resting current in outer hair cells by weakening the myosin motor force in stereocilia and does not increase the amount of force that myosin motors produce. Therefore, the underlying assumption must be that in the absence of calcium the myosin motor complexes provide enough force to keep transduction channels mostly open at rest. This means that the transduction channels attached to tip link 2 are constantly open and provide a source of calcium for myosins attached to tip link 1 along the same excitatory column. Even in 20 μM external calcium concentration, the calcium influx is enough to weaken the myosin motors on tip link 1 enough that the attached transduction channels are mostly closed at rest. If this were not the case, then the transduction current would be closer to 100 percent open at rest.

When the extracellular environment contains 1.5 mM external calcium, then the calcium influx is much larger. Calcium can diffuse down the second tallest stereocilia and back up into the tallest row

of stereocilia. This weakens the myosin motors connected to any tip link 2 so that they are mostly closed at rest. When these transduction channels are mostly closed at rest, the open probability is not zero but somewhere closer to 6 percent. This allows calcium to continue through the transduction channels located in the second tallest stereocilium. This produces enough calcium that myosin motors from all of the tip links are sufficiently weakened to keep them mostly closed at rest. This constant calcium feedback across stereocilia maintains a small open probability at rest.

Figure 5 displays the transduction current and intracellular calcium concentration for a full outer hair cell bundle in either 1.5 mM external calcium or 20 μM. The resting current for the 1.5 mM case is around 8% of the total and in 20 μM it is about 55%, which is in line with the reported values. These traces also show that adaptation is slower and less complete in the low calcium condition. Panel C and panel D show the calcium concentration along the middle column for the two calcium environments to the 60 nm deflections. The calcium concentration in the smallest stereocilium does not affect the force of a myosin motor complex but is a reflection of the open probability of the transduction channels located in that stereocilium. For the 1.5 mM case, the initial calcium concentration near the myosin motors for the middle stereocilium is 500 μM and it is 250 μM for the tallest stereocilium. Both of these concentrations are high enough to keep the myosin motors mostly closed at rest. The small open probability of the transduction channels is enough to keep the calcium supply near these concentrations. For a positive deflection, the calcium concentration rapidly rises in the smallest and middle stereocilia. The force reduction for tip link 1 causes the connected transduction channels to quickly close which decreases the calcium concentration in the smallest stereocilia. The calcium in the middle stereocilia takes some time to diffuse into the tallest stereocilia. This eventually reduces the force of myosin motors on tip link 2 which causes those channels to close. This reduces the calcium concentration in the middle stereocilia. The exact timing of this event varies across stereocilia which creates a more gradual decline in the current.

For the 20 μM case, the initial calcium concentration near the myosin motors for the middle stereocilium is 320 μM and it is 120 μM for the tallest stereocilium. A calcium concentration of 120 μM is not enough to make the connected transduction channels mostly closed at rest. Therefore, the transduction channels in the middle stereocilia are mostly open at rest and cause the calcium concentration to increase for those stereocilia. The low external calcium concentration limits the actual amount of calcium influx through the transduction channels which limits the amount of calcium that enters into the tallest row of stereocilia. For a positive deflection, the calcium concentration in the stereocilia with myosin motors does not change much as the state of the channels in the middle row of stereocilia does not differ much from rest. Upon a return of the bundle to the baseline position, the channels in the middle row of stereocilia close which reduces the overall calcium concentration. The large amount of rebound current arises because the myosin motors are moving along acting but not largely changing the state of the transduction channels for the initial step. This sets them up to respond to the bundle return to the baseline position. This is an effect that is also seen experimentally.

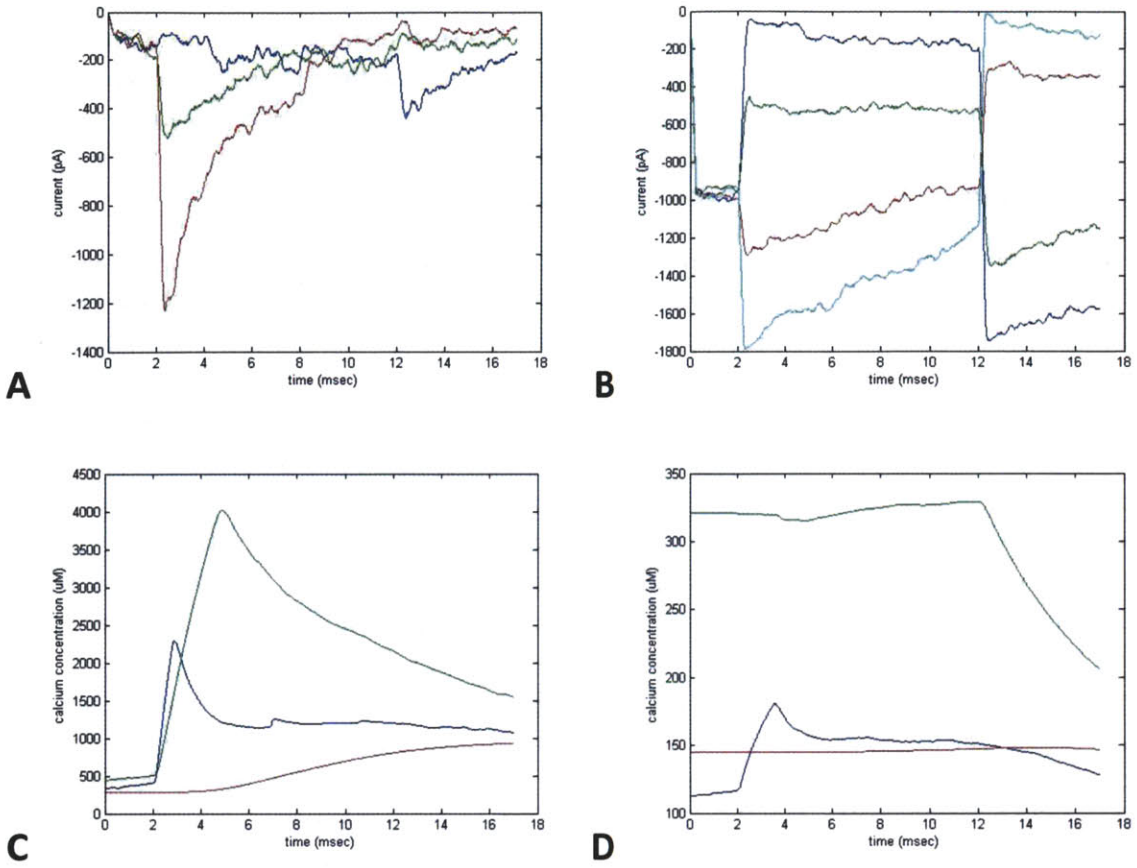

Figure 5. Transduction currents and calcium concentrations in a hair cell with a full outer hair cell bundle. The bundle was stimulated with a fiber with 20 pN/nm stiffness. **(A)** Transduction current in response to -30 nm (blue), 30 nm (green), and 60 nm (red) probe deflections for an external calcium concentration of 1.5 mM. **(B)** Transduction current in response to -60 nm (blue), -30 nm (green), 30 nm (red), and 60 nm (cyan) probe deflections for an external calcium concentration of 20 μM. **(C)** Intracellular calcium concentration near the myosin motors along the middle column for the smallest stereocilium (blue), middle stereocilium (green) and tallest stereocilium (red) along the column for a 60 nm deflection in 1.5 mM extracellular calcium concentration. **(D)** Same as in C but in 20 μM extracellular calcium concentration.

The case of calcium concentrations in between the two discussed is also fairly interesting. The resting current depends on the myosin drag coefficients as well as the motor forces. A low drag coefficient allows a myosin motor complex to make many transitions from a mostly open state to the mostly closed state and vice versa. This allows the transduction channels connected to a tip link to have an average current in between the two states, which alters the amount of calcium influx. If the myosin drag coefficient is too high, then each myosin motor complex will stay stuck in either the mostly open

state or mostly closed state depending on the motor force. This essentially limits the possible resting currents.

This difference is demonstrated in figure 6. For these stimulations the resting current was simply measured for various external calcium concentrations. β_{myosin}=200 pN-μsec/nm for blue and β_{myosin}=2000 pN-μsec/nm for green. For the high myosin drag coefficient, the current only existed near 50% or 6%. For the low myosin drag coefficient case, the resting current took on a wider range of possible values. Observing this effect would be evidence that there are two distinct sets of myosin motors within outer hair cell bundles. It also provides some insight into the drag coefficient for myosin-1C in outer hair cells. Based on fits to the available data, the drag coefficient should be closer to the lower case.

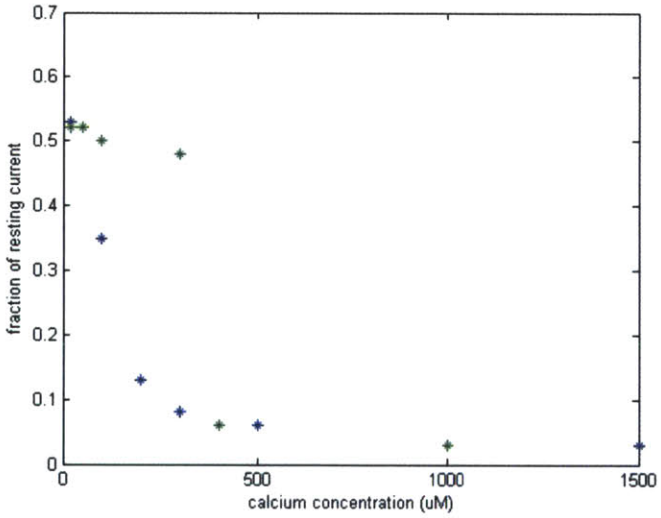

Figure 6. Fractional resting current versus calcium concentration for two different myosin drag coefficients. β_{myosin}=200 pN-μsec/nm for blue and β_{myosin}=2000 pN-μsec/nm for green.

Changing the holding potential can also be used to confirm that calcium influx through transduction channels is indeed responsible for the hair bundle moving further than the stimulus probe. This simulation is fairly straightforward and is shown in figure 7. The bundle is deflected with a 60 nm displacement to the base of the stimulus fiber. The membrane potential is changed to +80 mV either before the deflection, 5 msec after the deflection, or never. When the holding potential of -80 mV is held, the hair bundle moves past the base of the stimulus probe. For the case where there is no driving force for calcium, then myosin-1C is not weakened after the transduction channels open. This means that the bundle does not move as far as the stimulus for this case. Finally, if the calcium influx is removed after 5 msec, then additional positive motion of the bundle ceases. The bundle slightly moves in the negative direction which makes sense because the calcium is slowly being removed from the

stereocilia. This result is strong evidence that the motion further than the stimulus requires calcium influx after the deflection.

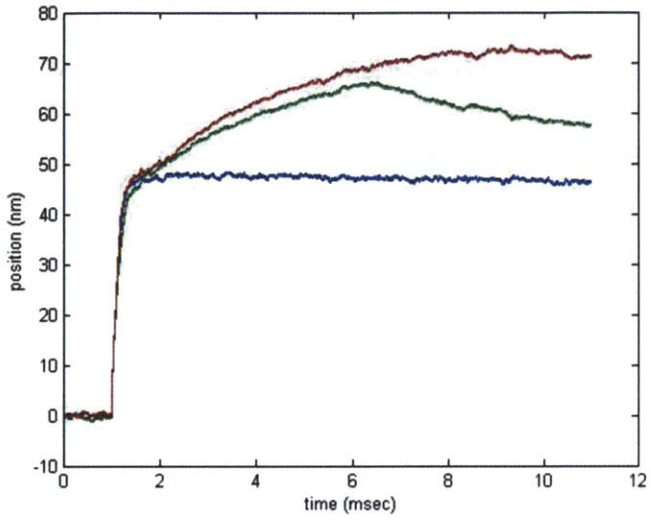

Figure 7. Position of the hair bundle in response to a 60 nm deflection with a 5 pN/nm probe. The holding potential was changed from -80 mV to +80 mV at 0 msec (blue), 6 msec (green) or never (red).

Conclusion

Outer hair cells are a complicated subtype of hair cell. They respond to a potentially complicated stimulus that originates from the interaction of the basilar membrane and tectorial membrane. In addition, they clearly change the motion of these structures by changes in the somatic length as well as active motion in the stereocilia. This feedback is further complicated by the fact that a population of outer hair cells in a local region all contribute to the feedback. Thus a thorough understanding of how outer hair cells effect mechanical amplification requires a complex physical model involving many outer hair cells in a region of the Organ of Corti.

This chapter explored the ability of the stereocilia to amplify a stimulus along the excitatory axis of the hair bundle. It was found that amplification is possible if the phase of the calcium feedback is aligned with the phase of the stimulus. This is difficult to obtain with a flexible fiber following a simple sinusoidal path. Future experiments on outer hair cells should explore new techniques to stimulate the stereocilia. This includes a better way of controlling all of the stereocilia as well as exploring new stimulus waveforms. Outer hair cells most likely respond best to a modified sinusoidal stimulus. Confirmation of this idea would not only provide insight into the behavior of outer hair cells but also provide insight into cochlear micromechanics.

Appendix A

Laser Tweezers User Guide

Introduction

This chapter describes a laser tweezers setup that was constructed in order to study intact epithelial preparations using an upright microscope. The goal of this setup was to attach silica beads of approximately 2 μm diameter to hair bundles from utricular and cochlear hair cells from mice. The benefit of a laser tweezers setup is that the stimulus force delivered can be precisely controlled and the position of the stimulus bead can be accurately measured with the resolution of a few nanometers.

Using laser tweezers as a stimulating technique proved to have a fatal difficulty. The laser power necessary to properly deflect the hair bundle had a damaging effect on hair bundle transduction. Repeatedly, transduction currents would diminish and then disappear over the course of less than half a minute when the laser power was high enough to deflect the bundle to elicit maximum transduction current. For an upright microscope, the laser path has to travel through the hair bundle and the hair cell body. This is not the case for dissociated hair cells in which the laser power seems to be less damaging to transduction.

This chapter does not seek to give a thorough description of optical trap theory. This chapter is more concerned with acting as a reference for future use of the laser tweezers setup. It is included in this thesis because laser tweezers are a potential experimental technique for some of the proposed future experiments. In particular, laser tweezers are the only possible technique to directly stimulate transduction channels from a single tip link. It proceeds with a description of the hardware setup followed by discussing the control and analysis software. Finally, a section describing some of the specific techniques that the laser tweezers utilized is presented with the idea that similar techniques can be useful for future experiments.

Hardware Setup

General Laser Tweezers Setup

The general optical setup for the laser tweezers is displayed in figure 1. The trapping laser is a 12W, 1064 nm, Nd:Yag diode-pumped laser. This laser is kept outside of the sound-proof chamber due to the excessive noise that the water cooling system produces. The output of the Nd:Yag laser is focused into a multi-mode fiber optic cable. The fiber optic output is in the sound proof chamber mounted on an optical breadboard. The optical breadboard is mounted on a floating physiology table in which all of the experiments are performed. The 1064 nm light path first enters through a 1064 nm $\lambda/2$ waveplate in order to achieve a vertically polarized light beam. The beam is reflected and aligned by two mirrors and then passes through a two-axis acousto-optic deflector. This creates multiple modes of the beam. The light is focused through a 75 mm plano-convex lens and only the first order mode in both dimensions is allowed to pass through an aperture. The beam is reflected off of two mirrors and then passed through a 300 mm plano-convex lens. The net effect of the telescoping lenses is to produce a

four time enlargement of the beam diameter. The beam is then reflected off of a dichroic mirror. The dichroic mirror directs the light through a 75 mm plano-convex lens and then directly into the side port of the microscope. The light is reflected off of a filter cube at a 45 degree angle down towards the objective. The back focal length of the objective is 75 mm. The objective focuses the beams at the focus of the microscope which allows small silica beams to be trapped.

The detection laser is a 250 mW 980 nm diode laser. The laser is mounted on a custom built platform directly on the floating table. The light path is directed into a laser power controller. The laser power controller monitors the laser power and performs a feedback loop to keep the laser power steady. The 150 mm separation between the laser and the laser power controller allows the beam to enter the device at its waist; this creates the best power control. The beam exits the power controller and proceeds through a -25 mm plano-concave lens and a 125 mm plano-convex lens. These lenses were empirically determined to provide proper beam expansion with a collimated output. An aperture changes the beam profile from a rectangle to a circle. The detection beam reflects off of two 45 degree mirrors and passes through two 125 mm plano-convex lenses. These four elements simply allow the beam to be co-aligned with the trapping laser. The detection laser follows the same path as the trapping laser into the microscope.

Both of the laser beams pass through the cover slip of the experimental chamber and are collected by the collector lens of the microscope. The beams are reflected off of a 45 degree dichroic mirror that reflects the 980 nm laser preferentially. Both beams then pass through two 1064 nm notch filters and one long-pass filter that preferentially pass the 980 nm light while rejecting light at 1064 nm. Finally, the light is collected by a position sensitive photodiode.

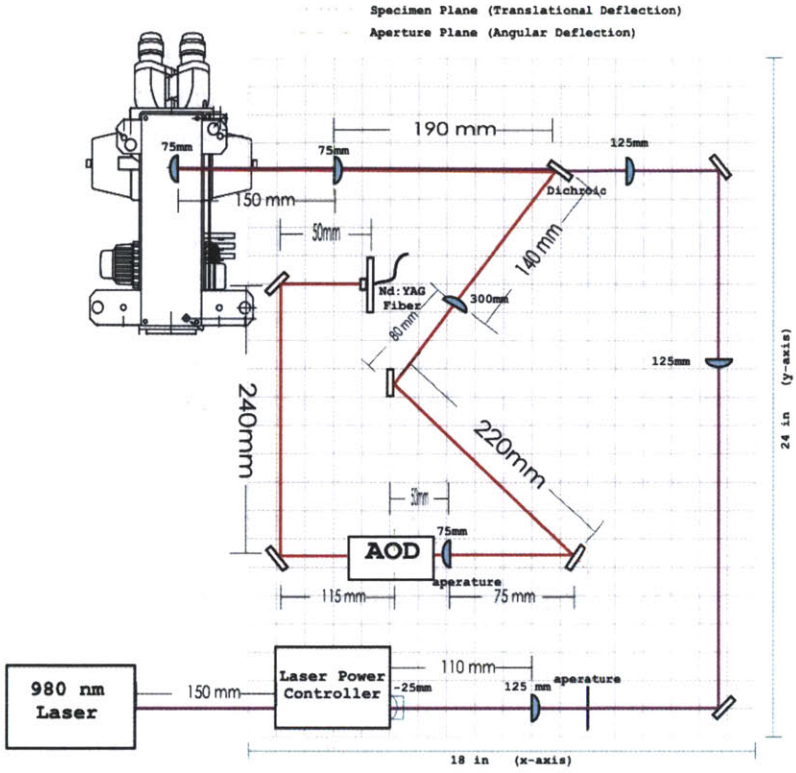

Figure 1. Schematic View of Laser Tweezers Setup.

External Laser Alignment through the Fiber Optic

The trapping laser consists of two diode pumping lasers that connect directly into a Nd:YAG laser. The diode pump lasers are connected to the Nd:YAG laser via two shielded fiber optic cables. These cables should be inserted into the Nd:YAG laser. The Nd:YAG laser also requires that the cooling system have both hose lines attached to it. To start the trapping laser, first turn on the cooling system and then flip the power switch on for the diode lasers. The diode lasers will take about 5 minutes to boot up. The boot up status will be displayed on the external display of the diode lasers box. Once the diodes are in the wait status, the laser may be started by software control read in via the serial port. The software control for the diode lasers is contained in the Labview routine, Laser1.vi. Run the vi. If a communication error occurs, just hit okay. Before the laser is turned on, make sure that the output of the Nd:YAG laser is blocked and that nobody is in danger of beam exposure. To turn on the laser, simply queue the diodes on and provide a power level of 2 W. This should be the initial power level. Once the value is reached, the power can be lowered; however, initially the laser power becomes unstable for values lower than 2 W.

Once the beam is on, extreme care should be taken not to touch or directly look at the beam. Protective goggles with an OD of 7 or higher at 1064 nm should be worn at all times. The Nd:YAG laser is housed within a black box mounted onto the side of the sound proof chamber. This provides increased mechanical stability of the beam aligned with the fiber optic. Within the box are three

components: the 1064 nm laser, an electronically controlled shutter, and the fiber optic mounting device. The laser should be mounted on one end of the optical breadboard with the beam directed along the length of the breadboard. The beam path should be roughly parallel with the optical breadboard. The shutter should be mounted such that the aperture is aligned with the beam path. Infrared sensor cards should be used to view the beam. Additionally, the laser will burn a line in a black plastic ruler. This technique can be used to measure beam positions along its path.

The fiber optic is extremely hard to align. A power of 500 mW should be used for the alignment. For the multimode fiber, 50 percent transmission efficiency should be as good as to be expected. Single mode fibers can achieve up to 90 percent transmission, but they are even harder to align. To align the fiber, the output of the fiber optic should be nearby with the output directly projecting onto an Infrared sensor card. It is also helpful if the lights are all out and it is dark outside. The fiber optic should be roughly mounted so that the input is about 2 feet from the output of the laser and coarsely aligned with the laser beam path. The 2 feet requirement is so that the fiber optic accepts the laser light at roughly the beam waist. Next, adjust the x and y manipulators of the fiber optic mount until a small amount of light is visible on the IR card. Once this occurs, an iterative process occurs for alignment. Adjust only one dimension at a time and a laser power meter will now have to be used. As the mount is moved throughout its range in one dimension, the light output from the fiber optic will disappear completely and then reappear either stronger or weaker. Find the position in that dimension in which the output produces the strongest power. After that, keep alternating dimensions using the same process until the fiber optic is optimally aligned. Once this is done, you can put the protective box back around the laser and hopefully never have to do this again. For the rest of the alignment, the initial laser power should be kept around 1 W or less.

Acoustic Optic Deflector Alignment

The light input into the Acoustic Optic Deflector (AOD) needs to be vertically polarized in order to be properly deflected. The $\lambda/2$ waveplate can rotate the polarization vector to achieve this. The polarization can either be checked by rotating the waveplate and measuring the laser power as the beam passes a polarizer, or by partially aligning the AOD and then adjusting the waveplate until maximum deflection efficiency occurs. After the waveplate, the beam should be roughly parallel to the optical breadboard and enter through the first aperture of the first AOD. The beam should be aligned with power on the first AOD before power is applied to the second AOD. The AOD requires a MHz control signal from the software to be sent to an external power amplifier box. The external power amplifier must be turned on by pressing the front panel power button. The easiest way to control the MHz signal for alignment is by using the angle.vi subroutine in the Tweezer Control.vi main control program. At the power amplifier box, unplug the cable to the second AOD in order to just deflect the beam in one dimension. Ideally, the exact power and frequency to the AOD should be adjusted for proper alignment of the AOD. For routine alignment, a small deflection in the angle program should be given in order to examine the beam deflection. Using an IR indicator card, several dots should appear on the card. The stationary dot is the zero order beam and the ones that move are the higher order beams. The knobs on the first deflector should be adjusted until the first order spot directly below the

zero order spot appears the brightest. Ideally, 75-85% of the input power can be redirected into this first order beam. This can be examined by blocking the other order beams with an aperture and measuring the power in the first order beam. This power should be maintained throughout the desired deflection range of motions. Once this deflector is aligned, do not touch it again or touch the mirrors aligning the beam into the deflector. Reconnect the cable to provide deflections to the second deflector. Adjust the angle so that deflections are only created in this new dimension. Repeat the alignment process for the second deflector so that the first order beam in each dimension contains 50%-70% of the input power throughout the desired range of deflections. After this, the beam is aligned through the AOD and only the first order beam in both dimensions should pass through an aperture placed right after the first converging lens.

Final Trapping Laser Alignment

The final alignment of the trapping laser should only involve the 3 mirrors and 2 lenses that come after the AODs. The mirrors deflect the beam at an unusual angle. This is to allow the dichroic mirror to properly reflect the 1064 nm light and pass the 980 nm light from the detection laser. In general, the beam should be roughly aligned so that it passes or reflects at around the middle of the optics. Following this, the beam should enter the side port of the microscope and be adjusted through either a low power objective lens or no objective lens so that the laser light shines on IR card where the specimen is usually placed. After this, place the 60x objective in position. The alignment will proceed from this point on by examining the laser light reflection off of the chamber cover slip onto the camera. To allow the laser light to pass to the camera, the IR filter just below the binoculars of the microscope should be removed. When the laser is on, protective eye wear should always be worn; this is especially the case when the IR filter is removed that normally blocks the laser binoculars. The reflection on the video monitor should ideally look like a series of concentric circles with each outward circle becoming weaker in intensity. Initially, the video monitor will have several laser spots with only a few of them appearing this way. A single spot will appear to be the brightest if not the nicest looking pattern. Adjust the mirrors and lenses until that spot appears as bright as possible and in the middle of the screen. Next, the image should be "walked" until the image starts looking like the desired series of concentric circles. This is accomplished by moving the beam in one direction by adjusting a mirror or lens and returning it to the original location by adjusting another optical element. Once the reflection of the trapping laser appears as a symmetric airy pattern, the focus of the laser should be adjusted until the width of the pattern is smallest at the top surface of the cover slip. After this point, the trapping laser is fully aligned. From this point on, only the lens directly in front of the side port of the microscope should be adjusted.

Detection Laser Alignment through the Laser Power Controller

The detection laser is a simple CW diode laser with an output power of 250 mW at 980 nm. The laser does not have an on/off switch and is turned on by simply plugging the power cable into an outlet. The platform mount for this laser should be adjusted with the adjustment nuts below the platform until

the laser beam is roughly parallel to the optical breadboard and roughly aligned with the laser power controller aperture. The laser power controller acts to reduce any fluctuations in the intensity of the output beam. It passes 90% of the input light and samples the intensity of the remaining 10% of light with a photo-detector. The output of the laser is modulated to a desired transmission percentage or power. To use the laser power controller, the laser should already be turned on and incident on the controller. Next, the laser power controller should be turned on by pressing the on switch on the control box. The power controller automatically performs a calibration once it is turned on. If the incident light is adjusted after the controller is already turned on, then the calibration button needs to be pressed in order to recalibrate the device.

The laser power controller box is easy to control. Nothing should be done until the calibration is complete which takes approximately 20 seconds. First, select the wavelength adjust button. Adjust the wavelength until the display reads 980 nm. Then, make sure that the mode is set to mode 1 which is the power control mode. Next, adjust the output power to the desired amount. Typically, a power around 50 mW is appropriate for experiments. Once the power is set, then the laser power has minimal noise, which is important for improving the resolution of the bead position detection system.

Final Alignment of the Detection Laser

The output of the detection laser immediately passes through a -25 mm plano-concave lens followed by a 125 mm plano-convex lens that is about 110 mm further down the beam path. This combination is an unconventional optics pair of lenses. The plano-concave lens diverges the beam until it encounters the plano-convex lens which properly converges the beam so that it is collimated. This pair was chosen to produce an expanded beam that is collimated in a short distance. The plano-convex lens should be adjusted slightly along the beam path to ensure that the output beam is indeed collimated.

The aperture just following the plano-convex lens is used to adjust the shape of the beam. The diode laser produces a rectangular shaped beam. The aperture simply shapes the beam into a circle. Ideally, one would like the direct output of the laser to be circular, but this is a practical solution that works for this system. A circular beam is easier to adjust and focus further down the beam path.

Following the aperture, there are 2 additional mirrors and 2 lenses that the beam must pass until in encounters the dichroic mirror. All adjustments to the detection laser path must be made with these four elements because adjustments made to the dichroic mirror or further also readjust the trapping laser. The two lenses in this path are telescoping lenses that both have a focal length of 125 mm and are placed roughly 250 mm apart, along the beam path. Therefore, these lenses do not produce any additional enlargement of the beam width and maintain beam collimation. They are used to make fine adjustments to the alignment of the laser beam path.

The first mirror should be adjusted until the laser beam hits the mirror directly in the center of its surface. The beam should be reflected parallel to the optical breadboard surface. The next lens should also be adjusted until the beam strikes it in the middle of its surface. This should be repeated for the following mirror and lens. Next, small adjustments should be made iteratively to all four elements until the beam strikes the dichroic mirror roughly in the same location as the trapping laser and proceeds along a similar path into the side port of the microscope. This technique involves a lot of patience and could take quite a bit of time.

Once the beam is roughly co-aligned with the trapping laser then the beam should be adjusted by examining the reflection off of the cover slip on the monitor. This technique should be performed in the same manner as the trapping laser was adjusted. The two mirrors and lenses in between them should primarily be adjusted in order to create the ideal airy pattern off of the cover slip. Once this shape has been established, the beam should gradually be adjusted so that it occupies the same location as the trapping laser. Care should be taken so that the shape of the reflection maintains an airy pattern. Once the two beams overlap each other then proper co-alignment should be tested by moving the final lens closest to the side port of the microscope. Any adjustment to this lens should now move the focus of both lasers an equal amount. If this is not the case, then adjustments should be made only in the detection laser path until this is true.

Alignment of the Photo-detector

Both lasers essentially have the same path as they proceed through the cover slip and into the collector lens. The idea behind the detection laser is that when the silica bead moves, it slightly adjusts the way it refracts the detection laser light. An infra-red wavelength is used for the detection laser so that there is minimal absorption by the experimental tissue. However, the trapping laser also uses an infra-red wavelength. It is therefore not a trivial matter to attenuate the light from the trapping laser while passing the light from the detection laser before it reaches the photo-detector.

For this alignment process, only the detection laser needs to be turned on. Several elements are held in an optical alignment cage. The first element is a dichroic mirror that preferentially reflects light below 1000 nm in wavelength. This already attenuates the 1064 nm wavelength light. This mirror should be placed directly above the light source for the microscope. The light should be reflected off this mirror parallel to the breadboard table that the microscope is mounted on. One additional element is held in the optical alignment cage: a notch filter that removes 99% of the laser light at 1064 nm. This element can be anywhere along the laser light path but an additional notch filter is also used to attenuate the remaining 1064 nm light. These two filters cannot be placed directly adjacent to one another as they lose their effect when used in this way.

The remaining light is directed at a position sensitive detector. The detector has two filters mounted directly in front it. First, a long-pass filter blocks out all visible light to remove any signal from the visible light in the room. Following this, an additional 1064 nm notch filter is placed right in front of

the detector. The detector is mounted on a custom built aluminum mount that holds the filters and detector as one single unit.

The photo-detector is a Pacific Silicon position sensitive detector which allows for the determination of an image in two dimensions. Three useful signals are outputs from the detector: an x signal, a y signal, and an overall light intensity signal. All of the signals from the detector are connected to a box that puts the detector signals into a coaxial line using a common ground. The x and y signals are sent to a differential amplifier. This allows for an offset and gain of the signal which are important preprocessing steps before the signals are digitized. The preprocessed signals are then sent to the National Instruments DAQ board to be read in by the software that will be described later.

It is difficult to properly align the detector because its surface is hidden behind the two filters. The laser should be roughly aligned so that it hits the middle of the first filter. Next, the overall intensity signal should be examined while the detector position is finely adjusted. The best adjustment occurs when this signal reaches a maximum for adjustments in both directions.

Final Alignment

The system is almost perfectly aligned. The final step is to place a solution of beads in the experimental chamber. The trapping laser should be able to trap a bead and hold it in the center of focus. This can be examined by using the monitor. If this is not the case, then this laser needs to be realigned following the earlier process. Only the optical elements past the acoustic optic deflector should be touched for additional alignment.

If trapping successfully works, then a small triangle deflection pattern should be given using the control software. The bead will slowly move back and forth. The x and y signal can be examined on an oscilloscope. If the response is not a triangle, then the optical signal is too large for the detector. The detector path should be realigned until a triangle response is observed for oscillations in both the x and y dimensions, while a near zero signal is observed on the non-stimulated channel. The easiest initial adjustment is to finely change the position of the 125 mm plano-convex lens that is located between the two mirrors on the detection laser path. Adjusting this lens along the direction of the beam path adjusts the size of the bead projection onto the detector, which usually allows the signal to become linear. If this has been successfully done then the optical paths are properly aligned.

The final step to perform is calibrating the motion of the bead with the detection signal. The motion of the bead can easily be observed on the monitor. Typically, the best micrometer is to use the diameter of the bead as this typically has a very tight tolerance. For a given deflection signal from the computer, the optical trap always moves a consistent amount. This calibration only needs to be performed when adjustments to the optical path are made. The signal from the detector versus the motion of the bead changes based on the environment. For example, the tissue below the bead will change the gain of this signal. Therefore, this calibration needs to be performed in free solution immediately before an experiment is performed. Furthermore, this calibration should be done as close to the actual location of the experiment in the chamber.

Software Setup

The control software has a few purposes. The software must control the output power of the trapping laser, send control signals to the acoustic optic deflectors, receive position signals, and control the patch clamp equipment. All of the software is written in Labview which directly sends and receives analog and digital signals through an attached DAQ board. The laser control is controlled by a separate program called Laser1.vi. Everything else is controlled by the master program called Tweezer Control.vi. There is an additional program that is used for analysis called Analysis.vi.

Laser Power Control

The program Laser1.vi directly controls the output from the diode laser box for the trapping laser. The diode lasers must already be turned on and the status should read ready before Laser1.vi is run. The control software communicates directly with the diode laser box through a serial cable. The control computer sends serial commands to increase the current sent to the two diode lasers contained within the diode laser box. The laser box sends back the current that each diode is receiving as well as the temperature of each diode laser.

There are multiple modes to control the laser. For the laser tweezers application, the only mode that should be used is the mode which controls the output power of the laser. In this mode, the power is set and the current needed to obtain this power is constantly monitored and adjusted by the program. To adjust the power, the Change Power button should be pressed, which brings up a slider that can slide from 0 to 12 W. The initial power should never be set to less than 2 W as the feedback control becomes unstable for values less than this. Once 2 W has been reached and the power is stable, then the power can be turned down as low as 0.5W. Any value below this makes the feedback unstable again, and occasionally the laser might turn off. Once the power is selected, then the new value command must be sent. To do this, the user must simply click the Send button at the bottom of the control panel.

Additionally, the diodes must be turned on for the laser to emit power. This can be done by clicking on the Control Toggle button to turn the diodes on. Again, the Send button must be hit to send this signal to the diode control box. The Send button can be clicked to change the power and turn the diodes on at the same time.

From this point, the laser should be turned on. This can be verified when the Laser Status box displays that the laser is on. The temperature will constantly be monitored and the laser will automatically be turned off if the temperature becomes too high. This should never be the case if the coolant system is turned on. During an experiment, this routine should rarely be used, except to potentially change the output power of the laser.

To turn the laser off, the diodes should first be turned off. If this is not done, then the laser will still be turned on, even if the control software is not active, which is dangerous. Once the laser status box reads that the laser is off, then the Stop button can be pressed. This stops Laser1.vi until the laser

needs to be used again. Finally, the outside power switch should be turned off to completely turn the diode lasers off.

Laser Tweezers Control Front Panel

The front panel for the main control program is organized so that the entire mechanical and patching systems can be controlled from the front panel. There are 2 graphical displays that show the voltage control stimulus and mechanical stimulus with respect to time, a graph that shows the recorded current, and three graphical displays that display the signals from the position detector. There are a few control buttons and additional displays. The files are automatically named based on the date and run number. This is displayed on the front panel. The acoustic optic deflectors are controlled by a card that uses a digital code. The actual digital code for this is also displayed on the front panel. A control variable is used to change the initial starting number for the files. This is useful if experiments from earlier in the day have already been saved. The Number of Runs control tells the software how many times a stimulus protocol should be run before the user is asked if they want to save the data. The Seal Test button runs a subroutine that delivers voltage pulses to the patch clamp. This is useful for determining the strength of the seal during patching. The Angle button changes the angle of the laser deflection. The Reset Parameters button is used to input in a new set of mechanical and voltage protocols. This can either be done manually or by loading in a saved parameter set. The Fire button runs the stimulus protocols for the given number of runs. Finally, the Stop button is used to stop the program completely.

Stimulus Protocol Setup

When the user first starts the main control program, then they are prompted to change the parameters. This can also be done at anytime by using the Reset Parameters button on the main control panel. The stimulus protocols are designed using Pclamp software as a model. Each stimulus is divided into epics, episodes and runs. An epic refers to using a given set of stimulus parameters throughout time. For instance, the user can have the voltage at a particular voltage for one epic. Changing it within the same signal waveform requires setting a new voltage level in the next epic. There can be up to 6 epics, with the number of epics used in an episode being set by a control variable. An episode is one presentation of the stimulus during a given period of time. Each episode can have a certain parameter change for an epic from the previous episode using the Δ controls. The number of episodes per run is a control variable. Finally, the number of runs refers to the number of times that the identical set of episodes is presented. This variable can be controlled with the other protocol parameters or on the main front panel.

Additional protocol parameters involve setting up the output and input of the device. The analog input channels can be user defined. They receive inputs in order for the current, x signal, y signal, and sum signal from the detector. The analog output channel refers to the analog output that contains the voltage control signal. The buffer size is the number of input samples that the buffer can

receive per episode. The current maximum value for this is 10000 per episode. The analog update rate is the sampling rate for the analog input data. This should not be set above 20000 samples/second. Finally, the digital update rate is the rate at which command words are sent out of the digital port to control the acoustic optic deflector control card. This value must be at least 100 times larger than the analog sample rate.

In addition to setting up the input and output settings, the protocol parameters also can set the initial angle of the laser deflections and the holding potential of the patch clamp. The holding potential added in addition to any additional voltage command. The angle control can be reset separately by using the Angle subroutine from the front panel. This is the best way to make sure that the stimulus angle is correct for the experiment.

The voltage and mechanical parameters are easy to change. They are updated in a similar manner. Each epic is set using controls aligned in order as a column. The main variable name changes that variable during that epic for the first episode. Changing the Δ variable makes an addition of the Δ value for each additional episode. Each epic can be defined as a square, triangle or sinusoidal stimulus. The Level defines the base position for the epic. The amplitude is only referenced for sinusoids and triangle patterns. This defines the amplitude of the stimulus that is added onto the baseline level. The frequency refers to the frequency of the repeating function as defined in Hz and the phase sets the phase with reference to a sine wave. The duration is the length of the epic in number of samples. These are the variables that are the same for both the mechanical and voltage protocols. The graphical panels to the right of the control panels display the stimulus for both sets of controls. These are the same graphs that are shown on the main front panel.

The mechanical control is slightly more complicated than the voltage control. First of all, the mechanical control shows the magnitude of the entire mechanical stimulus. The actual stimulus has x and y components that are calculated by the angle of the stimulus. In addition, there are controls called X power over and Y power over. These adjust the amount of power that goes to the acoustic optic deflectors. Typically, the power is calibrated so that the deflectors pass the maximum amount of laser power. By changing the power sent to the deflectors, the overall power of the trapping laser can be adjusted during the course of a single epic. This can be useful for rapidly changing the effective stiffness of the trapping laser. Using these parameters requires some empirical experimentation involving measuring the strength of the laser while changing the power over value. If this value is set to 0, then the power is automatically set to the best value for that particular deflection of the laser beam.

The protocols can also be saved and loaded fairly easily. To save the current protocol, the user simply presses the Save Parameters button. Then, the parameters are saved in the file named in the Protocol Name control box. If the Get Parameters button is pressed, then the user is prompted to select a filename. The parameters in that file are used to override the parameters on the screen. Once the parameters are satisfactory to the user, the OK button should be pressed to return to the main front panel.

Seal Test

The seal test is a standard device to measure the input seal resistance during patch clamping. A small voltage pulse is delivered and the current is measured. The seal resistance can therefore be easily determined. The Seal test subroutine can be used from the main front panel. Occasionally, this creates a problem with memory usage and causes the program to crash. It is advisable to open Seal Test.vi directly to avoid this problem.

The seal test front panel is very simple to use. There is a large graph that displays the measured current. From here, one can get a since of the capacitance of the seal as well, which is useful in determining if whole cell mode has been reached. The user can control several parameters. The length and duration of the voltage step are control variables. In addition, the holding potential can be set from this front panel. Usually, it is easier to set the holding potential from the Digidata control box. Once these values are changed, pressing the Reset Values button resets them. This subroutine automatically computes the seal resistance and displays this value on the front panel. The user can select how many times the voltage is presented and averaged for this calculation by changing the control parameter called # of averages.

Setting the Mechanical Angle

Changing the mechanical stimulus angle is performed by pressing the Angle button on the main front panel. This calls a subroutine that gives a square wave, triangle wave or sinusoidal output at the desired angle. The idea of this subroutine is that the user can observe the motion of the laser or trapped bead on the monitor and then adjust the angle to achieve the optimal stimulus. The angle can be adjusted from 0 to 360 degrees. This changes the angle of stimulus, sometimes with a slight delay before the system is updated. The amplitude of the stimulation can be adjusted by the Amplitude control. The frequency of the stimulation is not scientifically controlled as this subroutine should never be used for obtaining actual data. Increasing the Slow Gear control decreases the frequency on a course scale. Increasing the Speediness control finely increases the frequency. Once the Stop button is pressed the mechanical stimulus protocol is automatically updated to stimulate at the chosen angle. This subroutine also displays the digital code and x out and y out signal. These refer to values that are used to control the acoustic optic deflectors and will be discussed further in the following section.

Controlling the Acoustic Optic Deflectors

The acoustic optic deflectors require a high power and high frequency voltage signal in order to function. The frequency of the voltage source changes the amount that the laser beam is deflected. Adjusting this value can therefore allow the program to change the position of the trapping laser. The signal power affects the amount of laser power that goes into the 1^{st} order deflection for each deflector. Therefore, changing the amount of power in the signal can be used to attenuate the trapping laser

power which can change the effective stiffness of the optical trap. When a mechanical deflection protocol is created, the routine automatically uses a lookup table to get the appropriate frequency and power to create that deflection without changing the output power of the laser. This lookup table is determined empirically.

The control card that creates the MHz voltage signals is mounted in the control computer. This card can either be accessed by using custom Labview commands for the board or by a series of digital control commands from an external digital input. The direct computer access does not work quickly and is therefore not useful for changing the output frequency on a sub-second time scale. The card is custom built by the acoustic optic deflector company and has many glitches. Some of the commands tend to crash the card and cannot be used. A large portion of the code that creates the digital code uses techniques to bypass this problem. For instance, certain codes that produce deflections cannot be used, so the program uses the next viable deflection that does not crash the control card. This technique works but is not ideal.

Once the digital control command stream is created, the computer sends a digital command through the DAQ board. This is received by the high frequency generator card that is mounted on the same computer. This card sends two high frequency signals to a high power amplifier that it located outside of the sound proof chamber. This amplifies both signals above 2 W. One should take care not to directly attach an oscilloscope to this output before first attenuating the signal. The output is attached directly to the acoustic optic deflectors which deflect the beam.

Saving the Data

After the proper number of runs has been performed, the main program asks the user if they want to save the data. The user can then kindly accept the offer or rudely decline. If the data is to be saved, it is saved under the path that is listed on the front panel. The filename automatically takes on the name based on the date. An additional extension adds the run number to the tail of the filename. If the file already exists then the file is automatically overwritten. Therefore, care should be taken to ensure that the run number is unique and has not been used earlier in the day.

All of the mechanical, voltage, and general protocol parameters are automatically saved in the file name. In addition, the input values that were sampled from the analog inputs are saved as the recorded current, x position, y position, and sum data. The data can be opened as a word file and be examined in Excel or some other data analysis program. The easiest choice is to use the custom analysis Labview routine that will be described shortly.

Data Analysis

The Labview analysis program is called Analysis.vi. This program is custom designed to utilize the data collected by using the Tweezer Control.vi. To load in data, the user simply clicks the New File to Analyze button. This prompts the user to select a file to be loaded into the program. Once this file is

loaded, then the next or previous file in the folder can loaded by pressing the appropriate buttons. This allows the user to quickly examine all of the data taken during a given experiment.

The front panel is customized to optimally display whatever data the user wishes to observe. To examine the protocol, the user can chose to graphically see the mechanical stimulus, voltage stimulus, or AOD power signal for both deflectors by pressing the appropriate buttons. For the data, the user can see the x, y or sum signal from the position detector as well as the recorded current.

The user can automatically make a calibration for the data from a file. To do this, the calibration file should be loaded into memory. This should be a series of step deflections taken of the bead in the solution, close to the actual experimental location. By pressing the Make Calibration button, the proper scaling is applied to all future data. This determines the actual motion of the bead from the signal collected by the detector. This value also needs the motion of the laser per command size calibration which is a user control.

All of the episodes for a given run can be displayed on the graphs or the individual episodes can be selected individually. This is done by toggling between the All Trace or Single Trace mode button. In single trace mode, the traces can be quickly examined by pressing the Previous Trace or Next Trace buttons that only appear when the user is in single trace mode.

The user can make averages of the data. To do this, the Add Average button needs to be pressed when the desired run is displayed. This adds the trace to the average. The Number of Averages display is incremented to indicate how many runs are in the average. The user can add more files to the average by loading in new files and pressing the Add to Average button again. If the file is already in the average, then it can be subtracted out of the average by pressing the Subtract from Average button, which only appears if that file is already a part of the average. To display the average, the Display Average button needs to be pressed. To exit this mode, the Display Traces button can be pressed, or another file can be loaded into memory which automatically returns to the single file mode.

In addition to making averages, the user can also make combination plots to compare various traces on the same graph. This option simply adds whatever is being displayed on the data graphs to the combination collection. This mode can add a single trace, whole file, or even the average of files. To display the combination of traces, the Combo Mode button needs to be pressed. Individual traces or files can be removed from the combo by pressing the Subtract from Combo button. If a new combo is desired, then pressing the Clear Combo button removes all of the current traces from the combination.

Saving the data that is currently being displayed is easy by pressing the Export Current Traces button. This saves the data in the same format as the acquisition software. The base file path and name used to save it can be selected when the Save button is pressed or initially placed in the base file path that is displayed on the analysis front panel.

Useful Laser Tweezers Techniques

The laser tweezers are definitely quite complicated and have many potential perils, but they also represent a very interesting manner for applying force to an object. With the proper biochemistry, the beads can be used to stimulate single proteins. The stimulating bead also represents the entire physical stimulus, which makes them able to reach places that traditional stimulation techniques would have difficulty accessing. This section briefly mentions a few techniques that were utilized and might be useful for future users of the laser tweezers.

The first technique involves rapidly attenuating the laser power. A compliant stimulus is often used to apply a force to a hair bundle when the active forces within the hair bundle are to be observed. The compliant probe allows the intrinsic bundle forces to move the probe. One problem with this technique is that the rise time of a compliant probe is slow compared to a stiff probe. Many of the interesting forces could be occurring during the rise time of the probe and therefore go unnoticed. A stiff probe has a faster rise time but does not allow the hair bundle to move in order to measure the bundle forces. The stiffness of the optical trap is linearly proportional to the power of the trapping laser and the power can be changed very rapidly with the acoustic optic deflectors. Therefore, a stiff stimulus can be given to the hair bundle to quickly move it to a new position. After the hair bundle has reached its new position, then the power of the laser can be attenuated to any value. This effectively creates a compliant probe that is useful in measuring the active motions of the hair bundle. In this manner, the change in bundle force can be measured sooner after the stimulus. This technique can be used for hair bundles or for any system in which the active forces of the cell are being studied.

Another technique takes advantage of the small size of the stimulus beads. One problem with stimulating outer hair cell bundles is that they are very small and have a unique "v" or "w" shape. So, it is difficult to properly grasp and stimulate the hair bundle effectively. The overlying tectorial membrane properly stimulates outer hair cell bundles but is typically removed for an experiment to provide access for the stimulating probe. The tectorial membrane is relatively transparent and has little effect on the trapping laser. This allows a bead to be trapped and carefully maneuvered under the tectorial membrane to be placed adjacent to an outer hair cell bundle. This technique allows the bead, bundle, and a small portion of the tectorial membrane to move as one unit. This guarantees that the hair bundle is properly stimulated in a similar manner as *in vivo*. This idea is useful for stimulating outer hair cell bundles and can also be utilized to explore other cells in tight spaces.

Appendix B

A Complete List of Model Variables

There are a number of variables used to control the model. They are included here as a resource for controlling the model. They are grouped together by their function. All Boolean variables are true if the value is set to "1" unless otherwise specified.

Mode Parameters

Load_file: Holds the filename that seeds the initial conditions for the simulation.

Confocal_mode: Boolean variable that runs the confocal imaging code when true.

Stick_model: Boolean variable that runs the mechanical model section of code when true.

Calcium_model: Boolean variable that runs the calcium diffusion section of code when true.

Display_save_mode: Boolean variable that runs the display code when true.

Save_all_mode: Boolean variable that saves all of the values in memory. This should only be used with very long intervals between saves as it can quickly use up a lot of hard drive space.

Do_load: Boolean variable that loads the file in load_file when true.

Do_loop_continue: Boolean variable that loads the setup from the previous loop when true.

Mitochondria_on: Boolean variable that turns the mitochondrial buffers on when true.

Use_calcium_model_value: Boolean variable that is only evaluated if stick_model is true and calcium_model is false. If use_calcium_model_value is true then the calcium concentration from the setup file is used to determine the calcium feedback on the myosin motors and transduction channels.

Channel_mode: String variable that be "double_bottom," "double_top," or "either_end" and determines the location of the transduction channels with regard to the tip link, based on the variable name.

Fake_channel_mode: Boolean variable that is only evaluated if stick_model is false. If fake_channel_mode is true then the transduction current follows an exponential profile.

Buffer and Diffusion Related Parameters

Cylinder_depth: Determines the depth of the stereocilium cylindrical compartments (nm).

Down_cylinder: Determines the location of the boundary between the voxels and the cylindrical compartments in the stereocilia. The distance is a measure from the top of each stereocilium (nm).

Voxel_length: Determines the side of an edge of a voxel in the stereocilia (nm).

Body_voxel_length: Determines the side of an edge of a voxel in the hair cell body (nm).

Body_down_cylinder: Determines the location of the boundary between the voxels and the cylindrical compartments in the hair cell body. The distance is a measure from the top of the hair cell body (nm).

Body_cylinder_depth: Determines the depth of the cylindrical compartments in the hair cell body (nm).

Calcium_out: Sets the calcium concentration of the external solution (μM).

Calcium_in: Sets the calcium concentration of the internal solution (μM).

I_total: Sets the concentration of the indicator dye in the internal solution (μM).

B_total: Sets the concentration of the mobile calcium buffer in the internal solution (μM).

F_total: Sets the concentration of the fixed calcium buffer in the internal solution (μM).

C_total: Sets the concentration of the calcium cage in the internal solution (μM).

K_on_F: On rate for fixed calcium buffer (1/(uM-usec)).

K_D_F: Dissociation constant for fixed buffer (μM).

K_on_B: On rate for diffusible calcium buffer (1/(uM-usec)).

K_D_B: Dissociation constant for diffusible calcium buffer(μM).

K_on_I: On rate for diffusible calcium indicator dye(1/(uM-usec)).

K_D_I: Dissociation constant for diffusible calcium indicator dye (μM).

K_on_C: On rate for diffusible calcium cage (1/(uM-usec)).

K_D_C: Dissociation constant for diffusible un-phololyzed calcium cage (μM).

K_D_P: Dissociation constant for diffusible photolyzed calcium cage (μM).

D_I: Diffusion coefficient for bound and unbound calcium indicator dye ($nm^2/\mu sec$).

D_B: Diffusion coefficient for bound and unbound diffusible calcium buffer ($nm^2/\mu sec$).

D_C: Diffusion coefficient for bound and unbound un-photolyzed calcium cage ($nm^2/\mu sec$).

D_P: Diffusion coefficient for bound and unbound photolyzed calcium cage ($nm^2/\mu sec$).

upper_pump_density: density of calcium extrusion pumps in the upper portion of the stereocilia (nm^{-2}).

lower_pump_density: density of calcium extrusion pumps in the lower portion of the stereocilia (nm^{-2}).

body_upper_pump_density: density of calcium extrusion pumps in the upper portion of the hair cell body (nm^{-2}).

body_lower_pump_density: density of calcium extrusion pumps in the lower portion of the hair cell body (nm^{-2}).

upper_pump_down: defines the distance to the upper pump boundary as measured from the top of the stereocilia (nm).

body_upper_pump_down: defines the distance to the upper pump boundary as measured from the top of the hair cell body (nm).

mitochondria_top: defines the upper boundary of the mitochondria as defined as the distance from the top of the hair cell body (nm).

mitochondria_bottom: defines the lower boundary of the mitochondria as defined as the distance from the top of the hair cell body (nm).

K_m: sets the free to fixed ratio calcium ratio for the mitochondria.

Gamma_m: sets mitochondria volume ratio.

V_max_uni: sets the maximum transport rate of the mitochondria uniporter (μM/μsec).

K_uni: sets the half activation point of the mitochondria uniporter (μM).

V_max_NCX: sets the maximum transport rate of mitochondria sodium-calcium exchanger (μM/μsec).

K_NCX: sets the half activation point of the sodium-calcium exchanger (μM).

Uncaging Parameters:

Lambda: calcium uncaging wavelength of the laser (nm).

Extinction_coef: extinction coefficient of cage species (1/(μM-nm)).

Quatum_yield: photon percent that caused photo-activation.

P_max: the power of the excitation laser pulse (W).

Pulse_width: width of a single excitation pulse (μsec).

NA: numerical aperture of the microscope objective.

Excitation_on: Boolean that defines if the uncaging laser should be turned on.

Number_reps: number of presentations of the uncaging laser for one uncaging series.

Rep_rate: flash rate of laser (Hz).

Laser_start_time: time array that defines when the uncaging laser turns on, can have multiple times (μsec).

Excitation_x: x position of the uncaging laser focus.

Excitation_y: y position of the uncaging laser focus.

Excitation_z: z position of the uncaging laser focus.

Time Parameters

Delt_t: time step for mechanical portion of the model. This must be smaller than the other time steps (μsec).

Diffuse_delt_t: time step for voxel diffusion in the stereocilia (μsec).

Cylinder_diffuse_delt_t: time step for the cylinder diffusion in the stereocilia (μsec).

Body_diffuse_delt_t: time step for voxel diffusion in the hair cell body (μsec).

Body_cylinder_diffuse_delt_t: time step for cylinder diffusion in the hair cell body (μsec).

Save_delt_t: time step for saving important updated variables relating to the state of the hair cell (μsec).

Save_all_delt_t: time step for saving all of the parameters used during a simulation. This should be very large to avoid using too much computer memory (μsec).

Show_delt_t: time step for displaying the estimated completion time of a simulation (μsec).

Confocal_delt_t: time step for creating confocal images of the hair cell (μsec).

Wait_time: total simulation time before the hair bundle is stimulated (μsec).

Run_time: total simulation time that the stimulus is held in a deflected position (μsec).

Finish_time: total simulation time after the hair bundle is stimulated (μsec).

V_time_first: time that the voltage changes from the holding potential to the experimental voltage (μsec).

V_time_first_delt: differential time for V_time_first for each loop of the program (μsec).

V_time_second: time that the voltage returns to the holding potential (μsec).

V_time_second_delt: differential time for V_time_second for each loop of the program (μsec).

T_start_channel: time that the channels go from closed to open configuration in fake channel mode (μsec).

T_stop_channel: time that the channels go to the closed configuration in fake channel mode (μsec).

Fake_channel_fast_adapt: fast adaptation time constant in fake channel mode (μsec).

Fake_channel_slow_adapt: slow adaptation time constant in fake channel mode (μsec).

Bundle and Structure Parameters

K_tip: stiffness of an individual gating spring (pN/nm).

K_ankle: stiffness of individual rootlet spring (pN/rad).

Gate_swing: change in transduction channel length between the open and closed configurations (nm).

Calcium_slope_myosin_force: the calcium slope rate for the myosin force decrease.

Calcium_slope_myosin_drag: the calcium slope rate for the myosin drag decrease.

F_max_motor: the maximum force for a myosin complex without the effect of calcium (pN).

F_calcium_bound: the extra force needed to open the gate when calcium is bound to the transduction channel (pN).

K_F: forward rate constant for channel opening (μsec^{-1})

K_R: reverse rate constant for channel closing (μsec^{-1})

Mu: constant in channel probability equations that biases the channel towards the open or closed configuration.

K_top: stiffness of a single top connector (pN/nm).

Drag: drag coefficient of a single stereocilium which has to be set to give the entire hair bundle the appropriate collective drag coefficient (pN-μsec/nm).

Kill_fraction: percentage of the tip links that are randomly destroyed in the hair bundle.

Number_rows: number of stereocilia of the same height along the non-excitatory axis.

Number_columns: number of stereocilia of gradated height along the excitatory axis.

Height_array: height definition for stereocilia along a column (nm).

Ster_rad: radius of the stereocilia at their greatest thickness (nm).

Ster_step: distance between stereocilia rootlet attachment points (nm).

Height_taper: distance up the stereocilia that the stereocilia begin to taper into the rootlet attachment (nm).

Bottom_rad: smallest radius the stereocilia at the rootlet attachment point (nm).

Lower_back: distance that the lower insertion point is displaced from the excitatory edge of a stereocilium (nm).

Body_radius: radius of the hair cell body (nm).

Body_height: total height of the hair cell body (nm).

Body_y_shift: defines the shift of the smallest stereocilium with respect to the hair cell body in the excitatory dimension (nm).

Stimulus Parameters

Stimulus_mode: determines bundle deflection method, can be either "force" or "probe."

Stimulus_pattern: determine the shape of the stimulus, can be "step," "triangle," or "sine."

K_probe: stiffness of the stimulus probe (pN/nm).

Loop_times: number of times that a simulation executes while changing the "delt" parameters for each loop.

Start_loop_force: force stimulus for the first loop of execution (pN).

Delt_loop_force: increase in the force stimulus for each loop of execution (pN).

Start_loop_disp: probe displacement stimulus for the first loop of execution (nm).

Delt_loop_disp: increase in probe displacement for each loop of execution (nm).

Force_triangle_first: minimum force amplitude of triangle stimulus for all loops of execution (pN).

Force_triangle_second: maximum force amplitude of triangle stimulus for all loops of execution (pN).

Disp_triangle_first: minimum displacement amplitude of triangle stimulus for all loops of execution (nm).

Disp_triangle_second: maximum displacement amplitude of triangle stimulus for all loops of execution (nm).

Force_sine_first: force amplitude of sine stimulus for first loop of execution (pN).

Force_sine_delt: increase in force amplitude of sine stimulus for each loop of execution (pN).

Disp_sine_first: displacement amplitude of sine stimulus for first loop of execution (nm).

Disp_sine_delt: increase in displacement amplitude of sine stimulus for each loop of execution (nm).

Sine_freq_first: frequency of the sine stimulus for the first loop of execution (Hz).

Sine_freq_delt: increase in the frequency of the sine stimulus for each loop of execution (Hz).

V_hold: initial holding potential of the cell (mV).

V_step_first: Increase in voltage above the holding potential for the first loop of execution (mV).

V_delt: increase in the voltage step for each loop of execution (mV).

Fake_channel_rest: fraction of current open initially in fake channel mode.

Fake_channel_peak: fraction of current open maximally in fake channel mode.

Fake_channel_adapt_rest: fraction of current open after adaptation.

Display Parameters

Display_variable_name: calcium or buffer that is used to create an image for display.

Confocal_variable_name: calcium or buffer that is used to create an image in confocal mode.

Display_voxel_length: the voxel length used to create the display image (nm).

Display_x: the location of the cross section used for the y-z (side) display.

Display_Z: the location of the cross section used for the x-y (top) display.

Confocal_voxel_length: the voxel length used to create images in confocal mode (nm).

Confocal_lambda: the wavelength of the laser used to compute the confocal image (nm).

Confocal_extinction_coef: the extinction coefficient of the confocal (1/(μM-nm)).

Confocal_quatum_yield: The quatum yield for the confocal.

Confocal_P_max: The power of the confocal laser (W).

Confocal_pulse_width: width of the time spent per excited area (μsec).

Confocal_z_planes: a vector defining the z cross sections used to make confocal images (nm)

Bibliography

Ahmed ZM, Goodyear R, Riazuddin S, Lagziel A, Legan PK, Behra M, Burgess SM, Lilley KS, Wilcox ER, Riazuddin S, Griffith AJ, Frolenkov GI, Belyantseva IA, Richardson GP, Friedman TB (2006) The tip-link antigen, a protein associated with the transduction complex of sensory hair cells. *J. Neuroscience* **26(26):** 7022-7034.

Assad JA, Corey DP (1992) An active motor model for adaptation by vertebrate hair cells. *J. Neuroscience* **12(9):** 3291-3309.

Assad JA, Hacohen N, Corey DP (1989) Voltage dependence of adaptation and active bundle movement in bullfrog saccular hair cells. *PNAS* **86(8):** 2918-2922.

Assad JA, Shepherd GMG, Corey DP (1991) Tip-link integrity and mechanical transduction in vertebrate hair cells. *Neuron* **7:** 985-994.

Batters C, Arthur CP, Lin A, Porter J, Geeves MA, Milligan RA, Molloy JE, Coluccio LM (2004) Myo1c is designed for the adaptation response in the inner ear. *EMBO. J.* **23**: 1433-1440.

Beurg M, Fettiplace R, Nam JH, Ricci AJ (2009) Localization of inner hair cell mechanotransducer channels using high-speed calcium imaging. *Nat. Neurosci.* **5**: 553-558.

Beurg M, Nam JH, Chen Q, Fettiplace R (2010) Calcium balance and mechanotransduction in rat cochlear hair cells. *J. Neurophysiol.* **104**: 18-34.

Beurg M, Nam JH, Crawford A, Fettiplace R (2008) The actions of calcium on hair bundle mechanics in mammalian cochlear hair cells. *Biophys. J.* **94**: 2639-2653.

Beurg M, Evans MG, Hackney CM, Fettiplace R (2006) A large-conductance calcium-selective mechanotransducer channel in mammalian cochlear hair cells. *J. Neuroscience* **26(43)**: 10992-11000.

Bosher SK, Warren RL (1978) Very low calcium content of cochlear endolymph, an extracellular fluid. *Nature* **273:** 377-378.

Bozovic, D, Hudspeth AJ (2002) Hair-bundle movements elicited by transepithelial electrical stimulation of hair cells in the sacculus of the bullfrog. *PNAS* **100(3):** 958-963.

Brandt A, Striessnig J, Moser T (2003) $Ca_V1.3$ Channels are essential for development and presynaptic activity of cochlear inner hair cells. *J. Neurosci* **23(34):** 10832-10840.

Brown MC (1987) Morphology of labeled afferent fibers in the guinea pig cochlea. *J. Comp. Neuro.* **260(4):** 591-604.

Brown MC (1987) Morphology of labeled efferent fibers in the guinea pig cochlea. *J. Comp. Neuro.* **260(4):** 605-618.

Cheung ELM, Corey DP(2006) Ca^{2+} changes the force sensitivity of the hair-cell transduction channel. *Biophys. J.* **90**: 124-139.

Christensen AP, Corey DP (2007) TRP channels in mechanosensation : Direct or indirect activation? *Nat. Rev. Neurosci.* **8**: 510-521.

Corey DP, Garcia-Añoveros J, Holt JR, Kwan KY, Lin SY, Vollrath MA, Amalfitano A, Cheund ELM, Derfler DH, Duggan A, Geleoc GSG, Gray PA, Hoffman MP, Rehm HL, Tamasauskas D, Zhang DS (2004) TRPA1 is a candidate for the mechanosensitive transduction channel of vertebrate hair cells. *Nature* **432:** 723-730.

Corey DP, Hudspeth AJ (1979a) Ionic basis of the receptor potential in a vertebrate hair cell. *Nature* **281**: 675-677.

Corey DP, Hudspeth AJ (1979b) Response latency of vertebrate hair cells. *Biophys. J.* **26**: 499-506.

Corey DP, Hudspeth AJ (1983a) Analysis of the microphonic potential of the bullfrog's sacculus. *J. Neuroscience* **3(5)**: 942-961.

Corey DP, Hudspeth AJ (1983b) Kinetics of the receptor current in bullfrog saccular hair cells. *J. Neuroscience* **3(5)**: 962-976.

Crawford AC, Evans MG, Fettiplace R (1989) Activation and adaptation of transducer currents in turtle hair cells. *J. Physiol* **419**: 405-434.

Crawford AC, Evans MG, Fettiplace R (1991) The actions of calcium on the mechano-electrical transducer current of turtle hair cells. *J. Physiol* **434**: 369-398.

Dallos P, Wu X, Cheatham MA, Gao J, Zheng J, Anderson CT, Jia S, Wang X, Cheng W, Sengupta S, He DZZ, Zuo J (2008) Prestin-based outer hair cell motility is necessary for mammalian cochlear amplification. *Neuron* **58:** 333-339.

Denk W, Holt JR, Shepherd GMG, Corey DP (1995) Calcium imaging of single stereocilia in hair cells: localization of transduction channels at both ends of tip links. *Neuron* **15:** 1311-1321.

DeRosier DJ, Tilney LG, Egelman E (1980) Actin in the inner ear: the remarkable structure of the stereocilium. *Nature* **287**: 291-296.

Eatock RA, Corey DP, Hudspeth AJ (1987) Adaptation of mechanoelectrical transduction in hair cells of the bullfrog's sacculus. *J.Neuroscience* **7(9)**: 2821-2836.

Elgoyhen AB, Johnson DS, Boulter J, Vetter DE, Heinemann S (1994) Alpha 9: an acetylcholine receptor with novel pharmacological properties expressed in rat cochlear hair cells. *Cell* **79(4):** 705-715.

Ellis-Davies GCR (2008) Neurobiology with caged calcium. *Chem Rev.* **108(5):** 1603-1613.

Fuchs PA, Evans MG, Murrow BW (1990) Calcium currents in hair cells isolated from the cochlea of the chick. *J. Physiol (Lond)* **429:** 553-568.

Gale JE, Marcotti W, Kennedy H J, Kros CJ, Richardson GP (2001) FM1-43 dye behaves as a permeant blocker of the hair-cell mechanotransducer channel. *J. Neurosci.* **21:** 7013-7025.

Garcia JA, Yee AG, Gillespie PG, Corey DP (1998) Localization of myosin-1β near both ends of tip links in frog saccular hair cells. *J. Neuroscience* **18(21):** 8637-8647.

Gillespie PG, Corey DP (1997) Myosin and adaptation by hair cells. *Neuron* **19:** 955-958.

Gillespie PG, Cyr JL (2004) Myosin-1c, the hair cell's adaptation motor and adaptation by hair cells. *Annu Rev. Physiol.* **66:** 521-545.

Gillespie PG, Hudspeth AJ (1991) High-purity isolation of bullfrog hair bundles and subcellular and topological localization of constituent proteins. *J.Cell Biology* **112(4)**: 625-640.

Gillespie PG, Wagner MC, Hudspeth AJ (1993) Indentification of a 120 kd hair-bundle myosin located near stereociliary tips. *Neuron* **11:** 581-594.

Goodyear R, Richardson G (1999) The ankle-link antigen: an epitope sensitive to calcium chelation associated with the hair-cell surface and the calycal processes of photoreceptors. *J Neuroscience* **19(10)**: 3761-3772.

Grillet N, Xiong W, Reynolds A, Kasmierczak P, Sato T, Lillo C, Dumont RA, Hintermann E, Sczaniecka A, Schwander M, Williams D, Kachar B, Gillespie PG, Müller U (2009) Harmonin mutations cause mechanotransduction defects in cochlear hair cells. *Neuron* **62:** 375-387.

Gummer AW, Hemmert W, Zenner H (1996) Resonant tectorial membrane motion in the inner ear: its crucial role in frequency tuning. *PNAS* **93:** 8727-8732.

Hacohen N, Assad JA, Smith WJ, Corey DP (1989) Regulation of tension on hair-cell transduction channels: displacement and calcium dependence. *J Neuroscience* **9(11)**: 3988-3997.

Hille, B (1992) Ionic Channels of Excitable Membranes (Sinauer, Sunderland, MA), 2nd Ed., 54-57.

Holt JR, Gillespie SKH, Provance DW, Shah K, Shokat KM, Corey DP, Mercer JA, Gillespie PG (2002) A chemical-genetic strategy implicates myosin-1c in adaptation by hair cells. *Cell* **108**:371-381.

Howard J, Hudspeth AJ (1987) Mechanical relaxation of the hair bundle mediates adaptation in mechanoelectrical transduction by the bullfrog's saccular hair cell. *PNAS* **84**:3064-3068.

Howard J, Hudspeth AJ (1988) Compliance of the hair bundle associated with gating of mechanoelectrical transduction channels in the bullfrog's saccular hair cell. *Neuron* **1**:189-199.

Howard J, Roberts WH, Hudspeth AJ (1988) Mechanoelectrical transduction by hair cells. *Annu Rev Biophys Biophys Chem* **17**:99-124.

Hudspeth AJ (1982) Extracellular current flow and the site of transduction by vertebrate hair cells. *Neuroscience* **2**:1-10.

Hudspeth AJ, Choe Y, Mehta AD, Martin P (2000) Putting ion channels to work: mechanoelectrical transduction, adaptation, and amplification by hair cells. *PNAS* **97 (22)**: 11765-11772.

Hudspeth AJ, Corey DP (1977) Sensitivity, polarity, and conductance change in the response of vertebrate hair cells to controlled mechanical stimuli. *PNAS* **74 (6)**: 2407-2411.

Johnson SL, Beurg M, Marcotti W, Fettiplace R (2011) Prestin-driven amplification is not limited by the outer hair cell membrane time constant. *Neuron* **70**: 1143-1154.

Kachar B, Parakkal M, Kurc M, Zhao YD, Gillespie PG (2000) High-resolution structure of hair-cell tip links. *PNAS* **97(24)**: 13336-13341.

Karavitaki KD, Corey DP (2010) Sliding adhesion confers coherent motion to hair cell stereocilia and parallel gating to transduction channels. *J. Neuroscience* **30 (27)**: 9051-9063.

Kazmierczak P, Sakaguchi H, Tokita J, Wilson-Kubalek EM, Milligan RA, Müller U, Kachar B (2007) Cadherin 23 and protocadherin 15 interact to form tip-link filaments in sensory hair cells. *Nature* **449**: 87-91.

Kennedy HJ, Crawford AC, Fettiplace R (2005) Force generation by mammalian hair bundles supports a role in cochlear amplification. *Nature* **433:** 880-883.

Kennedy HJ, Evans MG, Crawford AC, Fettiplace R (2006) Depolarization of outer hair cells evokes active hair bundle motion by two mechanisms. *J. Neuroscience* **26 (10)**: 2757-2766.

Kozlov AS, Baumgart J, Risler T, Versteegh CP, Hudspeth AJ (2011) Forces between clustered stereocilia minimize friction in the ear on a subnanometre scale. *Nature* **474(7351):** 376-379.

Kwan KY, Allchorne AJ, Vollrath MA, Christensen AP, Zhang DS, Woolf CJ, Corey DP (2006) TRPA1 contributes to cold, mechanical, and chemical nociception but is not essential for hair-cell transduction. *Neuron* **50:** 277-289.

Le Goff L, Bozovic D, Hudspeth AJ (2005) Adaptive shift in the domain of negative stiffness during spontaneous oscillation by hair bundles for the internal ear. *PNAS* **102(47)**: 16996-17001.

Liberman MC, Gao J, He DZ, Wu X, Jia S, Zuo J (2002) Prestin is required for electromotility of the outer hair cell and for the cochlear amplifier. *Nature* **419:** 300-304.

Lumpkin EA, Hudspeth AJ (1998) Regulation of free Ca^{2+} concentration in hair-cell stereocilia. *J. Neurosci* **18(16):** 6300-6318.

Markin VS, Hudspeth AJ (1995) Gating-spring models of mechanoelectrical transduction by hair cells of the internal ear. *Annu Rev. Biophys.Biomol. Struct* **24**: 59-83.

Martin P, Bozovic D, Choe Y, Hudspeth AJ (2003) Spontaneous oscillation by hair bundles of the bullfrog's sacculus. *J. Neuroscience* **23(11)**: 4533-4548.

Martin P, Hudspeth AJ (1999) Active hair-bundle movements can amplify a hair cell's response to oscillatory mechanical stimuli. *PNAS* **96(25)**: 14306-14311.

Martin P, Hudspeth AJ, Jülicher F (2001) Comparison of a hair bundle's spontaneous oscillations with its response to mechanical stimulation reveals the underlying active process. *PNAS* **98(25)**: 14380-14385.

Martin P, Mehta AD, Hudspeth AJ (2000) Negative hair-bundle stiffness betrays a mechanism for mechanical amplification by the hair cell. *PNAS* **97(22)**: 12026-12031.

Meyers JR, MacDonald RB, Duggan A, Lenzi D, Standaert DG, Corwin JT, Corey DP (2003) FM1-43 loading of sensory cells through nonselective ion channels. *J. Neurosci.* **23:** 4054-4065.

Michalski N, Michel V, Caberlotto E, Lefevre GM, van Aken AFJ, Tinevez JY, Bizard E, Houbron C, Weil D, Hardelin JP, Richardson GP, Kros CJ, Martin P, Petit C (2009) Harmonin-b, an actin-binding scaffold protein, is involved in the adaptation of mechanoelectrical transduction by sensory hair cells. *Pflugers Arch – Eur J Physiol* **459:** 115-130.

Molloy JE, Burns JE, Kendrick-Jones J, Tregear RT, White DC (1995) Movement and force produced by a single myosin head. *Nature.* **9; 378(6553):** 209-212.

Nam JH, Cotton JR, Grant W (2007) A virtual hair cell, I: addition of gating spring theory into a 3-D mechanical model. *Biophys J.* **92(6):** 1918-1928.

Nam JH, Fettiplace R (2008) Theoretical conditions for high-frequency hair bundle oscillations in auditory hair cells. *Biophys. J.* **95(10)**: 4948-4962.

Peng AW, Belyantseva IA, Hsu PD, Friedman TB, Heller S (2009) Twinfilin 2 regulates actin filament lengths in cochlear stereocilia. *J.Neuroscience* **29(48)**: 15083-15088.

Pickles JO, Comis SD, Osborne MP (1984) Cross-links between stereocilia in the guinea pig organ of Corti, and their possible relation to sensory transduction. *Hear Res.* **15(2)**: 103-112.

Rayment I, Rypniewski WR, Schmidt-Base K, Smith R, Tomchick DR, Benning MM, Winkelmann DA, Wesenberg G, Holden HM (1993) Three-dimensional structure of myosin subfragment-1: a molecular motor. *Science* **261:** 50-58.

Ricci AJ, Crawford AC, Fettiplace R (2000) Active hair bundle motion linked to fast transducer adaptation in auditory hair cells. *J. Neuroscience* **20(19)**: 7131-7142.

Ricci AJ, Crawford AC, Fettiplace R (2002) Mechanisms of active hair bundle motion in auditory hair cells. *J. Neuroscience* **22(1)**: 44-52.

Ricci AJ, Crawford AC, Fettiplace R (2003) Tonotopic variation in conductance of the hair cell mechanotransducer channel. *Neuron* **40**: 983-990.

Ricci AJ, Kennedy HJ, Crawford AC, Fettiplace R (2005) The transduction channel filter in auditory hair cells. *J. Neuroscience* **25(34)**: 7831-7839.

Ricci AJ, Fettiplace R (1998) Calcium permeation of the turtle hair cell mechanotransducer channel and its relation to the composition of endolymph. *J. Neuroscience* **506(1)**: 159-173.

Ricci AJ, Wu Y-C, Fettiplace R (1998) The endogenous calcium buffer and the time course of transducer adaptation in auditory hair cells. *J. Neuroscience* **18 (20)**: 8261-8277.

Shepherd GM, Corey DP (1994) The extent of adaptation in bullfrog saccular hair cells. *J. Neuroscience* **14(10)**: 6217-6229.

Shotwell SL, Jacobs R, Hudspeth AJ (1981) Directional sensitivity of individual vertebrate hair cells to controlled deflection of their hair bundles. *Annals of the New York Academy of Sciences.* **374**: 1-10.

Siemens J, Concepcion L, Dumont RA, Reynolds A, Williams DS, Gillespie PG, Müller U (2004) Cadherin 23 is a component of the tip link in hair-cell stereocilia. *Nature* **428**: 950-955.

Söllner C, Rauch GJ, Siemens J, Geisler R, Schuster SC, Müller U, Nicolson T, Tübingen 2000 Screen Consortium (2004) Mutations in cadherin 23 affect tip links in zebrafish sensory hair cells. *Nature* **428**: 955-959.

Sotomayor M, Corey DP, Schulten K (2005) In search of the hair-cell gating spring: elastic properties of ankyrin and cadherin repeats. *Structure* **13:** 669-682.

Sotomayor M, Weihofen WA, Gaudet R, Corey DP (2010) Structural determinants of cadherin-23 function in hearing and deafness. *Neuron* **66:** 85-100.

Stauffer EA, Holt JR (2007) Sensory transduction and adaptation in inner and outer hair cells of the mouse auditory system. *J Neurophysiol.* **98**: 3360-3369.

Stauffer EA, Scarborough JD, Hirono M, Miller ED, Shah K, Mercer JA, Holt JR, Gillespie PG (2005) Fast adaptation in vestibular hair cells requires myosin-1c activity. *Neuron* **47:** 541-553.

Tinevez JY, Jülicher F, Martin P (2007) Unifying the various incarnations of active hair-bundle motility by the vertebrate hair cell. *Biophys. J.* **93**: 4053-4067.

Vollrath MA, Eatock RA (2003) Time course and extent of mechanotransducer adaptation in mouse utricular hair cells: comparison with frog saccular hair cells. *J Neurophysiol.* **90**: 2676-2689.

von Bekesy G (1960) Experiments in hearing. McGraw-Hill, *New York.*

Walker RG, Hudspeth AJ (1996) Calmodulin controls adaptation of mechanoelectrical transduction by hair cells of the bullfrog's sacculus. *PNAS* **93:** 2203-2207.

Wu YC, Ricci AJ, Fettiplace R (1999) Two components of transducer adaptation in auditory hair cells. *J Neurophysiol.* **82:** 2171-2181.

Yamoah EN, Gillespie PG (1996) Phosphate analogs block adaptation in hair cells by inhibiting adaptation motor force production. *Neuron* **17:** 523-533.

Zheng J, Shen W, He DZ, Long KB, Madison LD, Dallos P (2000) Prestin is the motor protein of cochlear outer hair cells. *Nature* **405:** 149-155.